

Aus dem Institut für Transfusionsmedizin und Immunologie  
der Medizinischen Fakultät Mannheim  
(Direktor: Prof. Dr. med. Harald Klüter)

## **Human macrophage programming by GDF-15**

Inauguraldissertation  
zur Erlangung des medizinischen Doktorgrades  
der  
Medizinischen Fakultät Mannheim  
der Ruprecht-Karls-Universität  
zu  
Heidelberg

vorgelegt von  
Lina Susana Silva Bermudez

aus  
Neiva, Kolumbien  
2023

Dekan: Prof. Dr. Sergij Goerd  
Referentin: Prof. Dr. Julia Kzhyshkowska

# TABLE OF CONTENT

	Page
ABBREVIATION LIST .....	7
1 INTRODUCTION .....	10
1.1 Healing, pro-fibrotic and tolerogenic functions of macrophages .....	10
1.2 Stabilin-1 .....	12
1.3 TGF- $\beta$ superfamily .....	13
1.4 GDF-15 .....	14
1.4.1 Regulators of GDF-15 expression .....	20
1.4.2 Known receptors of GDF-15 .....	21
1.4.3 GDF-15 physiological activities .....	22
1.4.4 GDF-15 and macrophages .....	23
1.4.5 Effects of rGDF-15 .....	24
1.4.6 GDF-15 in pathology .....	29
1.5 Aims and specific objectives .....	31
2 MATERIALS AND METHODS .....	33
2.1 Equipment .....	33
2.2 Chemicals and reagents .....	34
2.3 Consumables .....	35
2.4 Kits .....	35
2.5 Buffers and solutions .....	36
2.6 Cellular techniques .....	36
2.6.1 Monocyte isolation .....	36
2.6.2 Macrophage stimulation model .....	38
2.6.3 Collection of conditioned medium .....	40
2.7 Molecular biology methods .....	40
2.7.1 RNA isolation .....	40
2.7.2 cDNA synthesis .....	41

2.7.3	Real-time polymerase chain reaction (RT-PCR).....	42
2.8	Protein analysis and immunology methods .....	44
2.8.1	Enzyme-linked Immunosorbent Assay (ELISA) .....	44
2.9	Preparation of cells for immunofluorescence.....	45
2.9.1	Endocytosis assay .....	45
2.9.2	Cytospin sample preparation .....	45
2.9.3	Cell Fixation .....	45
2.9.4	Immunofluorescence staining .....	46
2.9.5	Confocal microscopy .....	48
2.10	Human sample preparation .....	49
2.11	Transcriptomic analysis.....	49
2.11.1	Correlation analysis and a principal component (PC) analysis .....	50
2.11.2	Differential gene expression (DEG) analysis .....	51
2.11.3	Functional enrichment analysis .....	51
2.12	In-silico analysis .....	51
2.13	Data analysis.....	51
3	RESULTS.....	53
3.1	GDF-15 levels in cultured macrophages and in serum of healthy human population.....	53
3.2	Analysis of macrophage pro-inflammatory cytokine expression induced by rGDF-15 after LPS stimulation .....	54
3.2.1	rGDF-15 priming for 48 hours suppresses TNF- $\alpha$ expression in response to LPS in macrophages.....	54
3.2.2	Macrophage co-differentiation with rGDF-15 suppresses TNF- $\alpha$ expression in response to LPS.....	56
3.2.3	rGDF-15 priming for 1 hour suppresses TNF- $\alpha$ and IL-1 $\beta$ expression in response to LPS in macrophages.....	56
3.3	Transcriptomic analysis in macrophages primed with rGDF-15 and challenged with LPS .....	58
3.3.1	Correlation analysis .....	59
3.3.2	Transcript quantification and DEG analysis .....	61
3.3.3	Functional enrichment analysis .....	64
3.3.4	Selection of candidate reference genes.....	74
3.4	In-silico analysis based on TCGA.....	87
3.4.1	Abnormal expression of GDF-15 in cancer.....	88

3.4.2	Abnormal expression of validated set of genes and its association with GDF15 expression in KIRC .....	90
3.5	Association between GDF-15 and Stabilin-1 .....	93
3.5.1	Abnormal expression of STAB1 and its association with GDF-15 expression in KIRC.....	94
4	DISCUSSION .....	99
4.1	GDF-15 levels in human serum and in culture media from primary human macrophages.....	99
4.2	Effect of rGDF-15 on the macrophage response to LPS-mediated inflammation .....	100
4.3	GDF-15 expression patterns and implications in cancer: focus on kidney renal clear cell carcinoma (KIRC) and tumor microenvironment .....	106
4.3.1	Stabilin-1 expression in the macrophage system and its implications in GDF-15-mediated processes with a focus on KIRC .....	109
5	SUMMARY .....	112
6	SUPPLEMENTARY DATA .....	114
6.1	GDF-15 serum levels in healthy plasma donors .....	114
6.2	DEG count for all the comparison groups .....	115
6.3	BCL2L14 expression is increased after LPS challenge in macrophages...	115
6.4	rGDF-15 treatment does not significantly change KLF2 expression in macrophages.....	116
6.5	PALD1 expression is not altered in activated macrophages.....	117
6.6	PROC expression does not change within activated macrophages challenged with LPS .....	118
6.7	SERPINB2 expression levels remain unchanged in macrophages after rGDF-15 treatment .....	119
6.8	rGDF-treatment does not change the GDF-15 expression in macrophages	121
7	REFERENCES .....	122
8	CURRICULUM VITAE .....	134

9 ACKNOWLEDGEMENTS.....	136
-------------------------	-----

## ABBREVIATION LIST

°C	celcius
α-SMA	Alpha Smooth Muscle Actin
μg	microgram
μL	microliter
μm	micrometer
acLDL	acetylated LDL
Akt	protein kinase B
AMPK	AMP-activated protein kinase
Arg-1	Arginase 1
ATF	activating transcription factor
bp	base pairs
BLCA	bladder urothelial carcinoma
BM	bone marrow
BMP	bone morphogenetic protein
BSA	bovine serum albumin
CCL	chemokine (C-C motif) ligand
CCR	C-C chemokine receptor
CD	cluster of differentiation
CD14	CD14 positive macrophages
cDNA	complementary deoxyribonucleic acid
CHOP	C/EBP homologous protein
CLP	chitinase-like proteins
COAD	colon adenocarcinoma
CRIF1	Cytokine response 6 (CR6)-interacting factor 1
CRP	C reactive protein
CSF	Colony-stimulating factor
CXCL	C-X-C motif chemokine ligand
DAPI	4',6-diamidino-2-phenylindole
DDIT3	DNA damage-inducible transcript 3
DEG	Differential gene expression
Dex	dexamethasone
DNA	deoxyribonucleic acid
ECM	extracellular matrix
EDTA	ethylene diamine tetra acetic acid
EGF	epidermal growth factor
EGFR	epidermal growth factor receptor
EGR1	early growth response 1
ELISA	enzyme-linked immunosorbent assay
ERK	extracellular-signal-regulated kinase
Fc	fragment crystallisable
FPKM	fragments per kilobase per million
g	gram / relative centrifugal force
GDF	growth differentiation factor
GDNF	glial cell-derived neurotrophic factor
GFRAL	GDNF family receptor α-like
GO	gene ontology

h	hour(s)
HIF	hypoxia-inducible factor
HRP	horseradish peroxidase
IgG	immunoglobulin G
IL	interleukin
IL-1Ra	Interleukin 1 receptor antagonist
IL17RB	Interleukin 17 receptor beta
INF- $\gamma$	interferon gamma
kD	kilodalton
KEGG	kyoto encyclopedia of genes and genomes
KIRC	kidney renal cell carcinoma
KLF	Kruppel-like factor
L	liter
LDL	low-density lipoprotein
LPS	lipopolysaccharide
LUAD	lung adenocarcinoma
LUSC	lung squamous cell carcinoma
M	molar concentration
M0	non-stimulated macrophages
M1	macrophages activated with INF- $\gamma$
M2	macrophages activated with IL-4
MACS	magnetic-activated cell sorting
MAPK	mitogen-activated protein kinase
M-CSF	macrophage colony-stimulating factor
MEM	minimal essential medium
mg	milligram
MI	myocardial infarction
min	minute(s)
ml	milliliter
mm	millimeter
MMP	matrix metalloproteinase
mRNA	messenger RNA
NAG-1	NSAID-activated gene-1
NAFLD	non-alcoholic fatty liver disease
NF- $\kappa$ B	nuclear factor kappa-light-chain-enhancer of activated B cells
ng	nanogram
NK	natural killer
nm	nanometer
NOS2	nitric oxide synthase 2
oxLDL	Oxidized LDL
padj	adjusted p-value
PBMC	peripheral blood mononuclear cell
PBS	phosphate buffered saline
PC	principal component
PCR	polymerase chain reaction
PDF	prostate-derived factor
PFA	paraformaldehyde
pg	picogram
PI3K	phosphatidylinositol 3-kinase



PPAR	proliferator-activated receptor
ppm	parts per million
PRAD	prostate adenocarcinoma
PTGF- $\beta$	placental transforming growth factor- $\beta$
RET	receptor tyrosine-protein kinase
Retnla	Resistin-like alpha
RNA	ribonucleic acid
ROS	reactive oxygen species
RPKM	reads per kilobase million
rpm	revolutions per minute
RT	room temperature
RT-qPCR/RT-PCR	reverse transcription real-time polymerase chain reaction
s	second(s)
SAT	subcutaneous adipose tissue
SFM	serum-free medium
Sp	Specificity protein
SPARC	secreted protein acidic and rich in cysteine
STAD	stomach adenocarcinoma.
STAT	signal transducer and activator of transcription
TAMs	tumor-associated macrophages
TGF	transforming growth factor
TGF $\beta$ R	transforming growth factor, beta receptor
TFEB	transcription factor EB
Th2	T helper cell type 2
THP-1	human acute monocytic leukemia cell line
TiNPs	titanium nanoparticles
TNF	tumor necrosis factor
UV	ultraviolet
VEGF	vascular endothelial growth factor
vs	versus
YAP	Yes-associated protein
YKL-40	Chitinase-3-like protein 1 (CHI3L1)

# 1 INTRODUCTION

## 1.1 Healing, pro-fibrotic and tolerogenic functions of macrophages

Macrophages are fascinating innate immune cells that act as key players in both inflammatory and healing processes, playing a pivotal role in maintaining tissue balance. These versatile cells are classically described in two distinct phenotypes, namely pro-inflammatory (M1) and regulatory (M2) macrophages, each with a unique set of functions. M1 differentiation is achieved by stimulating macrophages with interferon gamma (INF- $\gamma$ ) or with lipopolysaccharide (LPS). On the other hand, M2 are induced by exposure to IL-4 or IL-13. M1 produce cytokines such as IL-1 $\beta$  and tumor necrosis factor  $\alpha$  (TNF- $\alpha$ ), which induce a rapid inflammatory and cytotoxic response. This includes the recruitment of neutrophils and lymphocytes, and the generation of reactive oxygen species (ROS). In contrast, M2 are known to facilitate healing responses by promoting collagen synthesis and extracellular matrix (ECM) remodeling. They also secrete cytokines such as IL-10, IL-1Ra, and transforming growth factor  $\beta$  (TGF- $\beta$ ), and express scavenger receptors, such as stabilin-1 and mannose receptors<sup>1-3</sup>. Additionally, M2 generate crucial components for ECM remodeling, including matrix metalloproteinases (MMPs), arginase 1 (Arg-1), and resistin-like alpha (Retnla)<sup>4</sup>.

Macrophages are ubiquitous present in almost all human tissues and exert a profound influence on the healing and restructuring of damaged tissue. At the core of their impressive versatility lies their ability to rapidly polarize in response to cytokines. They have the capacity to clear local debris via phagocytosis and secrete various factors that promote angiogenesis and scar formation through auto- and paracrine mechanisms<sup>5, 6</sup>. This dynamic adaptability to their environment has made macrophages an essential component of the body's natural healing and tissue maintenance mechanisms<sup>7</sup>.

During injury, macrophage tissue infiltration increases, along with their production of pro-inflammatory cytokines, which induce the recruitment and proliferation of macrophage progenitor cells. A phenotypic transition to M2 favors the resolution of inflammation through the secretion of cytokines, such as IL-10, TGF- $\beta$  and vascular endothelial growth factor (VEGF), which supports fibroblast proliferation and promotes

angiogenesis. The initial macrophage infiltration then diminishes until wound resolution progresses<sup>8, 9</sup>.

The ontogeny of macrophages may influence their function during healing processes. Macrophage population in tissues can originate from resident cells that locally proliferate, from a spleen monocyte reservoir, or from blood peripheral circulating bone marrow(BM)-derived monocytes. The initial M1 response seems to be supported by spleen-derived monocytes that differentiate into macrophages, whereas the resolution-like M2 phenotype appears to be derived from resident macrophages and circulating monocytes<sup>10</sup>.

Although macrophages are considered less specialized than cells of the adaptive immune system, their response to various insults is quite specific and varies in different pathological contexts. For example, senescent macrophages with reduced polarization capacity, as well as, M1 are often found in impaired wound healing in diabetic patients<sup>11-13</sup>.

On the opposite end of the healing spectrum lies fibrosis, a process resulting from excessive ECM accumulation and defective remodeling<sup>14</sup>. Macrophages contribute to fibrogenesis by recruiting and activating fibroblasts, secreting TGF- $\beta$ 1 and modulating the tissue microenvironment. Similarly, they contribute to the resolution of fibrosis by secreting MMPs that degrade the ECM, such as MMP2 and MMP13, and by participating in the clearance of senescent cells<sup>15</sup>.

Given the impact of macrophages on healing, pro-fibrotic and tolerogenic functions in tissue homeostasis, it is not surprising that they play a significant role in the tumor microenvironment. Dysregulation within macrophage phenotypes has been linked to carcinogenesis<sup>15</sup>. One particular macrophage subtype, known as tumor-associated macrophages (TAMs), infiltrates tumor tissue and is implicated in tumorigenesis, angiogenesis, tumor invasion, and metastasis. TAMs can be derived from circulating monocytes, which are reprogrammed under the effect of CCL2, TGF- $\beta$  and VEGF-A, which are increased in hypoxic conditions, typical of tumor microenvironment. TAMs secrete various proangiogenic factors such as TNF- $\alpha$ , TGF- $\beta$ 1, S100A proteins, semaphorins and chitinase-like proteins (CLP), contributing to ECM degradation,

endothelial cell migration, vessel maturation, and invasion<sup>16</sup>. TAMs also display high plasticity, having a role in both tumor progression and anti-tumor immune responses<sup>17</sup>. For example, their presence can contribute to chemotherapy resistance<sup>18</sup>.

## 1.2 Stabilin-1

Stabilin-1 (STAB1, FEEL-1, CLEVER-1, KIAA0246) is a multifunctional scavenger receptor that mediates the endocytic and phagocytic internalization of various unwanted-self ligands, thereby contributing to tissue homeostasis<sup>19</sup>. Stabilin-1 is expressed by sinusoidal endothelial cells in the spleen, liver and lymphatic vessels, and by resident macrophages, excluding Kupffer cells<sup>20</sup>. Its extracellular domain contains 7 fasciclin, 2 laminin-type epidermal growth factor (EGF)-like and 16 EGF-like domains. Stabilin-1 owns a single short intracellular C-terminal domain with a complex sorting function<sup>19, 21</sup>.

Macrophages express stabilin-1 in response to IL-4 and dexamethasone, thus stabilin-1 is considered a marker of M2 polarization<sup>20</sup>. Besides stabilin-1 is abundantly expressed on TAMs<sup>16, 22</sup>. In contrast, M1 polarization is associated with reduced stabilin-1 expression<sup>23</sup>.

Some ligands known to interact with stabilin-1 extracellular domain include modified low-density lipoproteins (LDL) such as oxidized (oxLDL) and acetylated LDL (acLDL), and advanced glycation end products (AGEs)<sup>24, 25</sup>. Stabilin-1 also binds to gram-negative and gram-positive bacteria components, such as phosphatidylserine<sup>21, 26</sup>. Another ligand of stabilin-1 is secreted protein acidic and rich in cysteine (SPARC), a glycoprotein involved in tissue remodeling, wound healing, and inhibition of angiogenesis<sup>24, 25</sup>. Stabilin-1 also interacts with endogenous proteins such as stabilin interacting chitinase-like protein (SI-CLP), which is sorted from late Golgi to late endosomes for lysosomal degradation<sup>27</sup>. SI-CLP has been found in inflammatory diseases such as rheumatoid arthritis, liver cirrhosis and cancer<sup>25</sup>. Stabilin-1 is frequently found intracellularly due to rapid cycling between the plasma membrane and endosomal compartment. Nonetheless, its presence on the cell surface has also been demonstrated<sup>27</sup>. Functionally, stabilin-1 acts via a clathrin-dependent endocytosis pathway and mediates intracellular trafficking of the internalized ligands for their endosome sorting, and subsequent lysosomal degradation or storage in the trans Golgi network for recycling<sup>19</sup>.

Beyond its scavenging function, stabilin-1 expression has been linked to cellular adhesion. In non-continuous endothelial cells of lymphatic vessels, stabilin-1 mediates lymphocyte adhesion to the endothelium and subsequent transmigration<sup>28</sup>. Additionally, stabilin-1 exhibits high expression in various malignancies, including breast cancer, colorectal carcinoma, melanoma, urothelial cancer and leukemia, and its presence correlates with poor prognosis<sup>22, 29</sup>. It is hypothesized that stabilin-1 actively contributes to an immunosuppressive environment that favors metastasis. Therefore, recent immunotherapy initiatives have focused on stabilin-1 as a potential therapeutic target<sup>29</sup>. Besides acting as the scavenger receptor for SPARC, a mediator of angiogenesis, stabilin-1 is also expressed on blood vessels during tumor vascularization, and its inhibition decreases cell-cell interactions, highlighting its role in tumor progression<sup>21</sup>.

### 1.3 TGF- $\beta$ superfamily

The TGF- $\beta$  superfamily has 58 members, with 17 belonging to the bone morphogenetic protein (BMP) group, 8 to the Activin and 33 to the TGF- $\beta$  subfamily. This superfamily comprises secreted cytokines involved in various cellular processes, including growth, differentiation and immune regulation<sup>30</sup>. Among these, TGF- $\beta$  is the best-studied and well-characterized member. TGF- $\beta$  is strongly linked to fibrotic conditions such as defective scarring, cancer and atherosclerosis, as it contributes to ECM synthesis, remodeling and to the inhibition of matrix degradation. These effects are achieved through the secretion of factors such as tissue inhibitor of matrix metalloprotease 1 (TIMP1), alpha smooth muscle actin ( $\alpha$ -SMA), collagen I, and collagen II<sup>31</sup>. TGF- $\beta$  exists in three isoforms (TGF- $\beta$  1-3) each of which binds to the tetrameric receptor complexes transforming growth factor beta receptor I and II (TGF $\beta$ RI/TGF $\beta$ RII). Activation of downstream mediators occurs through MAP kinases, PI3K/AKT, and AMPK signaling pathways<sup>32</sup>. One of the most notable properties of TGF- $\beta$  is its paradoxical behavior in contexts such as cancer, where it acts both as a tumor suppressor and as a promoter of tumor growth and metastasis<sup>33</sup>.

All members are synthesized as dimeric precursors held together by three disulfide bonds, which are cleaved during maturation, leaving a secreted form linked by a unique disulfide bond<sup>30</sup>. Members of the growth differentiation factors (GDFs), within the TGF- $\beta$  superfamily, share the similar rigid structure of the BMPs. Noteworthy members of this subgroup include the recently discovered GDF-11 and GDF-15<sup>34, 35</sup>.

## 1.4 GDF-15

GDF-15, also known as MIC-1, PTGF- $\beta$ , PDF, and NAG-1, is a multifunctional cytokine recognized as a distant member of the glial cell-derived neurotrophic factor (GDNF) family and the TGF- $\beta$  superfamily<sup>36-38</sup>. Its discovery occurred in the late 1990s when it was identified as an autocrine cytokine capable of reducing the pro-inflammatory macrophage activation after LPS stimulation in the human myelomonocytic cell line U937<sup>37</sup>. In parallel, Lawton et al. discovered its expression in the placenta during early and late gestation<sup>39</sup>. Moreover, Paralkar et al. found elevated expression of this protein in the prostate and named it prostate-derived factor<sup>40</sup>. A few years later, Baek et al., observed that the treatment of HCT-116 colon cancer cells with NSAIDs induced GDF-15 expression<sup>41</sup>.

GDF-15 is present across the animal kingdom and is well-conserved within vertebrates, particularly in mammals<sup>42, 43</sup>. The GDF-15 gene is located in chromosome 19p12-13.1 and consists of two exons (309 bp and 891 bp) separated by a 2,9 kb intron<sup>39</sup>. Analogous to other members of the TGF- $\beta$  family, GDF-15 has a dimeric disulfide-bonded configuration and is synthesized as a proprotein. However, its disulfide bond configuration differs from that of the TGF- $\beta$  family<sup>36</sup>. Its general structure encompasses a propeptide, followed by an RXXR furine-like site and the mature protein. GDF-15 conserves the seven cysteine domains, typical of the TGF- $\beta$  family, sharing a 20% amino acid identity, that gives rise to its cysteine knot crystal motif (Figure 1A and C)<sup>37</sup>. Besides its proximity to the TGF- $\beta$  family, GDF-15 resembles the structure of the GDNF family ligands, sharing 16% amino acid identity (Figure 1B and C)<sup>36</sup>. The immature form consists of 308 amino acids, including a 9-amino acid signal peptide, 167-amino acid propeptide, and 112-amino acid mature protein. As part of its post-translational modifications, the immature form undergoes proteolytic cleavage, leaving the mature (13 kD) and propeptide (30 kD) forms, which are later cleaved at the RXXR furine-like site<sup>37</sup>. This site is recognized and sliced by proprotein convertase subtilisin/kexin type (PCSK)-3, -5, and -6 or by MMPs, facilitating GDF-15 maturation<sup>44-46</sup>. Upon dimerization, the mature form, consisting of 224 amino acids (25 kD), and the propeptide, are secreted. In contrast to the general structure of the TGF- $\beta$  family, GDF-15's propeptide lacks cysteine residues<sup>37</sup>. Interestingly, the propeptide seems to function autonomously<sup>47</sup>. Latent stromal stores of this immature form of GDF-15 have been found in diverse tissues and pathologies. These stores serve as a reservoir for

GDF-15<sup>48</sup>. Moreover, the secretion of the propeptide is faster than that of mature GDF-15<sup>49</sup>.

Under physiological conditions, GDF-15 is produced at high levels in the terminal villi of the placenta (up to 54000 pg/mL)<sup>50</sup>. In contrast, other human tissues produce lower levels of GDF-15, including skeletal muscle<sup>51</sup>, subcutaneous adipose tissue<sup>52</sup>, prostate epithelium<sup>53</sup>, bladder<sup>54</sup>, kidney<sup>55</sup> and lung<sup>56</sup>. Furthermore, GDF-15 has been found in most human fluids, including blood, amniotic fluid<sup>50</sup>, bronchoalveolar fluid, and cerebrospinal fluid<sup>57</sup> (Figure 2).

A diverse array of cell types, such as fibroblasts, adipocytes, macrophages, epithelial and endothelial cells contribute to the production of GDF-15 (Table 1). However, most of them express GDF-15 mainly under stress conditions, such as exposure to LPS, bleomycin, oligomycin, and tunicamycin<sup>58-60</sup>. Among the blood cells, the myeloid population exhibits higher expression levels of GDF-15 compared to the lymphoid population. Following clodronate-induced depletion of myeloid cells in mice, GDF-15 mRNA levels significantly dropped, highlighting a major myeloid contribution to systemic GDF-15 levels<sup>61</sup>. Ramirez et al., studied the expression of GDF-15 during the hematopoietic differentiation of CD34+ progenitors, revealing higher levels of GDF-15 expression and production within the erythroid cell lineage. In contrast, the myeloid cell lineage expressed marginal levels of GDF-15 during maturation<sup>62</sup>. During erythroblast maturation, GDF-15 levels are found up to 74000 ± 2580 pg/mL<sup>63</sup>. Recently, it was shown that the megakaryocytes are key cells expressing GDF-15 in the BM<sup>64</sup>.

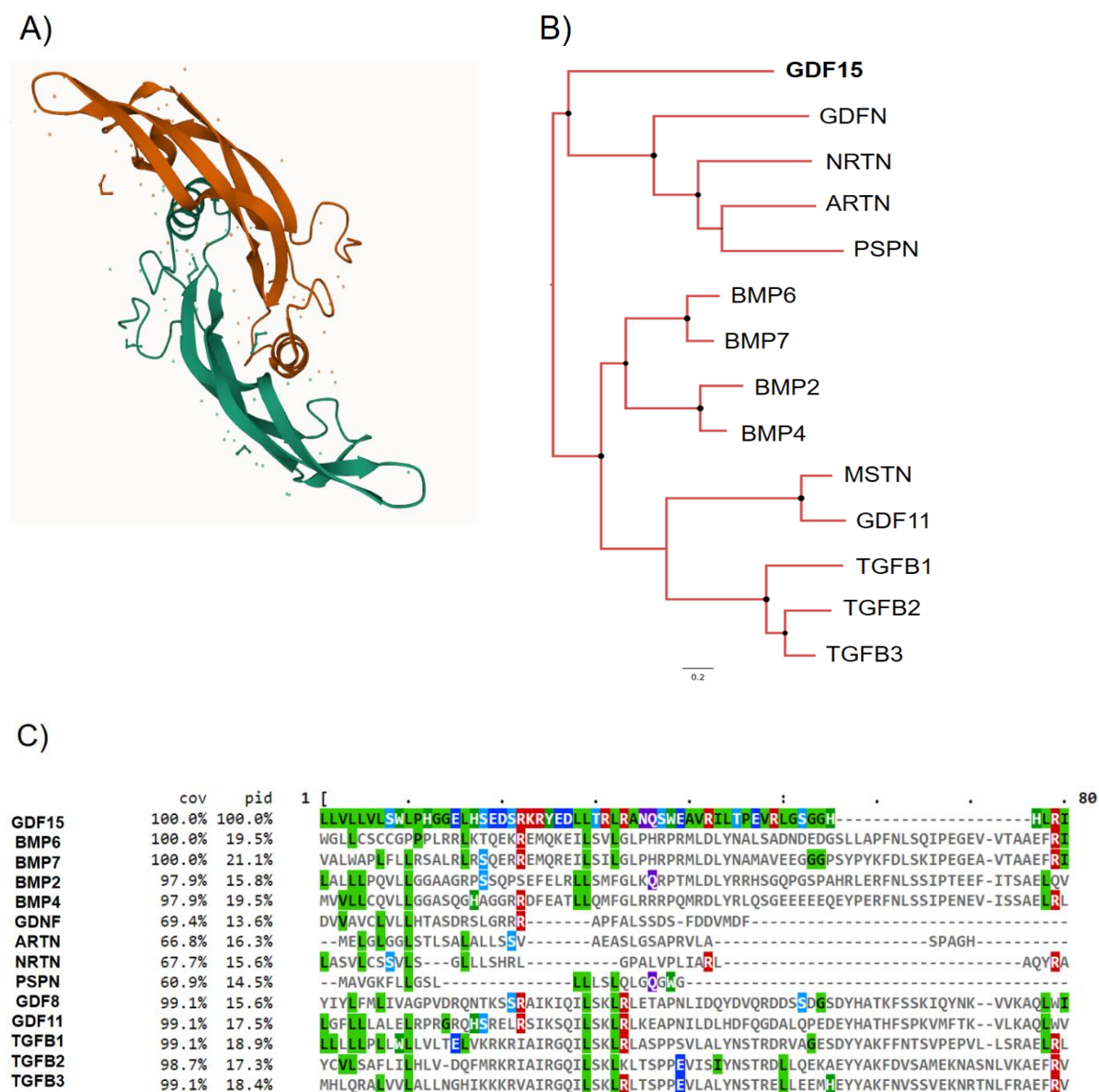


**Figure 1. GDF-15 crystal protein structure and phylogenetic associations.** A) Crystal structure of GDF-15 protein. Obtained from InterPro: <https://www.ebi.ac.uk/interpro/structure/PDB/5vt2/#table><sup>65</sup>. B) Phylogenetic tree illustrating relationships among GDF-15, TGF- $\beta$ , and GDNF superfamily members. Generated using TaxOnTree. (bioinfo.icb.ufmg.br/taxontree/#x). C) Protein sequence alignment of GDF-15 in comparison to TGF- $\beta$  and GDNF superfamily members. Sequence alignment was performed using Protein BLAST (blast.ncbi.nlm.nih.gov). cov: percentage of coverage, piv: percentage of identity.



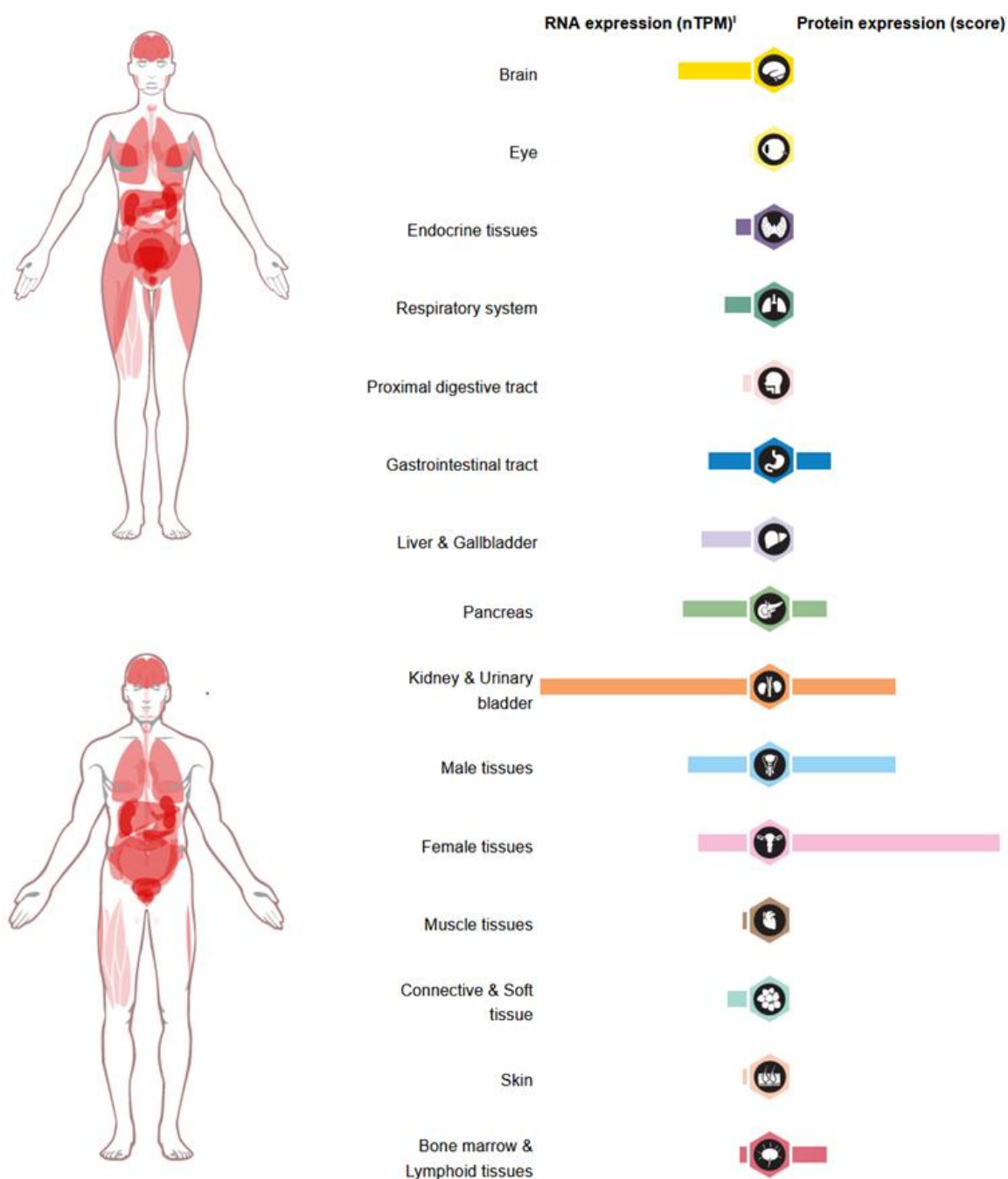


**Figure 2. GDF-15 RNA and protein expression in the human body.** GDF-15 expression is elevated in various tissues, including kidney, bladder, brain, and female and male tissues. RNA expression levels are represented using normalized transcript expression values (nTPM). Adapted from: Human Protein Atlas <https://www.proteinatlas.org/ENSG00000130513-GDF15/tissue>

**Table 1. GDF-15 producing cells**

<b>Cells</b>	<b>Species</b>	<b>Conditions</b>	<b>Measurement</b>	<b>Reference</b>
<b>Macrophages</b>	Human	Rosiglitazone-treated	Microarray	66
	Human – THP-1, RAW264.7	LPS	RT-PCR	67
<b>Endothelial colony-forming cells generated from adult blood</b>	Human	7 d	RT-PCR	68
	Human	7 d	ELISA	68
<b>Alveolar basal epithelial cells (A549)</b>	Human	Bleomycin treatment	RT-PCR	59
<b>Lung fibroblasts</b>	Mouse	Bleomycin treatment	RT-PCR	69
<b>Erythroid cells (increasing expression in higher differentiation states)</b>	Human	Maturation	RT-PCR	70
<b>Primary erythroblasts</b>	Human	7 and 14 d	RT-PCR	63
	Human	7 and 14 d	ELISA	63
<b>Cardiomyocytes</b>	Rat	Stretch conditions	RT-PCR	71
<b>Adipocytes</b>	Human	Differentiated from SAT	RT-PCR	60
	Human	Differentiated from SAT	ELISA	60
	Human	Oligomycin treated	ELISA	60
	Mouse	Recombinant IL-4 and IL-13	RT-PCR, ELISA	72
<b>Trophoblastic cells (BeWo)</b>	Human	24 h	ELISA	50
<b>Trophoblastic cells (BeWo)</b>	Human	7 d	ELISA	50
<b>Human aortic endothelial cells</b>	Human	Purified human recombinant C-reactive protein	RT-PCR, ELISA	73
<b>Colorectal cancer cells (HCT-116)</b>	Human	NSAID, Indometacyn	Northern and Western Analysis	41
<b>Adipose tissue macrophages</b>	Human	Obesity	RT-PCR	61

<b>Prostate cancer cells (LNCaP-C81 cell line)</b>	Human	Prostate cancer	Western blot analysis	74
<b>Androgen-sensitive (LNCaP-C33 cell line)</b>	Human	Prostate cancer	Western blot analysis	74
<b>C2C12 (myoblasts)</b>	Mouse	.	RT-PCR and Western blot analyze	75
<b>Mouse embryonic fibroblast cells</b>	Mouse	CRIF1 deficient muscle cells in mice	RT-PCR and Western blot analyze	75
<b>Hypopharyngeal carcinoma cells (FaDu cells)</b>	Human	Head and neck cancer	Western blot analysis	76
<b>Human epithelial carcinoma cells (KB cell line)</b>	Human	Head and neck cancer	Western blot analysis	76
<b>Human nasal epithelial cell</b>	Human	LPS treatment	RT-PCR	11
<b>Hepatocytes</b>	Mouse	Metformin treatment	RT-PCR	77
<b>Embryonic adipocyte-like cell line (3T3-L1)</b>	Mouse	Tunicamycin treatment	RT-PCR	58
<b>Adenocarcinoma alveolar basal epithelial cells (A549)</b>	Human	C5a treatment	RT-PCR	78

See list of abbreviations

### 1.4.1 Regulators of GDF-15 expression

Several transcription factors that induce GDF-15 expression have been identified (see Table 2). For example, upon exposure to C-reactive protein (CRP), p53 binds to the GDF-15 promoter and induces GDF-15 transcription in human aortic endothelial cells<sup>73</sup>. This highlights an association between the two biomarkers, GDF-15 and CRP, which are co-elevated in acute inflammatory conditions. However, its expression is not exclusively dependent on the presence of CRP. p53 has also been shown to increase GDF-15 expression following damage induced in enterocytes. In this context, GDF-15 functions as a pro-apoptotic factor and triggers the expression of activating transcription factor 3 (ATF3), a pro-survival protein induced during cellular stress<sup>79</sup>. The interaction between ATF3 and GDF-15 in human colorectal cancer cells was also reported by Lee et al<sup>80</sup>.

Recently, Kim et al found that the transcription factor EB (TFEB), a regulator of energy expenditure and an inducer of autophagy, binds to the GDF-15 promoter. This binding leads to increased GDF-15 expression following exposure to lysosomal stressors in adipose tissue macrophages. This mechanism mediates a reduction in metabolic inflammation during high-fat-induced obesity in mice<sup>61</sup>. In adipocytes, another transcription factor, STAT6, was also identified as an inducer of GDF-15 expression in response to IL-13 treatment. This mechanism appears to favor glucose tolerance<sup>72</sup>. In addition, under mitochondrial stress, C/EBP homologous protein (CHOP) promotes GDF-15 expression in murine myoblasts and hepatocytes<sup>75</sup>. Another recognized transcription factor is early growth response 1 (EGR1), which forms a positive feedback loop with GDF-15, serving itself as a promoter for EGR1<sup>76</sup>. For a comprehensive list of other transcription factors, Table 2 highlights the diverse range of GDF-15 inducers.

**Table 2. Known transcription factors of GDF-15 expression**

Transcription factors	Cells	Conditions	Reference
<b>ATF4</b>	human nasal epithelial cells	LPS treatment	11
	murine hepatocytes	Metformin treatment	77
	mouse embryonic 3T3-L1 adipocyte-like cell line	tunicamycin treatment	58
<b>CHOP</b>	PMA-differentiated THP-1, PBMCs	SFAs treatment	81
	murine C2C12 myoblasts	CRIF1 deficiency	75

	murine hepatocytes	Metformin treatment	77
<b>DDIT3</b>	mouse embryonic 3T3-L1 adipocyte-like cell line	tunicamycin treatment	58
<b>EGR1</b>	FaDu cells (a hypopharyngeal carcinoma cell line), KB cell line (human epithelial carcinoma cells)	.	76
<b>KLF5</b>	A549 (adenocarcinoma alveolar basal epithelial cells)	C5a treatment	78
<b>p53</b>	human aortic endothelial cells	CRP supplementation	73
<b>Sp1</b>	HCT-116 (colorectal cancer cells)	.	41
<b>Sp3</b>	HCT-116 (colorectal cancer cells)	.	41
<b>STAT6</b>	Murine adipocytes	IL-13 treatment	72
<b>TFEB</b>	human and murine adipose tissue macrophages	Obesity	61
<b>YAP*</b>	breast cancer cells and cytotrophoblast	.	82

\*YAP has been shown to act as a negative regulator of GDF-15 expression. See list of abbreviations

#### 1.4.2 Known receptors of GDF-15

In 2017, GDNF family receptor  $\alpha$ -like (GFRAL), a member of the GDNF receptor  $\alpha$  family, was identified as a receptor for GDF-15. This receptor is highly expressed in the area postrema and nucleus of the solitary tract of the hindbrain in mice, non-human primates, and humans<sup>83-85</sup>. Using an unbiased ligand-receptor coupling approach, Mullican et al. and Yang et al. found that GDF-15 binds exclusively to GFRAL, excluding high-affinity binding to other receptors including those of the TGF- $\beta$  receptor family<sup>84, 85</sup>. Other potential ligands for GFRAL, such as TGF- $\beta$  and GDNF-similar ligands (GFLs), were also discarded, highlighting an exclusive partnership between GDF-15 and GFRAL<sup>85</sup>. Together with Emerson et al, these three research groups dissected the mechanism of GDF-15-GFRAL binding and its effect on appetite regulation<sup>84</sup>. Moreover, the receptor tyrosine-protein kinase (RET) was found to be a co-receptor necessary for the metabolic actions of GDF-15 through GFRAL<sup>83, 84</sup>. Upon its binding, GDF-15 promotes the physical interaction between GFRAL and RET, and mediates the activation of RET phosphorylation and the intracellular phosphorylation cascade of extracellular-signal-regulated kinase (ERK), Akt, and phospholipase C<sup>83, 85</sup>. RET expression, like GFRAL, was shown to be particularly abundant in the area postrema and nucleus of solitary tract in the hindbrain of both mice and non-human primates. Beyond this, GFRAL expression was also found in the human spleen, thymus, testis, and adipose tissue, as well as in isolated adipocytes, but not in

macrophages<sup>51, 59</sup>. RET is expressed in most mouse tissues except liver, kidney and adrenal gland<sup>85</sup>. Recently, Siddiqui et al., found presence of GFRAL/RET in osteoblasts, using a mouse model of prostate cancer bone metastasis<sup>74</sup>. Furthermore, Moon et al., demonstrated GFRAL expression by Treg lymphocytes treated with recombinant human GDF-15 (rGDF-15)<sup>86</sup>. These findings highlight the GFRAL expression beyond the boundaries of the central nervous system, possibly arising in response to pathological stimuli and varying across different cell types or tissues.

To date, several other receptors have been investigated as possible peripheral mediators of GDF-15 actions. For instance, Takenouchi et al., found that rGDF-15 increases the phosphorylation of downstream components of the TGF- $\beta$  I receptor cascade, namely Smad2/3, in fibroblasts. This effect could be reversed by inhibiting the TGF- $\beta$  I receptor<sup>59</sup>. Other researchers demonstrated that GDF-15 binds to the TGF- $\beta$  I receptor through the use of inhibitors, effectively blocking the phosphorylation cascade triggered by the cytokine in human colorectal carcinoma and THP-1 cell lines<sup>87, 88</sup>. Nevertheless, concerns arose regarding the veracity of these findings due to the reported TGF- $\beta$  contamination in rGDF-15<sup>89</sup>. Other alternative mechanisms could explain GDF-15 peripheral effects, such as the existence of a soluble GFRAL that would form a complex with GDF-15 and facilitate its recognition and internalization in further tissues<sup>90</sup>. Another consideration is that GDF-15 may bind to other receptors depending on the cell type and underlying pathological condition. Therefore, the involvement of TGF- $\beta$  or other receptors in the response of cells to GDF-15 is still controversial.

GDF-15 is also recognized as a common endocytic ligand for both stabilin-1 and 2. Schledzewski et al. found an impaired clearance of GDF-15 in STAB-1/-STAB-2/- mice, which subsequently developed severe glomerular fibrosis and mild perisinusoidal hepatic fibrosis. They described for the first time the interaction between the extracellular fasciclin domains from stabilin-1 and -2, and GDF-15 by using GST pull-down assays. The functional endocytosis assay further validated the uptake of GDF-15 by stabilin-1 and stabilin-2<sup>91</sup>. The fate of GDF-15 after internalization by these receptors has not been investigated.

#### 1.4.3 GDF-15 physiological activities

GDF-15 basal plasmatic levels range from 337 to 1060 pg/mL. These levels may increase during certain physiologic changes, such as muscle contraction and exercise,

and under the pathological conditions reviewed in the following sections<sup>71, 85</sup>. Circulating GDF-15 levels increase with age and are not influenced by gender<sup>51, 60, 92</sup>. Notably, GDF-15 is significantly elevated at birth and during the first 4 months of life, reaching around threefold the average adult concentrations<sup>93</sup>. Its levels also progressively rise during pregnancy, correlating with gestational week and peaking in the third trimester<sup>50</sup>.

Under physiological conditions, GDF-15 expression positively correlates with higher maturation states in the erythroid line and its supplementation in erythroid cells reduces their metabolic activity and proliferation<sup>52</sup>. Moon et al., found that rGDF-15 accentuates the regulatory effect of Treg cells on activated T cells. Moreover, rs7226, a single nucleotide polymorphism associated with increased production of GDF-15 in humans, has been associated with an increased count of lymphocytes and monocytes and with a decreased concentration of innate immune cells and granulocytes<sup>86</sup>.

#### 1.4.4 GDF-15 and macrophages

In murine and human bone marrow-derived macrophages, as well as, in THP-1 and RAW264.7 cells, GDF-15 expression is increased under stimulation of pro- and anti-inflammatory mediators including IL-4, IL-1 $\beta$ , TNF- $\alpha$ , IL-2 and M-CSF<sup>66, 67</sup>. At the same time, GDF-15 has been widely associated with M2 differentiation and inhibition of M1 polarization<sup>59, 67, 72</sup>. Pence et al. studied the relationship between human GDF-15 serum levels and different parameters of monocyte immunosenescence. They found that GDF-15 levels were significantly higher in the elderly population as compared to the young individuals. Also, circulating GDF-15 levels exhibited a negative correlation with maximal monocyte respiratory capacity<sup>94</sup>.

GDF-15 production in macrophages has also been investigated in specific pathological contexts. For instance, in vitro LPS stimulation increases GDF-15 expression and secretion in THP-1 and RAW264.7 macrophages in a dose- and time-dependent fashion<sup>67</sup>. Likewise, in vivo LPS injection increases plasmatic GDF-15 concentrations in mice, rats and humans (in humans LPS was given in a 1 ng/kg doses)<sup>52, 95</sup>.

In the context of atherosclerosis, treatment of THP-1 with rGDF-15 was linked to lipid accumulation, whereas GDF-15 knockdown resulted in reduced lipid burden. In addition, rGDF-15 increased the levels of autophagy-related proteins, suggesting a possible role for GDF-15 in autophagosome formation in foam cells<sup>96</sup>. GDF-15 also

appears to improve the phagocytic and bactericidal function of macrophages in the THP-1 and RAW264.7 cell lines<sup>67</sup>.

Jung et al. investigated the effect of reduced mitochondrial oxidative function on insulin resistance in mice. They found that adipose tissue macrophages express low GDF-15 levels and show a shift toward M1 polarization. Further experiments demonstrated that treatment with rGDF-15 decreased the expression of IL-6, nitric oxide synthase 2 (NOS2) and TNF- $\alpha$ , and promoted M2 polarization by increasing the production of Arg-1, Retnla and CLP3<sup>66</sup>. Campderrós et al. found that GDF-15 produced by murine brown adipocytes suppressed the expression of TNF- $\alpha$ , CCL2 and IL-6 in M1-polarized RAW264.7. In contrast, M2 gene expression was unaffected by GDF-15<sup>97</sup>. A study by Takenouchi et al. examined GDF-15 expression in a mouse model of bleomycin-induced lung fibrosis. They found increased GDF-15 expression and protein levels in lung tissue, bronchoalveolar fluid, and plasma of mice with pulmonary fibrosis. Within the lung tissue, the highest GDF-15 positivity was found in epithelial cells and macrophages (see Table 3)<sup>59</sup>.

#### 1.4.5 Effects of rGDF-15

In vitro studies have explored the effects of GDF-15 using its recombinant form mainly by assessing its effect on transcriptome using RT-PCR. An overview of the main effects of rGDF-15 is given in Table 3. Besides studying the effect of rGDF-15 on the macrophage system, as reviewed above, Takenochi et al. also studied it on the fibroblast system, showing that rGDF-15 supplementation increases fibroblast activation measured by increased secretion of  $\alpha$ -SMA, an effect that was not mediated by GFRAL/RET activation pathway<sup>59</sup>. Other myeloid cells strongly affected by rGDF-15 treatment are erythrocytes. rGDF-15 supplementation leads to decreased erythroid colony formation and decreased transcription of erythroid differentiation factors<sup>70</sup>. In vitro rGDF-15 supplementation has also been linked to increased angiogenesis and increased VEGFA expression in glioblastoma cells<sup>98</sup>.

The parenteral supplementation of GDF-15 in in vivo models has also been evaluated in animal models including mice and primates, showing an impact in several metabolic parameters such as reduction of body weight, increased glucose tolerance and decreased appetite, which is reviewed in the following section<sup>83-85</sup>.

To date, no study has assessed the effects of rGDF-15 on the transcriptome using RNA-Seq. However, Deng et al evaluated the transcriptomic changes due to GDF-15



KO in the lung of mice exposed to ricin toxin. Mice deficient in GDF-15 showed an increased inflammatory response in lung tissue<sup>99</sup>.

**Table 3. Effects of rGDF-15**

Effects	Evidence		Species	Cells	Conditions	Method	Pathology	Product	Concentration	Reference
Increased M2 and decreased M1 polarization	Increased expression	Arg-1	Mouse	Peritoneal macrophages	IL-4, IL-13 ± rGDF15 for 48 h	RT-PCR	Pulmonary fibrosis	CHO-derived GDF-15; E. coli-expressed	100 ng/mL	<sup>59</sup>
	Decreased TNF-α, and secretion, decreased mRNA levels, increased CD163 mRNA levels	IL-6, MCP-1, IL-10 CD80 levels, CD163	Human	THP-1 and RAW264.7	rGDF15 for 48 h	RT-PCR, Flow cytometry	Inflammation			
Fibroblast activation	Increased α-SMA protein expression		Human	WI-38 (fibroblasts from lung tissue)	Preincubation for 48 h; rGDF15 for 72 h	Western blot	.	CHO-derived GDF-15; E. coli-expressed	0-100 ng/mL	<sup>59</sup>
	Increased Smad2/3 phosphorylation through TGF-β I receptor		Human	WI-38 (fibroblasts from lung tissue)	Preincubation for 48 h; rGDF15 for 20 min-1 h	Western blot	.	CHO-derived GDF-15; E. coli-expressed	100 ng/mL	<sup>59</sup>
Reduced metabolic activity in erythroid cells	Decreased optical density with increasing GDF-15 concentration in MTT assay		Human	K562 (lymphoblast BM)	Treatment with β-thalassemia serum containing 48 ng/mL of GDF-	RT-PCR, Flow cytometry, MTT assay	.	CHO-derived GDF-15	2-50 ng/mL	<sup>70</sup>

					15 or GDF-15 for 24h, 48h and 72h						
<b>Reduced proliferation in erythroid cells</b>	Decreased optical density with increasing GDF-15 concentration in MTT assay	Human	K562 (lymphoblast BM)	.	GDF-15 for 5 d	CFSE proliferation assay	.	CHO-derived GDF-15	10-50 ng/mL		<sup>70</sup>
<b>Decreased food intake</b>	Reduction of meal size and 24-h food intake reduction	Lean mice; Mice with diet-induced obesity; cynomolgus monkeys with spontaneous obesity	.	human or murine GDF-15 single	BioDAQ food-intake monitoring system	.	Self-purified	0,75 – 12 nmol/kg, 8 nmol/kg, 3 nmol/kg and 10 nmol/kg			<sup>83</sup>
<b>Reduction of body weight</b>	For 6 to 28 d	Lean mice; Mice with diet-induced obesity; cynomolgus monkeys with spontaneous obesity	.	human or murine GDF-15	Weight	Obesity	Self-purified	8 nmol/kg, 3 nmol/kg and 10 nmol/kg			<sup>83</sup>
<b>Improvement of glucose homeostasis</b>	Decreased glucose, For 13 d	blood OGTT	Mice under a normal chow diet	.	i.p every other d	Blood glucose, OGTT	.	Fc-GDF-15	0.1 mg/kg i.p		<sup>84</sup>
	Decreased glucose, For 13 d	blood OGTT	Mice on a high-fat diet for 16 weeks	.	i.p once every 3 d	Blood glucose, OGTT	Obesity	Fc-GDF-15	0.1 mg/kg i.p		<sup>84</sup>

	Reduced plasma leptin and insulin	Mice on a high-fat diet for 16 weeks	.	s.c daily	Blood leptin and insulin	Obesity	Saccharomyces cerevisiae-derived GDF-15	8 nmol in 4 ml/kg	<sup>85</sup>
<b>Increased angiogenesis</b>	Increased VEGFA expression	Human	U373 (glioblastoma cells), HBMV EC	3 d in culture	Tube formation assay, RT-PCR	Glioblastoma	CHO-derived GDF-15	100 ng/mL	<sup>98</sup>

CFSE: carboxyfluorescein succinimidyl ester; CHO: chinese hamster ovary; HBMVEC: human brain microvascular endothelial cells; MTT: (3-(4, 5-Dimethyl-2-thiazolyl)-2, 5-diphenyl-2H-tetrazolium bromide); OGTT: oral glucose tolerance test. See list of abbreviations

### 1.4.6 GDF-15 in pathology

The molecular mechanism and signaling pathway of GDF-15 have not been completely established. In general, GDF-15 is overexpressed in cellular stress states and its function seems to be protective. Several pathological conditions show elevated plasma GDF-15 levels, including metabolic, cardiovascular, hematological diseases and cancer, reaching concentrations up to one hundred times the physiological value (see Table 4)<sup>92</sup>.

**Table 4. GDF-15 serum levels in pathology**

Condition	Concentration (pg/mL)	Reference
<b><math>\alpha</math>-thalassemia syndrome</b>	5900 $\pm$ 1200	63
<b>Benign prostate hyperplasia</b>	731 $\pm$ 500	100
<b>Beta-thalassemia major</b>	66000 $\pm$ 9600	63
<b>Chronic pancreatitis</b>	2368 $\pm$ 2431	101
<b>Colorectal carcinoma</b>	783 $\pm$ 491	102
<b>COVID-19 in ICU</b>	12400	103
<b>Endometrial cancer</b>	1077	104
<b>Exercise</b>	200 -1000	51
<b>Heart failure</b>	2705	105
<b>Hereditary hemochromatosis</b>	720 $\pm$ 50	63
<b>Mitochondrial myopathy</b>	2711 $\pm$ 2459	106
<b>Ovarian cancer</b>	96 - 1876	107
<b>Pancreatic cancer</b>	5388 $\pm$ 3720	101
<b>Pregnancy</b>	6300-15300	50
<b>Prostate cancer</b>	860 $\pm$ 850	100
<b>Renal cell carcinoma</b>	1100 $\pm$ 150	63
<b>Sepsis</b>	4900	67
<b>Sickle cell anemia</b>	880 $\pm$ 160	63
<b>Smoking</b>	1835	59
<b>Stable coronary heart disease</b>	915 - 1827	108
<b>Systemic sclerosis</b>	1367	59

The most studied role of GDF-15 is its anorexigenic effect, mediating weight loss through reduced energy intake, an effect that is directly a consequence of GDF-15-GFRAL binding<sup>90</sup>. Its circulating levels have been consistently found elevated in obesity and its supplementation improves the metabolic profile in high-fat diet-induced obese mice, showing a significant reduction in body weight, food intake and glycemia. These effects may be a result of taste aversion rather than reduced energy expenditure or gastric motility<sup>109, 110</sup>. This anorexic effect is effectively abolished by blocking with a

monoclonal antibody directed against GDF-15 and by GDF-15 or GFRAL knock-out<sup>85, 109</sup>.

High GDF-15 levels are also found in the context of impaired glucose tolerance, insulin resistance, diabetes, and diabetes-related complications, but its role in glucose homeostasis is unclear. Other references provide a detailed review of this matter<sup>111, 112</sup>.

GDF-15 has also been proposed as a biomarker for elevated mortality risk and recurrent myocardial infarction (MI) after acute coronary syndrome and in heart failure, a common complication in patients with coronary heart disease<sup>108, 113</sup>. Indeed, GDF-15 positively correlates to cardiovascular mortality and all-cause mortality<sup>114</sup>. Kempf et al. also showed that mice deficient in GDF-15 have higher mortality after induced MI. They found that GDF-15 deficient mice display an increased recruitment of polymorphonuclear leukocytes, monocytes and macrophages in the myocardial tissue as compared to controls. Additionally, this recruitment was reduced upon treatment with rGDF-15, which decreased leukocyte adhesion, arrest and transmigration on the endothelium<sup>115</sup>. These data show that GDF-15 elevated levels after MI may exert a protective function by decreasing immune cell recruitment and, thereby, MI complications, such as cardiac remodeling and heart failure.

GDF-15 has also been associated with fibrotic diseases. Govaere et al found that hepatic tissue GDF-15 expression positively correlates to fibrosis progression in non-alcoholic fatty liver disease (NAFLD)<sup>116</sup>. Also, GDF-15 deficient mice expressed a NAFLD-like phenotype, which resolves with rGDF-15 treatment<sup>73</sup>. This effect may be a result of decreased M1 polarization and reduced pro-inflammatory cytokine expression within the liver<sup>117</sup>.

Serum GDF-15 levels have been found to be elevated in sepsis, regardless of the pathogen involved, and have been correlated with prognosis, severity, and survival<sup>67, 118-120</sup>. Li et al. assessed the diagnostic value of GDF-15 in sepsis, highlighting its role as a biomarker of sepsis severity, including septic shock. They found that GDF-15 positively correlates with procalcitonin, IL-6 and IL-10<sup>67</sup>. Santos et al. showed that GDF-15 knockout mice were protected against cecal ligation and puncture-induced sepsis, showing fewer severity symptoms, lower markers of inflammation and lower bacterial load<sup>120</sup>. Several other studies have proposed GDF-15 as a protector rather than a detractor in sepsis<sup>52, 121</sup>. Luan et al, showed that the increase in GDF-15 during bacterial inflammation stimulates beta-adrenergic sympathetic outflow and increases

hepatic triglyceride production, mediating cardiac protection, improving thermal homeostasis and promoting survival, which was shown to provide tolerance to inflammation<sup>121</sup>. Supporting this mechanism, Kim et al found elevated catecholamine-synthesis related gene expression and an increased thermogenesis in mice overexpressing GDF-15<sup>61</sup>. Recently, Wang et al. also proved that GDF-15 treated mice showed increased skeletal muscle noradrenaline and oxygen consumption, which is associated with an increased maintenance of energy expenditure<sup>122</sup>.

Elevated levels of GDF-15 have been observed in several hematologic disorders, including thalassemia, hemochromatosis, and refractory anemia with ring sideroblasts. The highest plasmatic levels of GDF-15 are reported in these conditions, reaching 66000 pg/mL beta-thalassemia major (see Table 4).

GDF-15 has been recognized as a potential diagnostic and prognostic biomarker for several gastrointestinal tumors including pancreas, colon, esophagus, hepatocellular and gastric carcinomas<sup>123</sup>. Additionally, other cancers such as glioblastoma, breast, lung, cervical, ovarian, endometrial, prostate, renal, urothelial, thyroid and melanoma have also shown elevated levels of GDF-15<sup>46, 124-126</sup>. As in the case of TGF- $\beta$ , the experimental results reveal a dualistic function of GDF-15 in the process of carcinogenesis. It shows an inhibitory effect on tumor growth in the early stages and subsequently facilitates progression and metastasis in the advanced stages<sup>127</sup>. However, different results have been documented in different cancer types and stages. For example, GDF-15 promotes cell proliferation through the activation of downstream factors such as AKT and ERK, while acting as an inhibitor of cell proliferation through SMAD2/3 activation<sup>126</sup>.

### 1.5 Aims and specific objectives

Although much has been investigated regarding the production of GDF-15 by macrophages and other cell types, less is known about the specific effect of GDF-15 in the macrophage system. The aim of the thesis project was to analyze the transcriptomic effects of rGDF-15 on primary human macrophages.

Specific aims:

1. To develop a model system to study the effect of rGDF-15 on macrophages, including dosing and incubation time

2. To identify the effects of rGDF-15 on pro-inflammatory cytokine expression in macrophages exposed to LPS
3. To analyze the changes induced by rGDF-15 alone and by rGDF-15 along with LPS in the transcriptional program from macrophages using Total-RNA-Sequencing (RNA-Seq), and to validate selected differentially expressed genes using RT-PCR
4. To analyze the implications of expression levels of GDF-15 in most relevant cancers
5. To assess the implications of expression changes in GDF-15-induced validated genes and its scavenger receptor stabilin-1 in kidney renal clear cell carcinoma (KIRC)



## 2 MATERIALS AND METHODS

### 2.1 Equipment

**Table 5. Equipment**

<b>Equipment</b>	<b>Company</b>
Accu-Chek Aviva	Roche
Balance	Kern
CasyTon Cell Counter	Schärfe Sytem – OLS
Cell culture incubator - Heracell™ 150	Thermo Fisher Scientific
Centrifuge ROTINA 420R	Hettich
Centrifuge 5415 C	Eppendorf
Centrifuge 5415 R	Eppendorf
Centrifuge 5804 R	Eppendorf
Cytospin 4	Thermo Scientific
Cytofunnel chamber	Thermo Scientific
Deep freezer (-80°C)	Thermo Fisher Scientific
Freezer (-20°C)	Liebherr
Fridge (4°C)	Liebherr
HydroFlex™ microplate washer	TECAN
Ice machine AF100	Scotsman
Laminar flow hood HERA safe	Thermo Fisher Scientific
Light sheet Microscope TCS SP8 DLS Leica inverted Microscope DMI9 CS Bino DLS	Leica Microsystems
MACS MultiStand	Miltenyi
Micropipettes Set (10ul, 20ul, 100ul and 1000ul)	Eppendorf
Microscope Axiovert 40 C	ZEISS
Millipore Milli-Q	Merck
Mini-plate centrifuge NG040	NIPPON GENETICS EUROPE
Multichannel pipet (10 raw)	Brand
Orbital Shaker DOS-10L	neoLab
Real-time PCR-device LighCycler 96	Roche
Rotator TRM 50	IDL
Staining dish	Neolab
Staining rack	Neolab
Tecan Infinite M200	TECAN
Thermomixer C	Eppendorf

Vacusaft <sup>TM</sup> Comfort	Integra Biosciences
Vortex Mixer Modell Vortex-Genie®	Scientific Industries

## 2.2 Chemicals and reagents

**Table 6. Chemicals and reagents**

<b>Chemicals and reagents</b>	<b>Company</b>
10x Earle´s balanced salt solution	Sigma
22x22 mm coverslips	Mariefeld
24x60mm coverslips	Mariefeld
acLDL–Alexa Fluor 488	Invitrogen
Aluminum foil	Roth
Bovine Serum Albumin (BSA)	Sigma Aldrich
CD14 MicroBeads	Miltenyi Biotec
CasyTON solution	OLS
D-(+)-Glucose solution 100 g/L	SIGMA
Dako Pen	DakoCytomation, Hamburg, Germany
DakoCytomation Fluorescent Mounting Medium	DakoCytomation, Hamburg, Germany
DEPC Water	Thermo Fisher Scientific
Dexamethasone-Water Soluble	Sigma Aldrich, #D2915
Dulbecco´s Phosphate Buffered Saline (DPBS)	Gibco
Ethanol	Roth
FcR Blocking Reagent, human	Miltenyi Biotec
Ficoll	GE Healthcare
LPS	Sigma Aldrich
MEM medium (Minimum essential medium Eagle)	Sigma
Nuclease free water	Omega Bio-tek
Paraformaldehyde (PFA)	Sigma-Aldrich
Percoll	GE Healthcare
Recombinant Human GDF-15/MIC-1 #120-28C	Peprtech
Recombinant Human IFN-γ # 300-02	Peprtech
Recombinant Human IL-4 # 200-04	Peprtech
Recombinant Human M-CSF #A300-25	Peprtech
Serum-free medium (SFM)	Gibco

Substrate reagent	R&D systems
Sulfuric acid (2N H <sub>2</sub> SO <sub>4</sub> )	Roth
Titanium nanoparticles	NanoAmor Europe
Triton X-100	Thermo Fisher Scientific
TGS (Tris/Glycine/SDS) buffer	Bio-Rad
Tween 20	Sigma Aldrich

## 2.3 Consumables

**Table 7. Consumables**

<b>Consumables</b>	<b>Company</b>
22 µm filter	Fisherbrand
CASY cups	Omni Life Sciences
Cell culture flasks	Greiner Bio-One
Cell culture 6- and 12-well plates	Thermofisher
Cell scrapes 25 cm	Roth
Disposable hypodermic needle	Braun
Elisa plate sealers	R&D systems
Elisa Plates	R&D systems
Falcon tubes (15ml, 50ml)	Cellstar Greiner Bio-One
Filter card (Cytospin)	Thermo Fisher
Inject syringe	Braun
LS columns	Miltenyi Biotec
Parafilm	American National Can
Pipettes tips (10/20µL, 200µL, 1000µL)	Eppendorf
qPCR plates	Axon Labortechnik
qPCR plate sealers	Axon Labortechnik
Safe-Lock Eppendorf Tubes, 1.5 ml	Eppendorf
Scalpel	Feather
Serological pipettes	Star Labs
Sterile pipette tips	Star Labs, Nerbeplus
Transfer pipettes	SARSTEDT

## 2.4 Kits

**Table 8. Kits**

<b>Kits</b>	<b>Company</b>
DuoSet® ELISA Human GDF-15 CAT #	R&D Systems

DY957	
E.Z.N.A. Total RNA kit I	Omega Bio-tek
MACS manual cell separator	Miltenyi Biotec
RNeasy mini kit	Qiagen
SensiFAST cDNA Synthesis Kit	BIOLINE
SensiMix II Probe Kit	BIOLINE

## 2.5 Buffers and solutions

**Table 9. Buffers and solutions**

Wash buffer for ELISA	500 µl of Tween 20 was pipetted into 1 L of PBS. The beaker was stirred on a magnetic stirrer for 30 min and the solution was stored at RT
MACS buffer	500 ml of PBS, 2,5 g of BSA and 2 ml of 0,5M EDTA
Solution for blocking (3% BSA)	50 ml of PBS and 1,5 g BSA

## 2.6 Cellular techniques

### 2.6.1 Monocyte isolation

Buffy coats were obtained from healthy blood donors out of the German Red Cross Blood Service Baden-Württemberg – Hessen after informed consent. The following procedure was carried out under sterile conditions under a hood (HERA safe from Thermo Scientific) and exemplifies the protocol per each donor:

- 1 First gradient: One 50 mL falcon tube was filled with 15 mL Ficoll (GE Healthcare) at RT.
- 2 The protective bag of the buffy coat was opened with a sterile scalpel and a T-75 cell culture flask was filled with the blood (~ 30 mL per donor). The blood was diluted 1:1 with sterile DPBS (Dulbecco's Phosphate Buffered Saline from Gibco) and mixed by rotating.
- 3 25 mL of the cell suspension was slowly added to the Ficoll without mixing.
- 4 The falcon tube was centrifuged for 30 minutes at 420 rcf and 20°C without brake.
- 5 The second layer (white ring portion) was collected, which corresponds to peripheral blood mononuclear cells (PBMCs), with a sterile plastic Pasteur pipet and pipetted into a fresh 50 mL falcon tube. The resting portion was discarded. The falcon tube was filled with DPBS up to 50 mL.
- 6 The tube was centrifuged for 10 minutes at 420 rcf and 20°C with brake.

- 7 The supernatant was collected (~ 45 mL) into a new 50 mL falcon tube and the pellet was resuspended with 5 mL of DPBS.
- 8 The tubes containing the supernatants and the resuspended pellets were centrifuged for 10 minutes at 420 rcf and 20°C with brake.
- 9 The supernatant (~ 45 mL) was discarded and the pellet from all the tubes was resuspended with 3 mL of DPBS and combined.
- 10 Second gradient: Percoll gradient solution was prepared by mixing 13,5 mL Percoll (GE Healthcare), 15 mL MEM medium (Minimum essential medium Eagle from Sigma) and 1,5 mL 10x Earle's balanced salt solution (Sigma) for a final volume of 30 mL in a 50 mL falcon tube. The resuspended pellets were slowly added to the Percoll solution without mixing them for further purification of PBMCs.
- 11 The falcon tube was centrifuged for 30 minutes at 420 rcf and 20°C without brake.
- 12 The white ring portion was collected with a sterile plastic Pasteur pipet and pipetted into a fresh 50 mL falcon tube. The resting portion was discarded. The falcon tube was filled with DPBS up to 50 mL.
- 13 Centrifugation was done for 10 minutes at 420 rcf and 20°C with brake.
- 14 The supernatant was aspirated and discarded. The pellet was resuspended in 2 mL of PBS. The content was transferred into a 15 mL falcon tube and filled till 10 mL.
- 15 Pre-count step: 10 µL aliquot was taken for cell counting from the 10 mL suspension and mixed with 10 mL of CasyTon (from OLS) solution. The CasyTon Cell Counter (Schärfe System – OLS) was used for quantification. The cell count was considered for calculations, as follows:  
$$\text{MACS } (\mu\text{L}) = (\text{Cell Count} \times 10) \times 95$$
$$\text{MicroBeads } (\mu\text{L}) = (\text{Cell Count} \times 10) \times 7,5$$
- 16 Centrifugation of the 15 mL falcon tube was done for 10 minutes at 420 rcf and 20°C with brake.
- 17 The supernatant was aspirated and discarded. The cell pellet was resuspended in 95 µL of MACS buffer (0.5% BSA, 2 mM EDTA dissolved in DPBS) + 5 µL CD14 MACs MicroBeads (Miltenyi Biotec) per  $10^7$  cells.
- 18 The mixture was incubated for 20 minutes on a rotator at 4°C.
- 19 The sample was filled to 10 mL with MACS buffer.

- 20 Centrifugation was done for 10 minutes at 420 rcf and 20°C with brake.
- 21 The cell pellet was resuspended in 1000 µL of MACS buffer.
- 22 Monocyte CD14 magnetic positive selection: One LS column (MACS® Column Technology) was placed in the magnetic separation unit (Miltenyi Biotec) and washed with 3 mL MACS buffer. The cell pellet suspension was applied to the column.
- 23 The column was washed with 3 mL of MACS buffer and the flow-through was collected in a fresh 15 mL falcon tube. This wash step was repeated twice.
- 24 The LS column was removed from the magnetic separation unit and placed into a fresh 15 mL falcon tube. 5 mL MACS buffer were added and the flow-through was collected. The liquid was pressed through the column with a piston. Additional 5 mL were added for a final volume of 10 mL.
- 25 Final count step: 10 µL aliquot were taken for cell counting and mixed with 10 mL of CasyTon solution.
- 26 Centrifugation of the sample was done for 10 minutes at 420 rcf and 20°C with brake.
- 27 The supernatant was aspirated and discarded.
- 28 The cell pellet was resuspended with SFM (serum-free medium from Gibco) supplemented with 5 mM glucose at a concentration of  $1 \times 10^6$  cells/mL, following the final count measurement in the CasyTon. Glucose concentration was controlled by Accu-Chek glucose monitor.
- 29 The cells were seeded into cell culture dishes. Different stimulation factors were added according to the Macrophage stimulation model.
- 30 5 million monocytes were transferred to fresh tubes, 350 µL of TRK lysis (for E.Z.N.A. Total RNA kit I) or 350 µL of RLT lysis buffer (for RNeasy Mini Kit) were added and the tubes were frozen at -80°C freezer until further use.

#### 2.6.2 Macrophage stimulation model

Macrophages were differentiated in the presence of M-CSF at 5 ng/mL (Peprotech; #A300-25B) and Dex  $10^{-8}$  M (Sigma, #D2915). For M1 polarization IFN- $\gamma$  was used at the concentration of 100 ng/mL (Peprotech; # 300-02), and for M2 polarization, IL-4 was used at the concentration of 10 ng/mL (Peprotech; #200-04). No cytokines were added for M0 differentiation.

### 2.6.2.1 Stimulation with titanium nanoparticles

For immunofluorescence analysis, the model included the differential culturing in the presence or absence of titanium nanoparticles (TiNPs). TiNPs were purchased from NanoAmor Europe, France. The stock solution was initially diluted to 1:4 in DPBS, followed by another 10-fold dilution in 5 mM glucose SFM media to achieve the final dilution factor (1:4000). The TiNPs were added for a final concentration of 0,0100% (100ppm). The dilution was sterilized via UV-light for 1 hour.

The conditions were maintained for 6 days with 7,5% CO<sub>2</sub> at 37°C in the incubator (Hera cell 150 Thermo Scientific). A daily microscopic check-up was performed to evaluate the health status of the cells. The following table illustrates the stimulation model:

**Table 10. Stimulation model with TiNPs**

M0	IFN- $\gamma$ (M1)	IL-4 (M2)
M0 100ppm TiNPs	IFN- $\gamma$ (M1) 100ppm TiNPs	IL-4 (M2) 100ppm TiNPs

### 2.6.2.2 Stimulation with rGDF-15 and LPS

Monocytes were cultured in the presence or absence of rGDF15 (Peprotech) at different concentrations, according to the experimental design (Table 11). Three different incubation times were used. One of them was a 48 hour-incubation under cytokine stimulation in the presence or absence of rGDF15 (Model 1). Another incubation time was done under cytokine stimulation in the presence or absence of rGDF15 for 6 days (Model 2). Finally, model 3 included a 6-day incubation under cytokine stimulation, and 1 hour-treatment with or without rGDF-15 (Figure 4, Results). After this, the differentiated macrophages from the 3 incubation times were treated with LPS 100 ng/mL and further incubated for 6 hours.

**Table 11. Experimental design with rGDF-15 and LPS**

M0 $\pm$ LPS 100 ng/mL	M1 $\pm$ LPS 100 ng/mL	M2 $\pm$ LPS 100 ng/mL
M0 + rGDF-15 10 ng/mL $\pm$ LPS 100 ng/mL	M1 + rGDF-15 10 ng/mL $\pm$ LPS 100 ng/mL	M2 + rGDF-15 10 ng/mL $\pm$ LPS 100 ng/mL
M0 + rGDF-15 25 ng/mL $\pm$ LPS 100 ng/mL	M1 + rGDF-15 25 ng/mL $\pm$ LPS 100 ng/mL	M2 + rGDF-15 25 ng/mL $\pm$ LPS 100 ng/mL
M0 + rGDF-15 50 ng/mL $\pm$ LPS 100 ng/mL	M1 + rGDF-15 50 ng/mL $\pm$ LPS 100 ng/mL	M2 + rGDF-15 50 ng/mL $\pm$ LPS 100 ng/mL

M0 + rGDF-15 100 ng/mL ± LPS 100 ng/mL	M1 + rGDF-15 100 ng/mL ± LPS 100 ng/mL	M2 + rGDF-15 100 ng/mL ± LPS 100 ng/mL
---	---	---

### 2.6.3 Collection of conditioned medium

- 1 After respective stimulation, the conditioned medium was collected into 1,5 mL Eppendorf tubes and was centrifuged for 10 minutes at 2000 rpm at RT.
- 2 The supernatants were transferred to fresh tubes.
- 3 350 µL of TRK lysis (for E.Z.N.A. Total RNA kit I) or 350 µL of RLT lysis buffer (for RNeasy Mini Kit) was added to wells and the cells were harvested in ice.
- 4 The cell suspension was added and resuspended on the remaining the cell pellet from the centrifugation.
- 5 The samples were frozen at -80°C freezer until further use (see Protein techniques).

## 2.7 Molecular biology methods

### 2.7.1 RNA isolation

#### 2.7.1.1 RNA isolation using E.Z.N.A. Total RNA kit

E.Z.N.A. Total RNA kit I from Omega Bio-tek was used for RNA isolation for the samples in which TNF-α and IL-1β were assessed with RT-PCR.

- 1 An equal volume of 70% ethanol was added to the cell lysate previously mixed with TRK lysis (see Monocyte isolation) and the sample was mixed thoroughly by vortexing. The suspension was applied to a HiBind RNA spin column and placed into a 2 mL Eppendorf collection tube.
- 2 The column was centrifuged at 10000 rpm for 60 seconds at 4 °C. The flow-through was discarded and the tube was reused.
- 3 500 µL of RNA Wash Buffer I was added to the column and was centrifuged at 10000 rpm for 60 seconds at 4 °C.
- 4 The flow-through was discarded and the tube was reused.
- 5 500µL of RNA Wash Buffer II was added to the column and the column was centrifuged at 10000 rpm for 60 seconds at 4 °C. The flow-through was discarded and the tube was reused.
- 6 500µL of RNA Wash Buffer II was added to the column and the column was centrifuged at 10000 rpm for 60 seconds at 4 °C. The collection tube was discarded and replaced with a new one.
- 7 The column was centrifuged at maximum speed at 4 °C for 2 minutes.



- 8 The column was transferred into a new 1,5mL RNase-free Eppendorf tube. 40µL of Nuclease-free water were added to the column and left to incubate for 1 minute at RT. The RNA was eluted by centrifuging at maximum speed for 1 minute at 4 °C.
- 9 The concentration of isolated RNA was determined by spectrophotometry TECAN (Tecan Infinite® 200). Samples with RNA concentrations of lower than 10 ng/µL or with RNA/DNA ratios of lower than 1,8 were discarded. Isolated samples were stored at -80°C until use.

#### 2.7.1.2 RNA isolation using RNeasy Mini Kit

RNeasy Mini Kit from Qiagen was used for the samples in which RNA-Seq was performed.

- 1 An equal volume of 70% ethanol was added to the cell lysate previously mixed with TRK lysis (see Monocyte isolation) and the sample was mixed thoroughly by vortexing.
- 2 The suspension was applied to an RNeasy mini column, placed in a 2 mL collection tube and centrifuged at 10000 rpm for 15 seconds.
- 3 The flow-through was discarded, the column was reused and 700 µL of RW1 buffer were added to the column and centrifuged at 10000 rpm for 15 seconds.
- 4 The flow-through was discarded, the column was reused and was washed with 500 µL of RPE buffer followed by a 15 seconds centrifugation at 10000 rpm.
- 5 The flow-through was discarded, the column was reused and was washed with 500 µL of RPE buffer followed by a 2 minute-centrifugation at 10000 rpm.
- 6 The column was placed in a new collection tube and was centrifuged at maximum speed for 2 minutes.
- 7 The columns were placed in a fresh 1,5 RNase-free Eppendorf tube, 35 µL of Nuclease-free water was added directly to the column membrane, followed by a 1 minute-centrifugation at 10000 rpm for RNA elution.
- 8 The concentration of isolated RNA was determined by spectrophotometry TECAN (Tecan Infinite® 200). Isolated samples were stored at -80°C until use.

#### 2.7.2 cDNA synthesis

cDNA was synthesized using the SensiFAST cDNA Synthesis Kit from Bioline according to the manufacturer's instructions.

- 1 The master mix was prepared on ice including 4  $\mu$ L of 5x TransAmp Buffer and 1  $\mu$ L of Reverse Transcriptase per tube. The amount of RNA was calculated according to the concentration and filled with DNase/RNase-free water up to 20  $\mu$ L per tube. All the components were mixed in a single tube.
- 2 The tubes went through the following heating cycles for primer annealing and transcription:
  - 25 °C for 10 min (primer annealing)
  - 42 °C for 15 min (reverse transcription)
  - 85 °C for 5 min (inactivation)
- 3 cDNA sample was diluted 10 times with DNase/RNase free-water and stored at -20 °C until use.

### 2.7.3 Real-time polymerase chain reaction (RT-PCR)

Diluted cDNA was amplified using RT-PCR. 18S was used as an endogenous control. Duplicates were performed per each sample. Water was used for negative control. TaqMan primer mix from Eurofins (Germany) for each gene was prepared according to Table 12. Primer sequences are shown from the 5' end to 3' end direction.

**Table 12. List of primers designed in the lab.** F: forward, R: reverse, Pr: probe. All primers and probes were ordered from Eurofins

Target Gene	Primer name	Sequence (5'-3' direction)
18srRNA	FP2242	CCATTGGAACGTCTGCCCTAT
	RP2242	TCACCCGTGGTCACCATG
	Pr2242	ACTTTCGATGGTAGTCGCCGTGCCT
ID3	FP1259	ACATGAACCACTGCTACTCC
	RP1259	AGGTCGAGAATGTAGTCGATG
	Pr1259	ACTCAGCTTAGCCAGGTGGAAATCCTACAGCG
IL-1beta	FP2150	ACAGATGAAGTGCTCCTTCCA
	RP2150	GTCGGAGATTCGTAGCTGGAT
	Pr2150	CTCTGCCCTCTGGATGGCGG
TNF- $\alpha$	F896	TCTTCTCGAACCCCGAGTGA
	F896	AGCTGCCCCTCAGCTTGA
	Pr896	AAGCCTGTAGCCCATGTTGTAGCAAACC

**Table 13. List of Taqman ready-made mixes.** All ready-made mixes were ordered from Thermo Fisher

Target Gene	Assay code
BCL2L14 (BCLG)	Hs00373302_m1
CCL15 (HCC-2, HMRP-2B, LKN-1, LKN1, MIP-1 delta, MIP-1D, MIP-5, MRP-2B, NCC-3, NCC3, SCYA15, SCYL3, SY15)	Hs01929667_s1
CLEC12A (CD371, CLL-1, CLL1, DCAL-2, MICL)	Hs00370621_m1
GAS7 (MLL/GAS7)	Hs00243470_m1
GDF-15 (GDF-15, MIC-1, MIC1, NAG-1, PDF, PLAB, PTGF-B)	Hs00171132_m1
IL17RB (CRL4, EVI27, IL17BR, IL17RH1)	Hs00218889_m1
KLF2 (LKLF)	Hs00360439_g1

PALD1 (KIAA1274, PALD)	Hs01012869_m1
PMEPA1 (STAG1, TMEPAI)	Hs00375306_m1
PROC (APC, PC, PROC1, THPH3, THPH4)	Hs00165584_m1
PTP4A3 (PRL-3, PRL-R, PRL3)	Hs02341135_m1
SERPINB2 (HsT1201, PAI, PAI-2, PAI2, PLANH2)	Hs01010736_m1
SMAD6 (AOVD2, HsT17432, MADH6, MADH7)	Hs00178579_m1

For the gene analysis, each well contained the following reagents:

**Table 14. Reaction set-up for RT-PCR**

Reagents	Per well
SensiMix II BIOLINE	5 $\mu$ L
Assay Primer Mix (Target Gene or Reference Gene)	0.5 $\mu$ l
H <sub>2</sub> O	3.5 $\mu$ L
cDNA or H <sub>2</sub> O for negative control	1 $\mu$ L
<b>Total</b>	<b>10 <math>\mu</math>L</b>

The experiment was performed as follows:

- 1 Two master mixes for duplicate were prepared without cDNA, one for each primer of interest, according to Tables 12 and 13, for the planned amount of reactions (~ 40 reactions). After that, each one was vortexed and spun down briefly.
- 2 The master mixes were distributed into 1.5 mL nuclease-free labeled Eppendorf tubes for each condition of interest (see Table 14).
- 3 2  $\mu$ L of cDNA were added into each tube, according to the labeling. Each one was vortexed and spun down briefly.
- 4 9.5  $\mu$ L of the solution was added to each RT-PCR plate well per duplicate. The plate was sealed and centrifuged for 1 minute.
- 5 Amplification was performed using a LightCycler 480 instrument owned by the Institute of Transfusion Medicine and Immunology. The protocol for the RT-PCR was adapted from the host laboratory and the program was repeated for 50 cycles as follows:

**Table 15. RT-PCR program**

PCR program	Temperature	Time
Initial denaturation	95°C	3 minutes
Denature	95°C	10 seconds
Anneal and extension	60°C	30 seconds

One final cycle of cooling (35°C) finalized the RT-PCR program.

## 2.8 Protein analysis and immunology methods

### 2.8.1 Enzyme-linked Immunosorbent Assay (ELISA)

Serum concentration of GDF-15 from healthy controls was measured according to the recommendation of the manufacturer using ELISA Human GDF-15 from R&D Systems.

- 1 A 96-well plate was coated with Capture Antibody provided in the kit, previously diluted in PBS 1:180 without carrier protein. Each well was coated with 100  $\mu$ L, covered with a plastic strip and the plate was incubated overnight.
- 2 The next day the wells were washed 3 times with 200  $\mu$ L Wash Buffer (0.05% Tween® 20 in PBS pH: 7,2-7,4) using an automatic microplate washer (HydroFlex™ from TECAN) and incubated with 300  $\mu$ L Reagent Diluent (1% BSA/PBS pH: 7,2-7,4) for 1 hour for blocking.
- 3 After blocking, the 96-well plate was washed 3 times with 200  $\mu$ L Wash. 50  $\mu$ L of Reagent Diluent were added to each well for the sample wells and 100  $\mu$ L were added for the standard wells.
- 4 Additional 50  $\mu$ L of the supernatants for the sample wells. The standard was added according to the manufacturer's instructions and incubated for 2 hours.
- 5 After incubation, the plate was washed 3 times with Wash Buffer, as described above.
- 6 100  $\mu$ L of detection antibody (1:180) was added according to the manufacturer's instructions and incubated for 2 hours.
- 7 100  $\mu$ L of working dilution from Streptavidin-HRP (1:200) were added to each well. The plate was covered and incubated for 20 minutes in dark conditions.
- 8 The plate was washed 3 times with Wash Buffer, as described above.
- 9 100 $\mu$ L Substrate Solution was added to each well. The plate was covered and incubated for 20 minutes in dark conditions.
- 10 50  $\mu$ L of Sulfuric acid (2N H<sub>2</sub>SO<sub>4</sub>) was added to stop the reaction and the plate was gently mixed to ensure thorough mixing.
- 11 The optical density was determined in a Tecan Infinite 200 at 450 nm, according to the manufacturer's instructions.
- 12 Concentration was calculated by regression analysis of a standard curve.

## 2.9 Preparation of cells for immunofluorescence

### 2.9.1 Endocytosis assay

- 1 M0, M1 and M2 macrophages were grown on coverslips and cultured for 6 days in the presence of 7,5% CO<sub>2</sub> at 37°C as described in Table 11.
- 2 At day 6, culture medium was removed, leaving minimum 200 µL per well (for a 24-well plate).
- 3 acLDL-Alexa488 was added at a final concentration of 5 µg/mL.
- 4 The cells were incubated in the presence of 7,5% CO<sub>2</sub> at 37°C for 30 minutes.
- 5 Cessation by immediate fixation with PFA, as described below, for M1, M1 and M2 treated with TiNPs, and for M1 non-treated with TiNPs.

### 2.9.2 Cytospin sample preparation

Since M1 and M2 non-treated with TiNPs were almost completely suspensional, sample preparation for these cells was performed using a Cytospin™ 4 centrifuge (Thermo Fisher Scientific), as follows:

- 1 The well content was transferred to fresh 1,5 mL Eppendorf tubes.
- 2 Centrifugation was done for 10 minutes at 2,0 rcf and RT.
- 3 The supernatant was discarded.
- 4 The cells were resuspended with 750 µL PBS.
- 5 Microscope slides were washed with 100% ethanol and attached to a filter card and a Cytofunnel.
- 6 100 µL of the cell dilution was added to each Cytofunnel chamber.
- 7 Centrifugation was done for 4 minutes at 700 rpm.
- 8 The chambers were disassembled and the microscope slides with the cellular monolayer were left to dry at RT.

### 2.9.3 Cell Fixation

Cells prepared with Cytospin were fixated at RT as follows:

- 1 The microscope slides were submerged in a tray containing 2% PFA for 10 minutes.
- 2 The tray was submerged in a 0,5% Triton X-100/1X PBS solution for 15 minutes.
- 3 The tray was submerged in 4% PFA for 10 minutes.
- 4 The tray was shortly washed with PBS.

- 5 The tray was submerged in PBS for 10 minutes under shaking. This step was repeated two times.
- 6 The microscope slides were left to dry under the laminar flow.
- 7 The slides were stored at -80°C until further use.

For M1, M1 and M2 treated with TiNPs and for M1 non-treated with TiNPs, fixation was done directly in the 24-well plates. The following steps were performed at RT.

- 1 1400 µL of supernatant were aspirated and discarded, resting 100 µL per well.
- 2 2 mL 2% PFA per well were added and incubated for 10 minutes. The content was aspirated and discarded.
- 3 2 mL 0,5% Triton X-100/1X PBS followed by 15-minute incubation. The content was aspirated and discarded.
- 4 2 mL 4% PFA per well were added and incubated for 10 minutes. The content was aspirated and discarded.
- 5 The wells were washed with PBS for 10 minutes under shaking. This step was repeated 3 times.
- 6 The content was aspirated and 2 mL PBS were added to each well.
- 7 The plates were sealed and stored under 4 °C until further use.

#### 2.9.4 Immunofluorescence staining

The following steps describe the immunofluorescence staining for the samples prepared with Cytospin and were done at RT. From step 7 on, the experiment was performed under dark conditions.

- 1 The microscope slides were taken out of -80 °C and left to dry.
- 2 The cell monolayer was encircled using a Dako Pen and was left to dry for 1 minute.
- 3 The microscope slides were submerged in a tray containing PBS for 5 minutes under shaking. This step was repeated once.
- 4 The tray was submerged in a 0,1% Tween® 20 in 1xPBS solution for 30 seconds.
- 5 100 µL of 3% BSA was added to each monolayer and left to incubate for 1 hour in a humidity chamber.
- 6 The antibodies used are shown in Tables 16 and 17.
- 7 The primary antibodies were diluted accordingly in 1% BSA.
- 8 100 µL of the dilution was applied to the cell monolayer and incubated for 1,5 hours.

- 9 After incubation, the slides were washed three times with 1xPBS for 5 minutes under shaking.
- 10 An additional wash with 0,1% Tween® 20 in PBS was done for 30 seconds.
- 11 The secondary antibodies and nuclear staining were diluted accordingly in 1% BSA.
- 12 100 µL of the dilution was applied to the cell monolayer and incubated for 45 minutes.
- 13 The slides were washed four times with 1xPBS for 5 minutes under shaking.
- 14 One drop of Dako fluorescent mounting media was pipetted onto the cell monolayer and was covered with cover slips.
- 15 The slides were stored at 4°C until further use.

For the cells grown on glass coverslips, the following staining steps were performed under RT. Upon step 6, the experiment was performed under dark conditions.

- 1 The plates were taken out of 4°C.
- 2 The content of the 24 well-plate was aspirated and the wells were washed with 2 mL of 0,1% Tween® 20 in 1xPBS for 30 seconds.
- 3 The content was aspirated and 1 mL of 3% BSA was added to each well, followed by a 1-hour incubation.
- 4 The wells were washed with 2 mL of 0,1% Tween® 20 in 1xPBS for 30 seconds.
- 5 The antibodies used are shown in Tables 16 and 11.
- 6 The primary antibodies were diluted accordingly in 1% BSA.
- 7 100 µL of the dilution was applied to each cover slip and incubated for 1,5 hours.
- 8 After incubation, the wells were washed three times with 1 mL of 1xPBS for 5 minutes under shaking.
- 9 An additional wash with 1 mL of 0,1% Tween® 20 in PBS was done for 30 seconds.
- 10 The secondary antibodies and nuclear staining were diluted accordingly in 1% BSA.
- 11 100 µL of the dilution was applied to each well and incubated for 45 minutes.
- 12 The wells were washed four times with 1xPBS for 5 minutes under shaking.
- 13 Microscope slides were labeled and washed with 100% ethanol and left to dry.
- 14 One drop of Dako fluorescent mounting media was pipetted onto the microscope slides.

15 The glass coverslips from the wells were transferred with a scalpel and small tweezers and mounted upside down on the microscope slide. The slides were covered with coverslips.

16 The slides were stored at 4°C until further use.

**Table 16. Primary antibodies**

<b>Antibody</b>	<b>Concentration in stock</b>	<b>Dilution</b>	<b>Species</b>	<b>Company</b>
anti-hstabilin-1 polyclonal serum RS1		1:800	Rabbit	Self-produced (Politz et al., 2002)
monoclonal anti-EEA-1	250 µg/ml	1:500	Mouse	BD Biosciences
Preimmune Serum to N2RS1 isotype control		1:800	Rabbit	Self-produced (Politz et al., 2002)
Purified Mouse IgG1, κ Isotype Control	0,5 mg/mL	1:1000	Mouse	BD Pharmingen™

**Table 17. Secondary antibodies and labelling agents**

<b>Antibody/labelling agent</b>	<b>Dilution</b>	<b>Species</b>	<b>Company</b>
Cy3-conjugated anti-rabbit IgG	1:400	Donkey	Dianova
Alexa647-conjugated anti-mouse IgG	1:400	Donkey	Dianova
DAPI (nuclear staining)	1:1000	N/A	Roche

### 2.9.5 Confocal microscopy

Confocal microscopy was performed using a Leica laser scanning spectral confocal microscope, model DM IRE2, equipped with an HCX PL Apo 63 ×/1.32 numeric aperture oil objective (Leica Microsystems, Wetzlar, Germany) from the Live Cell Imaging Mannheim (LIMa). Excitation was achieved with an argon laser emitting at 488 nm, a krypton laser emitting at 568 nm, and a helium/neon laser emitting at 633 nm. Images were acquired using a TCS SP2 scanner and Leica Confocal software, version 2.5 (Leica Microsystems). Images were acquired using a sequential scan mode. For panel assembly, Adobe Photoshop version 6.0 (Adobe Systems, San Jose, CA) was used.



## 2.10 Human sample preparation

Blood samples were obtained from healthy plasma donors participating in the CORE (COVID-19 Reconvalescent) trial conducted at the German Red Cross Blood Service Baden-Württemberg – Hessen and the Institute of Transfusion Medicine and Immunology in Mannheim. The Medical Faculty of Mannheim's Ethical Committee approved the conduct of the study (Ref: 2020-643N). All donors provided the CORE trial written informed consent. The participants were included if they had no persistent serious organ dysfunction, no fever at the time of blood sampling, and were between 18 to 68 years old. The baseline characteristics of the participants were self-reported using an online questionnaire. Venous blood samples were collected into tubes and centrifuged at 3500 rpm for 15 minutes at 25°C. Plasma and serum were separated and stored at -80°C until analysis. ELISA Human GDF-15 from R&D Systems was used to measure the plasma concentration of GDF-15 in accordance with the manufacturer's instructions, as described above.

## 2.11 Transcriptomic analysis

Total RNA was extracted following the steps previously described for RNA isolation. The concentration of the purified samples was quantified using a NanoDrop® spectrometer, while the quality was assessed using agarose gel electrophoresis. Total RNA samples with a concentration exceeding 300 ng were selected for RNA-Seq. RNA-Seq was performed by the company Novogene (Cambridge, United Kingdom). Briefly, mRNA was purified using poly-T oligo-attached magnetic beads. The first strand of cDNA was synthesized with random hexamer primers, followed by the second strand of cDNA synthesis using dUTP. The double-stranded cDNA libraries were achieved using the SMARTTM PCR cDNA Synthesis Kit. Sequencing was performed on the Illumina HiScanSQ based on the mechanism SBS (sequencing by synthesis) platform. The raw data generated by the sequencer was provided in FASTQ format.

Because of failure during library preparation and uncertainty of RNA integrity, 2 of the 45 samples were discarded (M0121424 from the M0 + rGDF-15 + LPS group and M2121424 from the M2 + rGDF-15 + LPS group), leaving 43 samples for the sequencing (Table 18). The maximal acceptable error rate was 6%. All the samples had an error rate of a maximum of 3%. Additionally, to assess the potential of AT/GC separation, GC content distribution was evaluated. To avoid low-quality reads, a

filtering process was conducted on the raw sequencing data, which included removing reads containing adaptors, more than 10% uncertain nucleotides and those containing low-quality nucleotides.

**Table 18. List of the sequenced samples.** In red are the samples that failed the library preparation

Group Name	Sample ID	Group Name	Sample ID	Group Name	Sample ID
M0	M0121421	M2	M2121421	Monocytes	Mo12142
	M0121431		M2121431		Mo12143
	M0121441		M2121441		Mo12144
	M0121721		M2121721		Mo12172
	M0121731		M2121731		Mo12173
M0 + rGDF-15	M0121422	M2 + rGDF-15	M2121422		
	M0121432		M2121432		
	M0121442		M2121442		
	M0121722		M2121722		
	M0121732		M2121732		
M0 + LPS	M0121423	M2 + LPS	M2121423		
	M0121433		M2121433		
	M0121443		M2121443		
	M0121723		M2121723		
	M0121733		M2121733		
M0 + rGDF-15 + LPS	M0121424	M2 + rGDF-15 + LPS	M2121424		
	M0121434		M2121434		
	M0121444		M2121444		
	M0121724		M2121724		
	M0121734		M2121734		

Alignment of the sequences was performed by HISAT2. Mapped regions were classified in exon, intron or intergenic region. The most abundant reads were exons, which supported the high-quality mRNA isolation. Gene expression quantification was normalized to the sequencing depth and length of the genes (RPKM). The logarithm to base 2 of the quotients of the RPKM values was given as a log2 fold change. The p-value and padj (adjusted for multiple comparisons using the Benjamini-Hochberg procedure) indicate the probability of error.

#### 2.11.1 Correlation analysis and a principal component (PC) analysis

Correlation analysis and a PC analysis were performed using the normalized RNA-Seq data accounted for total reads sequenced for each sample, to examine the reproducibility of the samples and the grouping of the comparison groups. Data was provided by Novogene.

### 2.11.2 Differential gene expression (DEG) analysis

The DEG was analyzed using the DESeq2 R package and the normalized method DESeq. A gene was considered differentially expressed if it differed more than twice in expression between two sets of samples. To correct for false positive results, a padj was calculated. Among differentially expressed genes, relevant genes were selected if they had a  $|\log_2(\text{FoldChange})| \geq 1$  and a  $\text{padj} \leq 0.05$ . To visualize the output, volcano plots were generated using GraphPad Prism9.

### 2.11.3 Functional enrichment analysis

Functional enrichment analysis was used to categorize genes into relevant functional gene ontology (GO) terms to elucidate their biological roles and associations. To visualize the transcriptomic changes in the biological system, KEGG pathways were also analyzed. GO and KEGG analysis were performed using the clusterProfiler R package. Data was provided by Novogene.

### 2.12 In-silico analysis

The gene expression patterns of pan-cancer samples obtained from the TCGA database were evaluated utilizing Xena and Tumor Immune Estimation Resource 2.0 (TIMER 2.0) platforms. These platforms offer comprehensive bioinformatics analysis tools for RNA-Seq data and clinical information about various tumors encompassed in the TCGA database. The dataset comprises gene expression profiles derived from both cancerous and healthy tissue samples, along with details regarding tumor stages, subtypes, and other clinicopathological characteristics. The association between mRNA levels of CCL15, CLEC12A, GAS7, GDF15, ID3, IL17RB, PMEPA1, PTP4A3, SMAD6, and STAB1 and the clinical information specifically related to KIRC was investigated. Immune tumor infiltration was assessed using TIMER2.0 and CIBERSORT performing a partial Spearman's correlation adjusted by tumor purity.

### 2.13 Data analysis

The significance of the differential gene expression data was determined using the Wilcoxon matched-pairs rank test for non-normally distributed data or the Student's paired t-test for normally distributed data, according to the test for normal distribution (Shapiro-Wilk test). ANOVA Kruskal-Wallis test was used for multiple comparison analysis and an unpaired t-test was performed for the analysis of gene expression within tumor tissue and clinical correlates. The survival analysis was performed using

the Log-rank (Mantel-Cox) test. Simple linear regressions were performed for the clinical characteristics and GDF-15 plasmatic level association in healthy donors. All statistical analyses were generated using GraphPad Prism 9. The significance of the data of correlation was analyzed using the Spearman test for non-normal distribution. A two-tailed p-value of less than 0.05 was considered to indicate statistical significance (confidence level 95%). ns = non-significant,  $p < 0.05$ ,  $p \leq 0.05^{**}$ ,  $p \leq 0.01$ ,  $^{***}p \leq 0.001$  and  $^{****}p \leq 0.001$ . A p-value of  $<0.05$  was considered to be statistically significant.

### 3 RESULTS

#### 3.1 GDF-15 levels in cultured macrophages and in serum of healthy human population

To assess the levels of GDF-15 secreted by macrophages, the samples of conditioned medium from macrophages cultured for 6 days were collected. The experimental groups included non-stimulated M0 macrophages, as well as M1 macrophages differentiated under stimulation with IFN- $\gamma$ , and M2 macrophages differentiated under stimulation with IL-4. The GDF-15 concentration was assessed by ELISA. No statistical difference in GDF-15 levels was observed between the macrophage phenotypes (Figure 3).

To determine the physiological levels of GDF-15, peripheral blood was collected from a group of healthy plasma donors, ranging in age from 19 to 68 years. Subsequently, serum was isolated from the collected blood samples. Detailed information on the characteristics of the participants can be found in Supplementary Table 1. Quantification of GDF-15 in the serum samples was conducted using ELISA. Spearman analysis between plasma GDF-15 levels and age, as well as with erythrocyte count showed a significant positive correlation (Supplementary Figure 1). The mean serum GDF-15 concentration in healthy donors was 382,7 pg/mL (85,3-1830). Compared to the culture concentration, the serum concentration was significantly higher (for M0, M1 and M2 vs. serum  $p < 0,0001$ ) (Figure 3).

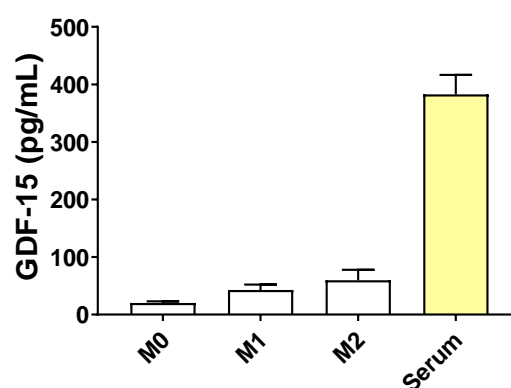


**Figure 3. GDF-15 levels** in cultured M0, M1 and M2 macrophages after 6 days (M0  $n=6$ , M1  $n=10$ , M2  $n=10$ ) and in serum from healthy donors ( $n=68$ ). Data are presented as mean  $\pm$  SEM.

### 3.2 Analysis of macrophage pro-inflammatory cytokine expression induced by rGDF-15 after LPS stimulation

To evaluate the effect of rGDF-15 on the inflammatory response of macrophages to LPS, macrophages were primed with varying concentrations of rGDF-15 at different time points, and were subsequently challenged with LPS, according to the experimental design (Table 19 and Figure 4). In all models, macrophages were harvested after 6 hours of LPS co-culture. RNA was then isolated and cDNA was synthesized. The relative expression of the pro-inflammatory cytokines TNF- $\alpha$  and IL-1 $\beta$  was measured by RT-PCR.

**Table 19.** Experimental design

M0 $\pm$ LPS 100 ng/mL	M1 $\pm$ LPS 100 ng/mL	M2 $\pm$ LPS 100 ng/mL
M0 + rGDF-15 10 ng/mL $\pm$ LPS 100 ng/mL	M1 + rGDF-15 10 ng/mL $\pm$ LPS 100 ng/mL	M2 + rGDF-15 10 ng/mL $\pm$ LPS 100 ng/mL
M0 + rGDF-15 25 ng/mL $\pm$ LPS 100 ng/mL	M1 + rGDF-15 25 ng/mL $\pm$ LPS 100 ng/mL	M2 + rGDF-15 25 ng/mL $\pm$ LPS 100 ng/mL
M0 + rGDF-15 50 ng/mL $\pm$ LPS 100 ng/mL	M1 + rGDF-15 50 ng/mL $\pm$ LPS 100 ng/mL	M2 + rGDF-15 50 ng/mL $\pm$ LPS 100 ng/mL
M0 + rGDF-15 100 ng/mL $\pm$ LPS 100 ng/mL	M1 + rGDF-15 100 ng/mL $\pm$ LPS 100 ng/mL	M2 + rGDF-15 100 ng/mL $\pm$ LPS 100 ng/mL

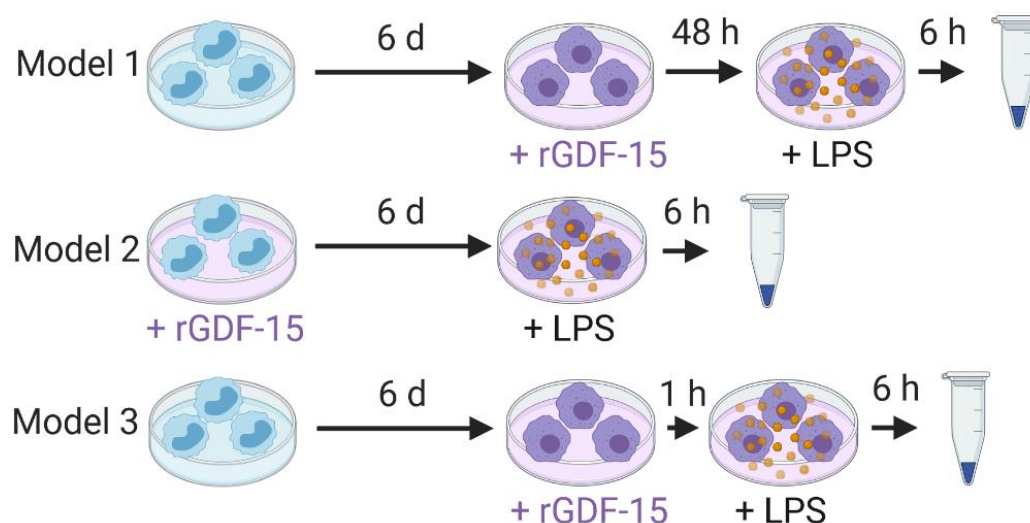


**Figure 4. Schematic representation of the different model systems.** After CD14 isolation, monocytes were differentiated into macrophages in culture medium for 6 days. In model 1, rGDF-15 was added on day 6 of incubation for 48 hours, followed by the LPS challenge for 6 hours. In model 2, rGDF-15 was added after monocyte isolation. LPS challenge was performed on day 6. In model 3, rGDF-15 was added for 1 hour on day 6 of incubation, followed by the LPS challenge for 6 hours. Created with Biorender.com.

#### 3.2.1 rGDF-15 priming for 48 hours suppresses TNF- $\alpha$ expression in response to LPS in macrophages

To investigate the influence of rGDF-15 priming on macrophages, model 1 was performed in which rGDF-15 treatment occurred 48 hours before the cells were challenged with LPS. The expression levels of TNF- $\alpha$  in macrophages from this

particular model are depicted in Figure 5. Macrophages treated with rGDF-15 alone showed no significant difference in TNF- $\alpha$  expression compared to control, regardless of rGDF-15 concentration. In contrast, LPS treatment significantly increased TNF- $\alpha$  expression in macrophages compared to those treated with rGDF-15 alone and control. Finally, TNF- $\alpha$  expression was significantly downregulated in M0 and M1 primed with high doses of rGDF-15 for 48 hours before the LPS challenge ( $p=0,0313$  for M0 and  $p=0,0156$  for M1). A similar trend was evident in M2 without reaching statistical significance. Although not statistically significant, a dose-response trend is evident, particularly in M0 and M1.

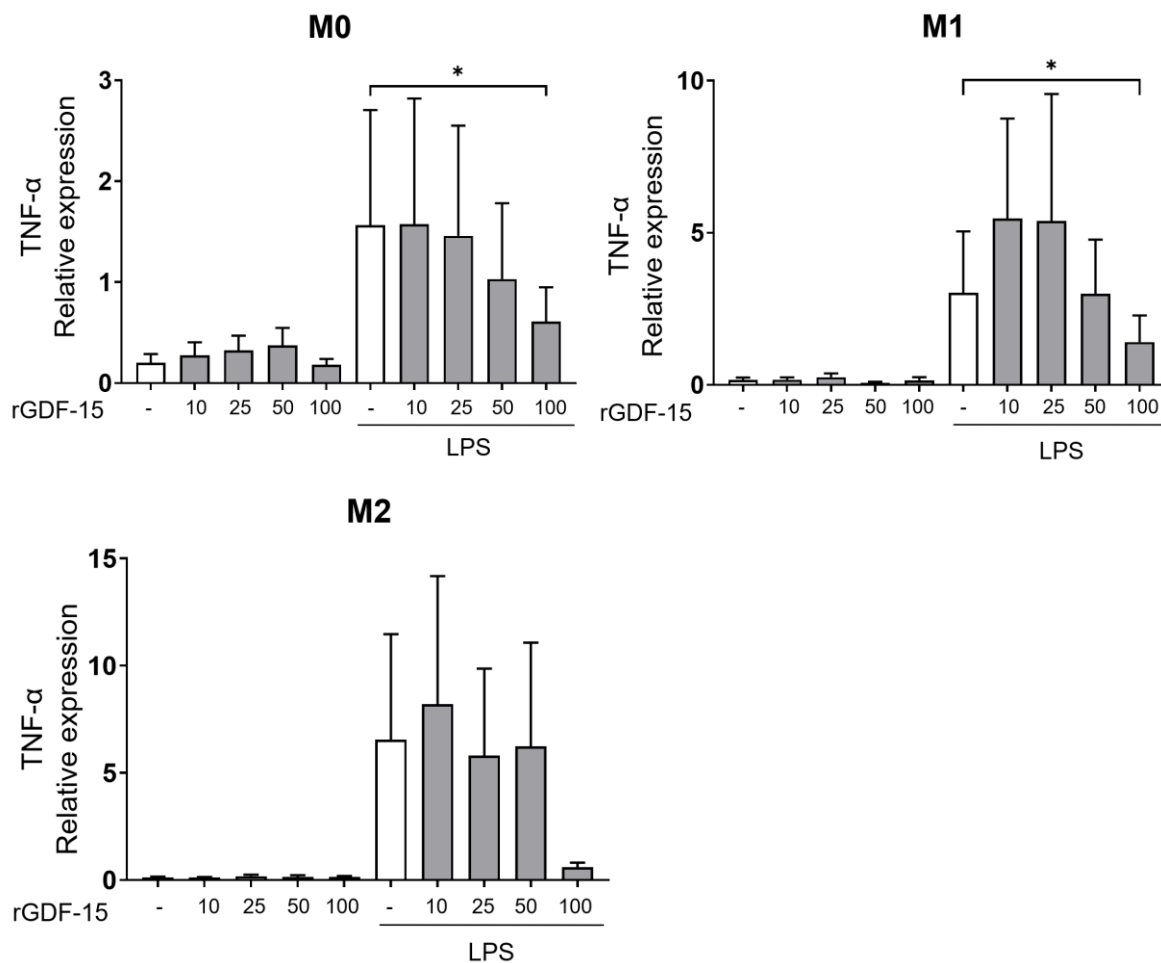


**Figure 5. Effect of rGDF-15 pretreatment for 48 hours on TNF- $\alpha$  expression in M0, M1 and M2 macrophages challenged with LPS.** mRNA expression was analyzed by RT-PCR in macrophages cultured for 6 days, primed with rGDF-15 at increasing concentrations (10, 25, 50 or 100 ng/mL) for 48 hours and challenged with LPS (100 ng/mL) for 6 hours.  $n=6$  for M0,  $n=4$  for rGDF15 10 ng/mL, 25, 50, 10 + LPS, 25 + LPS, 50 + LPS,  $n=7$  for 100, LPS and 100 + LPS,  $n=7$  for M1, rGDF15 100 ng/mL and LPS, 100 + LPS,  $n=4$  for 10, 25, 50, 10 + LPS, 25 + LPS, 50 + LPS,  $n=6$  for M2, rGDF15 100 ng/mL,  $n=4$  for 10, 25, 50, 10 + LPS, 25 + LPS, 50 + LPS,  $n=7$  for LPS,  $n=5$  for 100 + LPS. Data are presented as mean  $\pm$  SEM normalized to 18S rRNA expression levels. \* $p<0.05$ .

### 3.2.2 Macrophage co-differentiation with rGDF-15 suppresses TNF- $\alpha$ expression in response to LPS

The effect of rGDF-15 on the monocyte-to-macrophage differentiation was assessed in model 2, in which rGDF-15 was added after monocyte isolation for 6 days, followed by a 6-hour challenge with LPS. There was a decreasing trend in TNF- $\alpha$  expression in M0 and M1 macrophages with increasing concentrations of rGDF-15. However, this was not statistically significant. This trend was not observed in M2 (Figure 6).

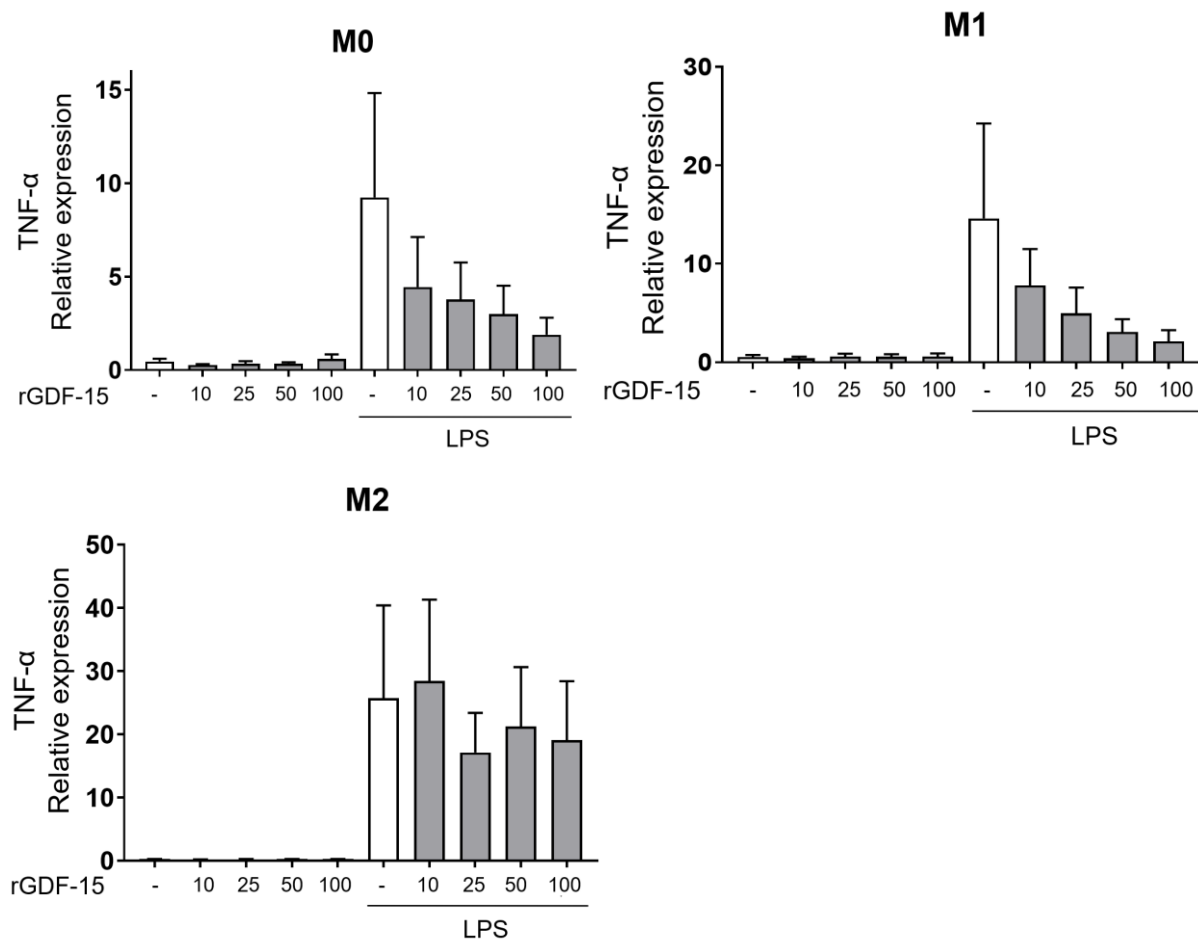


**Figure 6. Effect of rGDF-15 co-culture on the gene expression of TNF- $\alpha$  in M0, M1 and M2 macrophages challenged with LPS.** mRNA expression was analyzed by RT-PCR in macrophages cultured with rGDF-15 at increasing concentrations (10, 25, 50 or 100 ng/mL) for 6 days and challenged with LPS (100 ng/mL) for 6 hours. M0 n=4, M1 n=4, M2 n=4, n=2 for rGDF15 10 ng/mL + LPS, 50 + LPS and 100. Data are presented as mean  $\pm$  SEM normalized to 18SrRNA expression levels.

### 3.2.3 rGDF-15 priming for 1 hour suppresses TNF- $\alpha$ and IL-1 $\beta$ expression in response to LPS in macrophages

In order to assess the effect of shortened exposition time to GDF-15, rGDF-15 was added to the culture media for only 1 hour on day 6 in model 3. TNF- $\alpha$  expression was significantly reduced in response to LPS in M0 and M2 macrophages primed with



rGDF-15. A dose-dependent trend with increasing rGDF-15 concentration was observed in M2 (Figure 7).

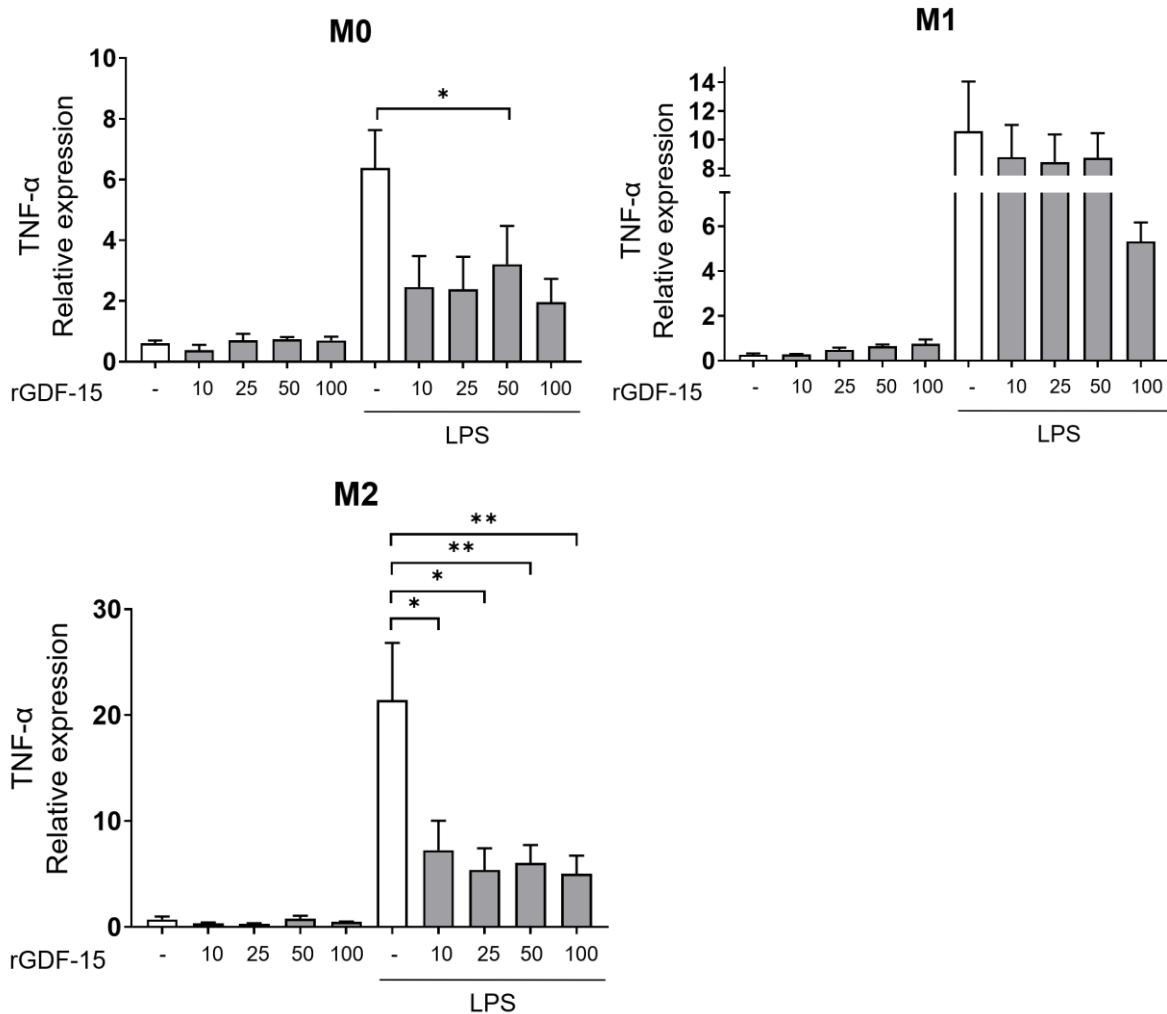


**Figure 7. Effect of rGDF-15 priming on the gene expression of TNF- $\alpha$  in M0, M1 and M2 macrophages challenged with LPS.** mRNA expression was analyzed by RT-PCR in macrophages cultured for 6 days, primed for 1 hour with rGDF-15 at increasing concentrations (10, 25, 50 or 100 ng/mL) and challenged with LPS (100 ng/mL) for 6 hours.  $n=9$  for M0, rGDF15 50 ng/mL, LPS and 50 + LPS.  $n=3$  for 10, 25, 100, 10 + LPS, 25 + LPS, 100 + LPS, M1  $n=4$ ,  $n=10$  for M2, 50, LPS and 50 + LPS.  $n=4$  for 10, 25, 100, 10 + LPS, 25 + LPS, 100 + LPS. Data are presented as mean  $\pm$  SEM normalized to 18SrRNA expression levels. \* $p<0.05$ , \*\* $p<0.01$ .

IL-1 $\beta$  expression was assessed in M0 and M2 macrophages primed with 50 ng/dL rGDF-15. A decrease in IL-1 $\beta$  expression was evident in macrophages treated with rGDF-15 and challenged with LPS compared to those challenged with LPS alone in both M0 and M2. In M0, an increased IL-1 $\beta$  expression was found in macrophages treated with rGDF-15 compared to control (Figure 8).

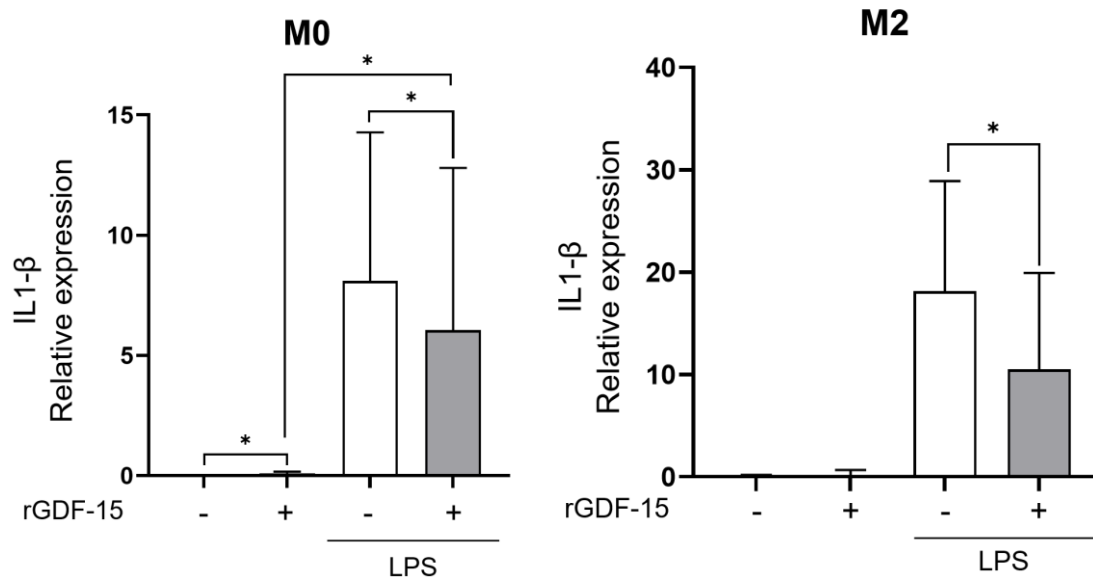


**Figure 8. Effect of rGDF-15 priming on IL-1 $\beta$  gene expression in M0 and M2 macrophages challenged with LPS.** mRNA expression was analyzed by RT-PCR in macrophages cultured for 6 days, primed with rGDF-15 50 ng/mL for 1 hour, and challenged with LPS (100 ng/mL) for 6 hours. M0 n=8, M2 n=7. Data are presented as mean  $\pm$  SEM normalized to 18S rRNA expression levels. \*p<0.05.

All three models successfully confirmed the well-established inhibitory effect of rGDF-15 on TNF- $\alpha$  expression. Nevertheless, model 3 was selected to advance with transcriptomic analysis via Total-RNA-Sequencing (RNA-Seq) because it demonstrated significant TNF- $\alpha$  suppression even at low doses of rGDF-15 and after a shortened exposure time. Furthermore, this model revealed a dose-dependent effect within M2 macrophages. In addition, RNA-Seq analysis was conducted specifically on M0 and M2 phenotypes, while M1 was excluded due to the lack of any observable significant effect on TNF- $\alpha$  expression following rGDF-15 treatment in model 3.

### 3.3 Transcriptomic analysis in macrophages primed with rGDF-15 and challenged with LPS

To analyze the effect of rGDF-15 priming on the global differential mRNA expression in macrophages challenged with LPS, RNA-Seq was performed. Total RNA was isolated from monocytes and from macrophages under cytokine stimulation to achieve M0 and M2 phenotypes for 6 days, according to the experimental design (Figure 4). On day 6, rGDF-15 was added to the culture media and incubated for 1 hour, followed by a 6 hours LPS challenge. Macrophages were immediately harvested and RNA was isolated for RNA-Seq. RNA quality was assessed by agarose gel electrophoresis. RNA-Seq was performed by Novogene (Cambridge, UK) using Illumina HiScanSQ based on the sequencing by synthesis (SBS) mechanism. RNA-Seq data consisted of

four to five replicates for 9 conditions. In total, the available RNA-Seq transcriptomes consisted of 43 samples, as shown in Methods (Table 18).

The transcriptomic analysis involved a number of key steps. First, correlation analysis and a principal component analysis were performed to examine the reproducibility of the samples and the grouping of the comparison groups. Next, DEG and Kyoto encyclopedia of genes and genomes (KEGG) analyses were performed to identify genes with significant changes in expression. Finally, functional enrichment analysis was used to categorize genes into relevant functional GO terms to elucidate their biological roles and associations.

### 3.3.1 Correlation analysis

In order to evaluate the reproducibility within samples, a Pearson correlation analysis was performed on the normalized RNA-Seq data to account for the total number of reads sequenced for each sample. Figure 9 illustrates the inter- and intragroup variability of macrophage and monocyte samples. Intergroup similarity is high within macrophage conditions, showing a  $R^2$  greater than 0.8, consistent with each group belonging to an activated phenotype. Monocytes from different donors show high intragroup similarity but lower intergroup similarity, which is also an expected result considering their undifferentiated state.

The two-dimensional PC plot (Figure 10) depicts the grouping of replicates within conditions and across samples. This plot shows all 43 samples along PC1 and PC2, which describe 33.09% and 24.09% of the variability within the expression data set, respectively. Conditions including LPS are grouped in the negative portion of the X- and Y-axis, regardless of macrophage phenotype or additional pretreatment with GDF-15, highlighting the strong effect of this treatment on the transcriptome. Conditions without LPS are grouped in the negative X-axis and positive Y-axis, supporting that although M0 and M2 are different macrophage phenotypes, they share most of their transcriptome and there is no major shift of it in the presence of rGDF-15.

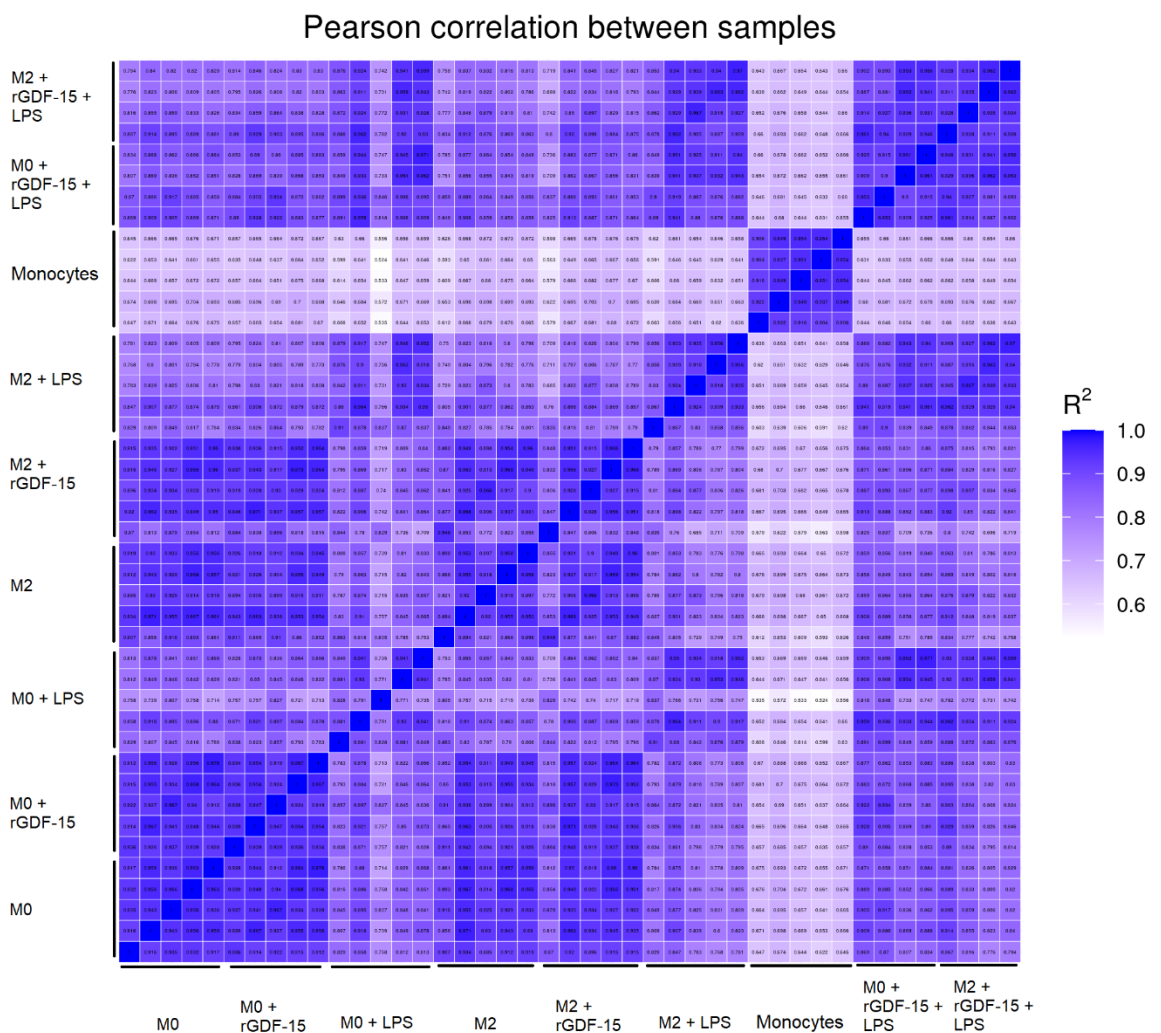


**Figure 9. Intersample correlation heat map.** Individual sample ID clarification is shown in Methods. R<sup>2</sup> indicates the square of the Pearson coefficient.

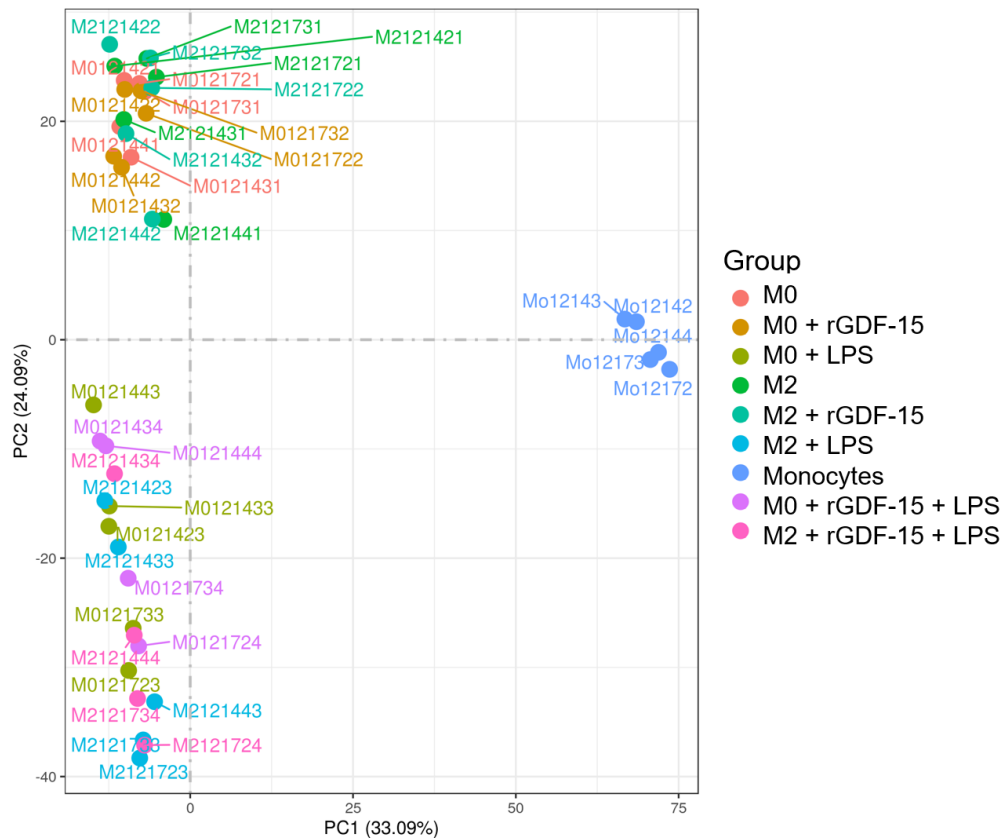


**Figure 10. PC analysis of biological replicates.** Percentages indicate the relative contribution of the 2 principal components (PC1–PC2). Clarification of individual sample IDs is provided in Methods.

### 3.3.2 Transcript quantification and DEG analysis

To elucidate the impact of rGDF-15 in activated macrophages, the following comparisons were made: M0 vs. M0 + rGDF-15 and M2 vs. M2 + rGDF-15. Furthermore, to evaluate the transcriptomic influence of rGDF-15 on macrophage response to LPS, the comparisons M0 + rGDF-15 + LPS vs. M0 + LPS and M2 + rGDF-15 + LPS vs. M2 + LPS were focused on (Figure 11). RNA-Seq overall count of differentially up- and/or downregulated DEGs for the selected comparisons of interest is shown in Table 20. The gene expression level threshold was 1 for FPKM. DESeq2  $p$ -value  $\leq 0.05$  and  $|\log_2\text{FoldChange}| \geq 0.0$  were selected as screening criteria. The numbers of differentially expressed genes in the resting comparisons is shown in Supplementary Figure 2.

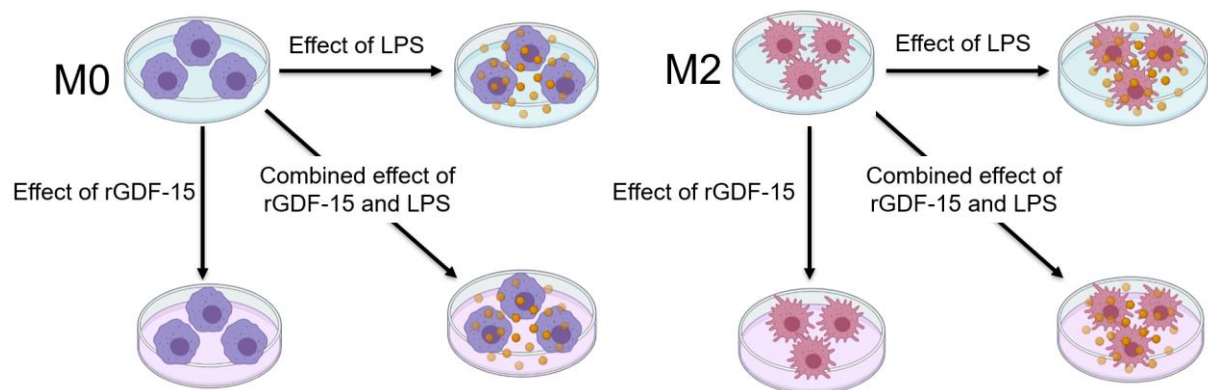
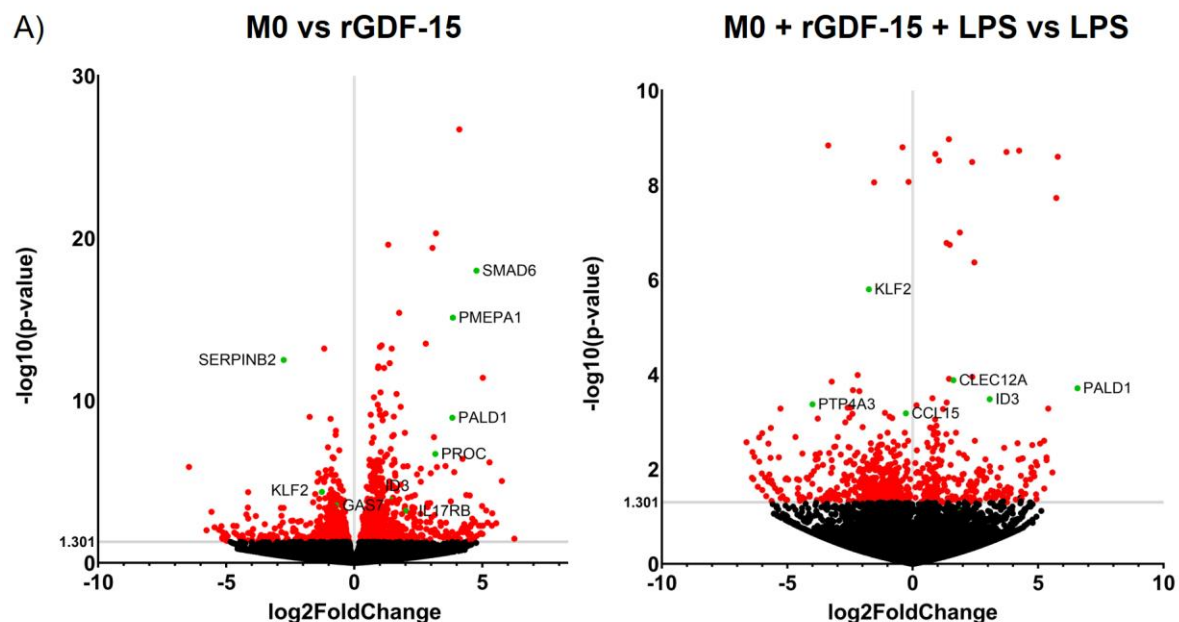


**Figure 11. Schematic representation of the comparison of interest in the model system.**

**Table 20. Differences in DEG counts between the comparison groups**

	<b>M0</b>		<b>M2</b>	
	rGDF-15	rGDF-15+LPS vs. LPS	rGDF-15	rGDF-15+LPS vs. LPS
downregulated	674	266	461	227
upregulated	526	462	342	211

To get an overview of the expression profile, Volcano plots were generated, plotting the log<sub>2</sub> fold change against the 2log<sub>10</sub> p-value for pairwise comparisons in M0 and M2, respectively (Figure 12). The set of genes that were selected for further RT-PCR validation are displayed in green, as mentioned below.



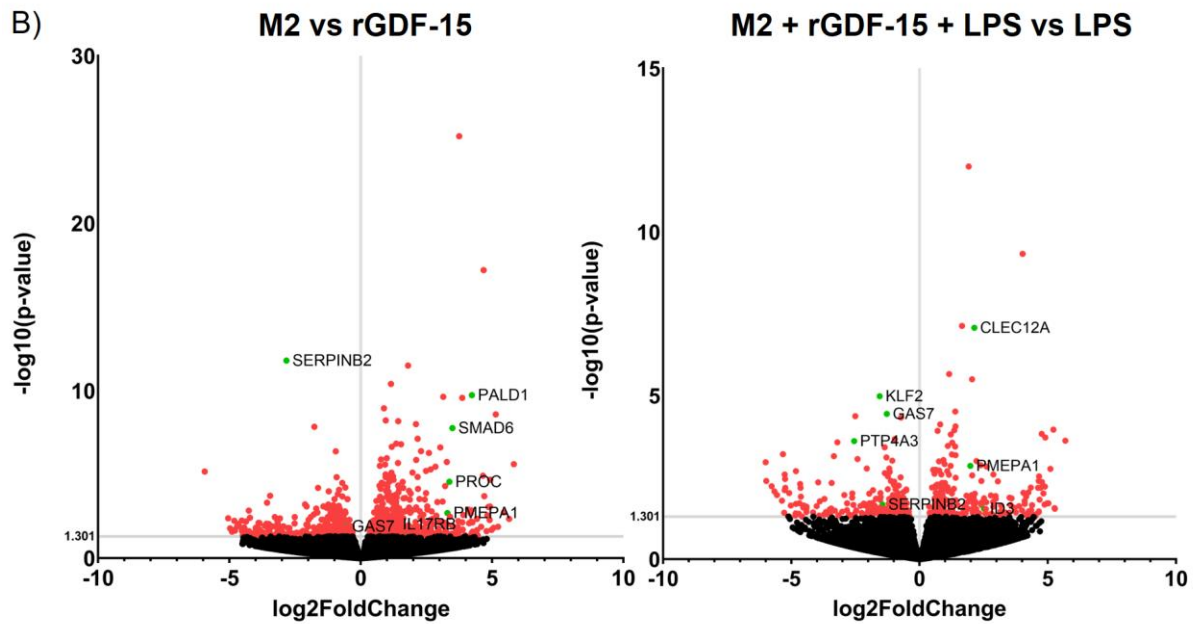


**Figure 12. Volcano plot for differential gene expression in M0 and M2.** A) Gene expression changes between M0 primed with rGDF-15 and non-primed M0 and between M0 primed with rGDF-15 and challenged with LPS and M0 after LPS challenge, as well as, B) between M2 primed with rGDF-15 and non-primed M2 and between M2 primed with rGDF-15 and challenged with LPS and M2 after LPS challenge. The X-axis is the log<sub>2</sub> fold change of gene expression levels and the Y-axis is  $-\log_{10}$  padj based on  $-\log_{10}$ . Up- and downregulated differentially expressed genes with a false discovery rate less than 0.05 are shown in red. The black dots indicate genes with no statistically significant difference. The grey line is showing the threshold for differential gene screening. The green dots represent the genes selected for validation.

A total of 328 and 512 genes were differentially expressed after rGDF-15 priming for 1 hour in M0 and M2, respectively (Figure 13A and 13B). Overlap within and between macrophage phenotypes was considered. For the comparison groups, 1055 genes were differentially expressed in M0 and M2 after rGDF-15 priming for 1 hour followed by LPS challenge vs. LPS challenge alone. In this comparison, 616 genes were differentially expressed in M0 and 326 in M2, sharing a total of 113 differentially expressed genes (Figure 13C). A total of 822 genes were differentially expressed in M0 in all three conditions: control; challenged with LPS alone, and primed with rGDF-15 and challenged with LPS (Figure 13D). Figure 13E shows the total differential expression between M2 conditions.



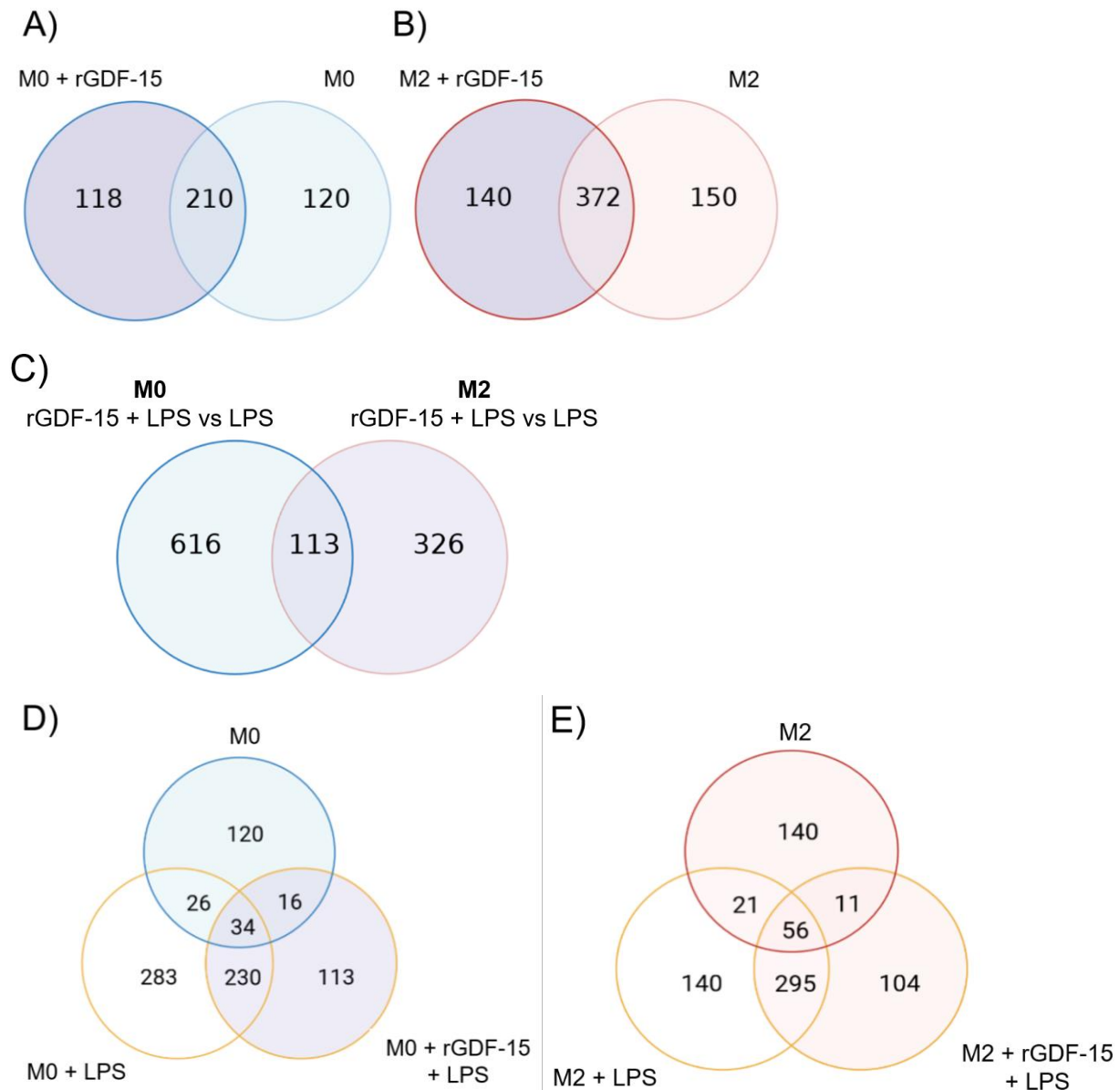


**Figure 13. Significant overlapping genes for the different culture conditions.** A) Venn's diagram of the number of genes that are uniquely expressed by M0 + rGDF-15 vs. M0, as well as the overlapping gene expression within groups. B) Venn's diagram of the number of genes that are uniquely expressed by M2 + rGDF-15 vs. M2, as well as the overlapping gene expression within groups. C) Differential gene expression for the condition of interest rGDF-15 priming vs. LPS challenge and rGDF-15 priming in M0 and M2. D) Venn's diagram of differential gene expression in M0 in rGDF-15 priming, in LPS challenge and in rGDF-15 priming and LPS challenge. E) Venn's diagram of differential gene expression in M2 in rGDF-15 priming, in LPS challenge and in rGDF-15 priming and LPS challenge.

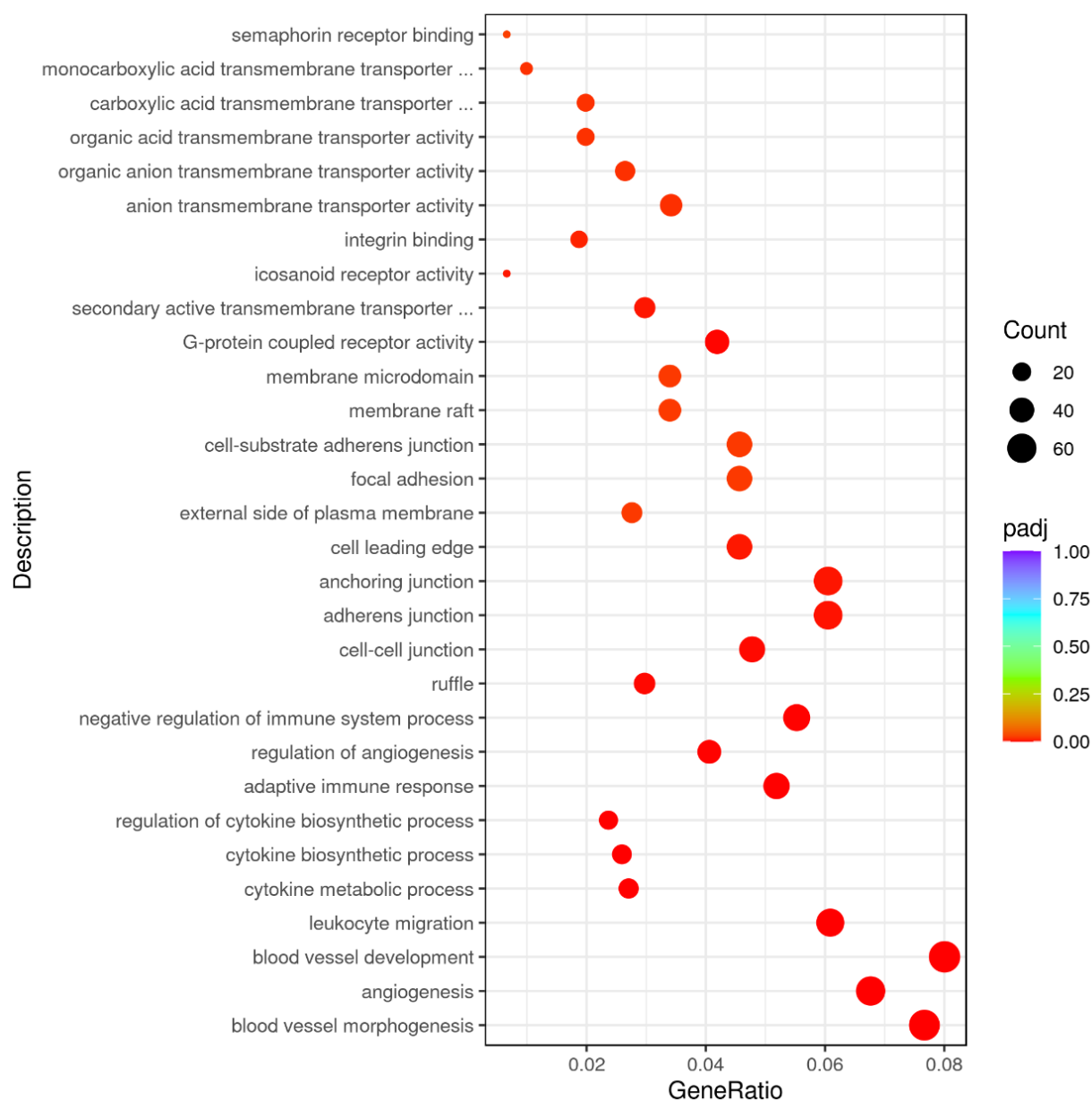
### 3.3.3 Functional enrichment analysis

To better understand the spectrum of the DEGs, GO and KEGG analysis was performed. DEGs were categorized by cellular component (CC), molecular function (MF), and biological process (BP) based on their GO annotations. Figure 14A and B show the top 30 significant GO terms for the M0 vs. M0 + rGDF-15 comparison and their corresponding biological category. 464 GO terms showed significant changes in

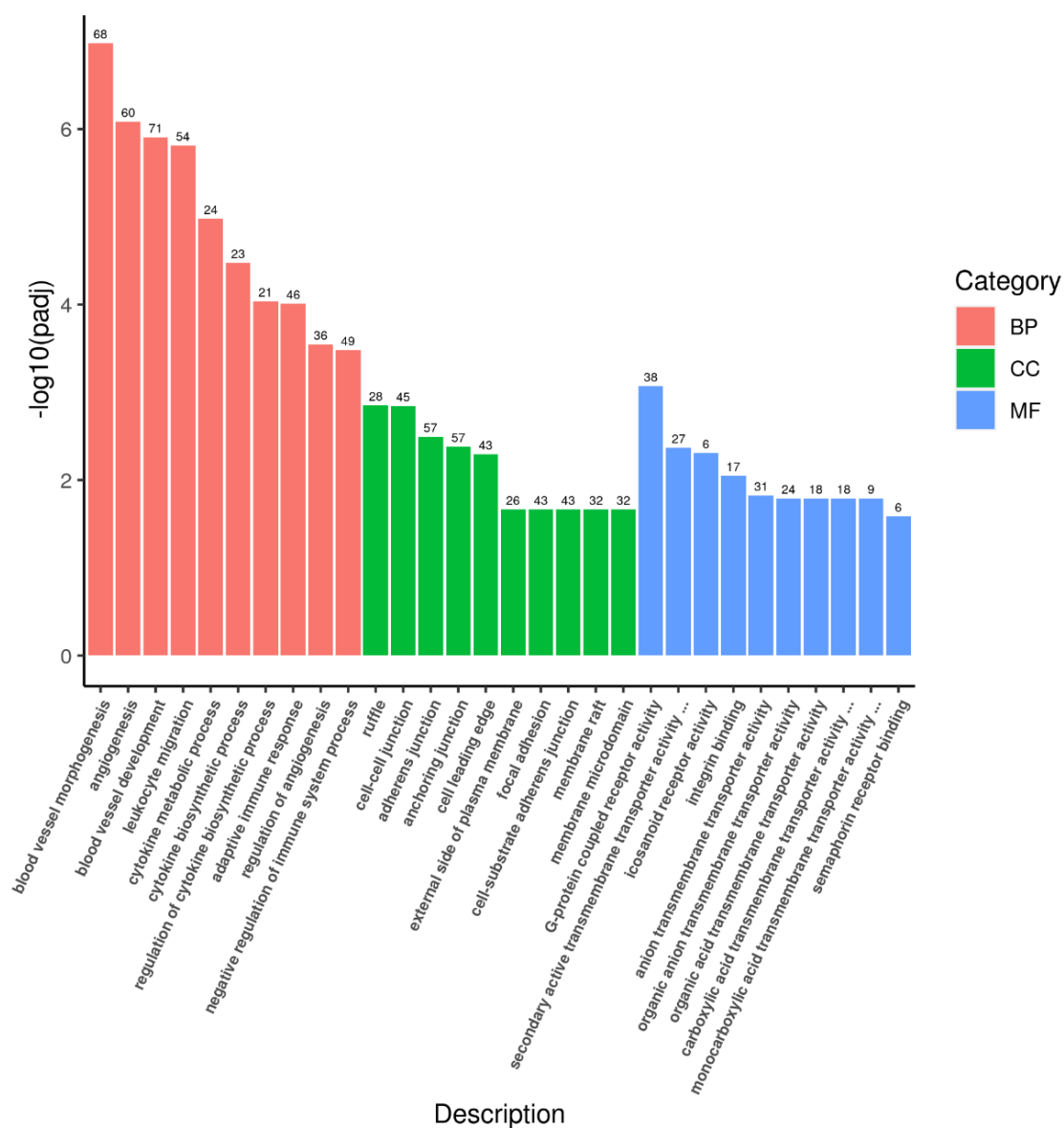


the M0+rGDF-15 vs. M0 comparison. Within this comparison group, the upregulated DEGs identified were mainly associated with blood vessel morphogenesis, development and angiogenesis. The top downregulated GO terms were platelet activation, adaptive immune response and leukocyte cell-cell adhesion. KEGG analysis showed that most of the DEGs are involved in Transcriptional dysregulation in cancer, Leishmaniasis, Pathways in cancer and Cytokine-cytokine receptor interaction (Figure 14C).

A)



B)



C)

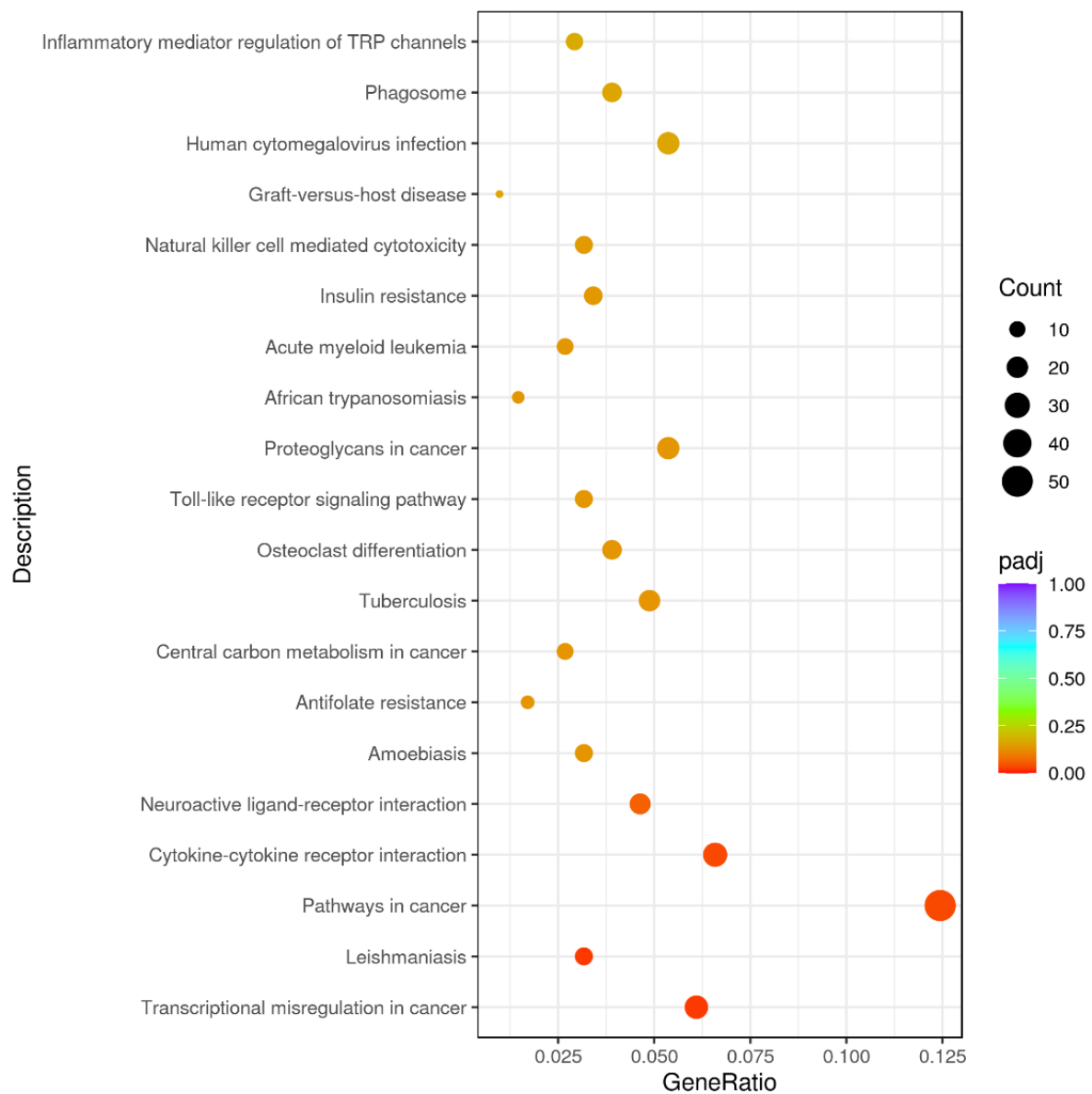
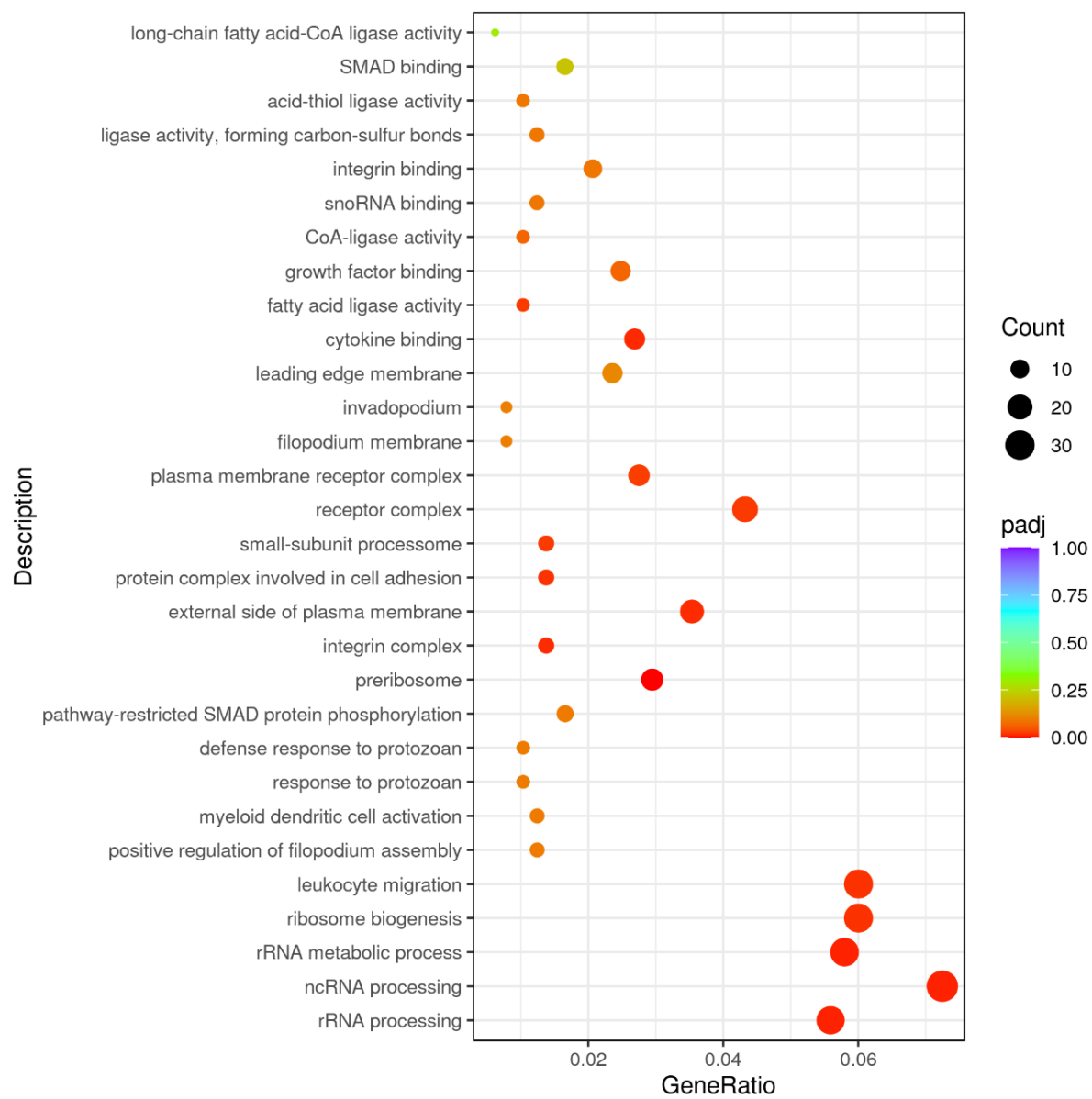


**Figure 14. GO and pathway analysis of DEGs for M0 vs. M0 + rGDF-15 comparison.** A) Dot plot of the top 30 significant GO terms. The Y-axis shows the GO categories, and the X-axis represents the  $-\log_2(p\text{-value})$  of the significant GO terms. B) Histogram of the top 30 significant GO terms classified by GO functional category. C) Dot plot of the top 30 KEGG pathways. The size of the dots is proportional to the fold enrichment.

The results of GO analysis showed that 14 GO terms were related to M0+rGDF-15+LPS vs. M0+LPS. The top downregulated GO terms were mainly involved in rRNA metabolism and ribosome biogenesis, whereas the upregulated ones were related to TGF- $\beta$  receptor signaling pathway and receptor complex formation (Figure 15A and B). KEGG analysis revealed no statistically significant pathway for this comparison group.

A)



B)

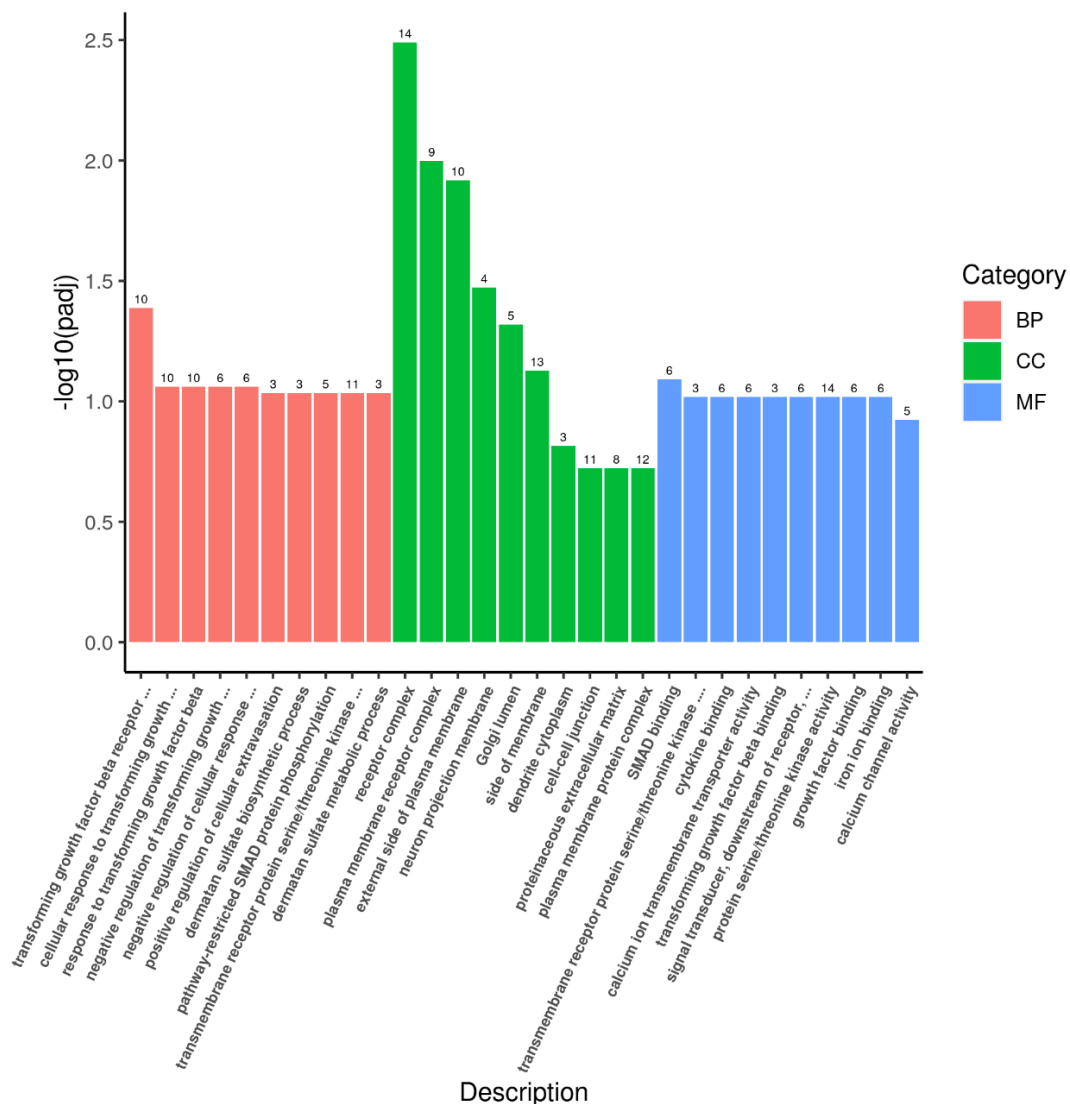
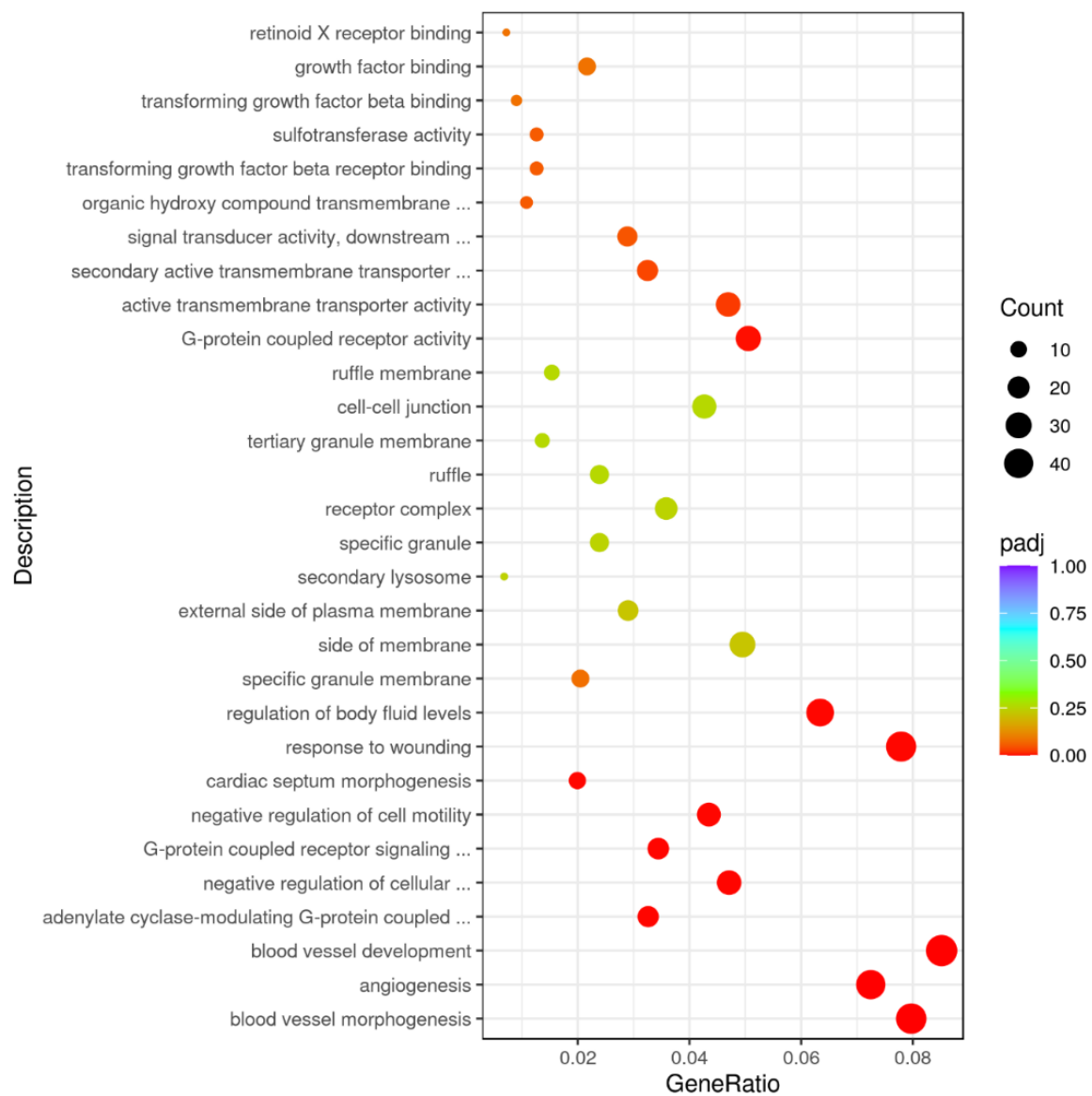


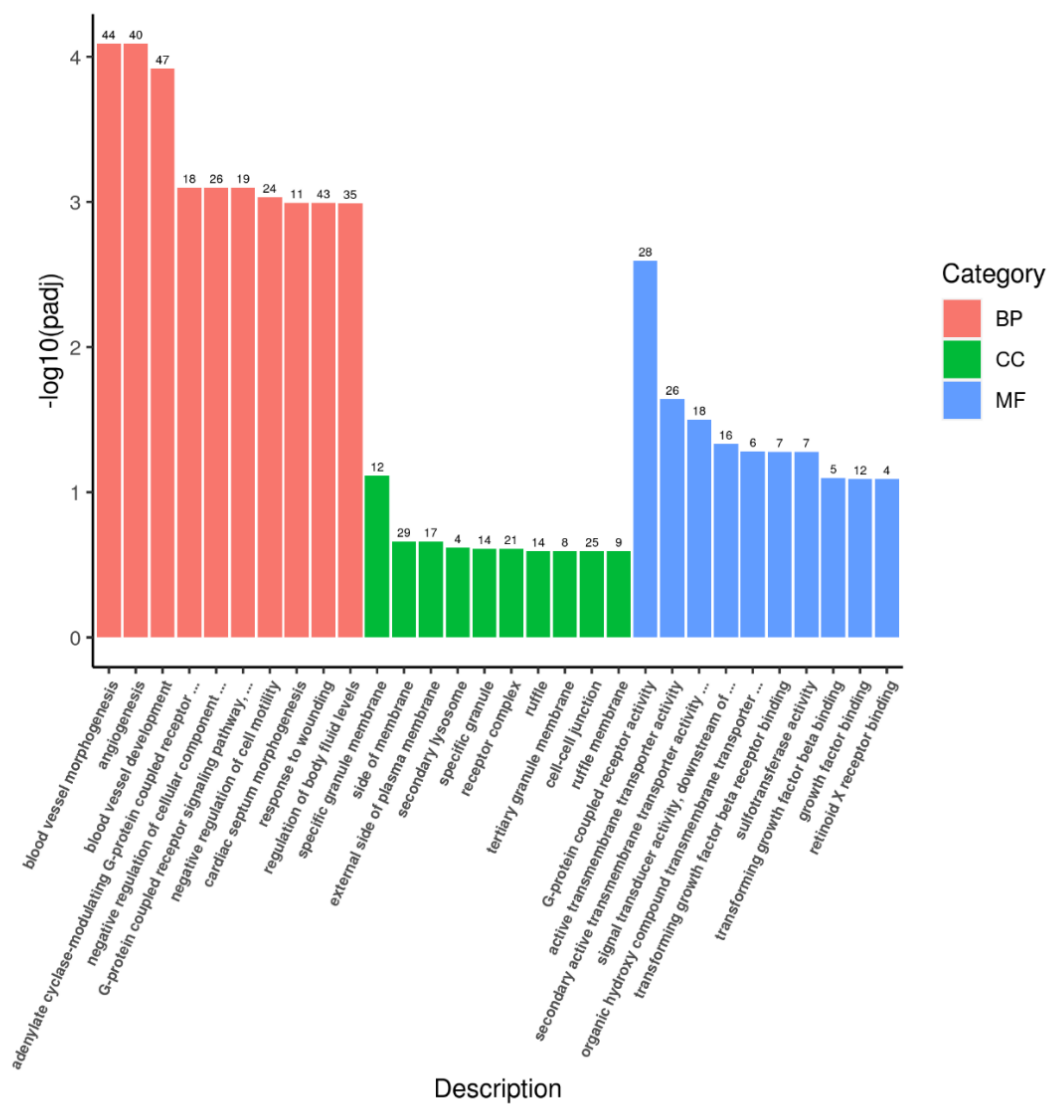
**Figure 15. GO and pathway analysis of DEGs for M0 + rGDF-15 + LPS vs. M0 + LPS comparison.** A) Dot plot of the top 30 significant GO terms. The Y-axis shows the GO categories, and the X-axis represents the  $-\log_2$  (p-value) of the significant GO terms. B) Histogram of the top 30 significant GO terms classified by GO functional categories.

A total of 119 GO terms were significantly altered in M2 macrophages treated with rGDF-15 compared to control. Similar to M0 treated with rGDF-15, genes were enriched in processes related to angiogenesis and leukocyte migration. Other important pathways that were significantly changed in the model involved the response to transforming growth factor beta. KEGG pathway analysis showed that a large number of genes in the “Calcium signaling pathway” and “Pathways in cancer” were upregulated in this comparison group.

A)



B)



C)

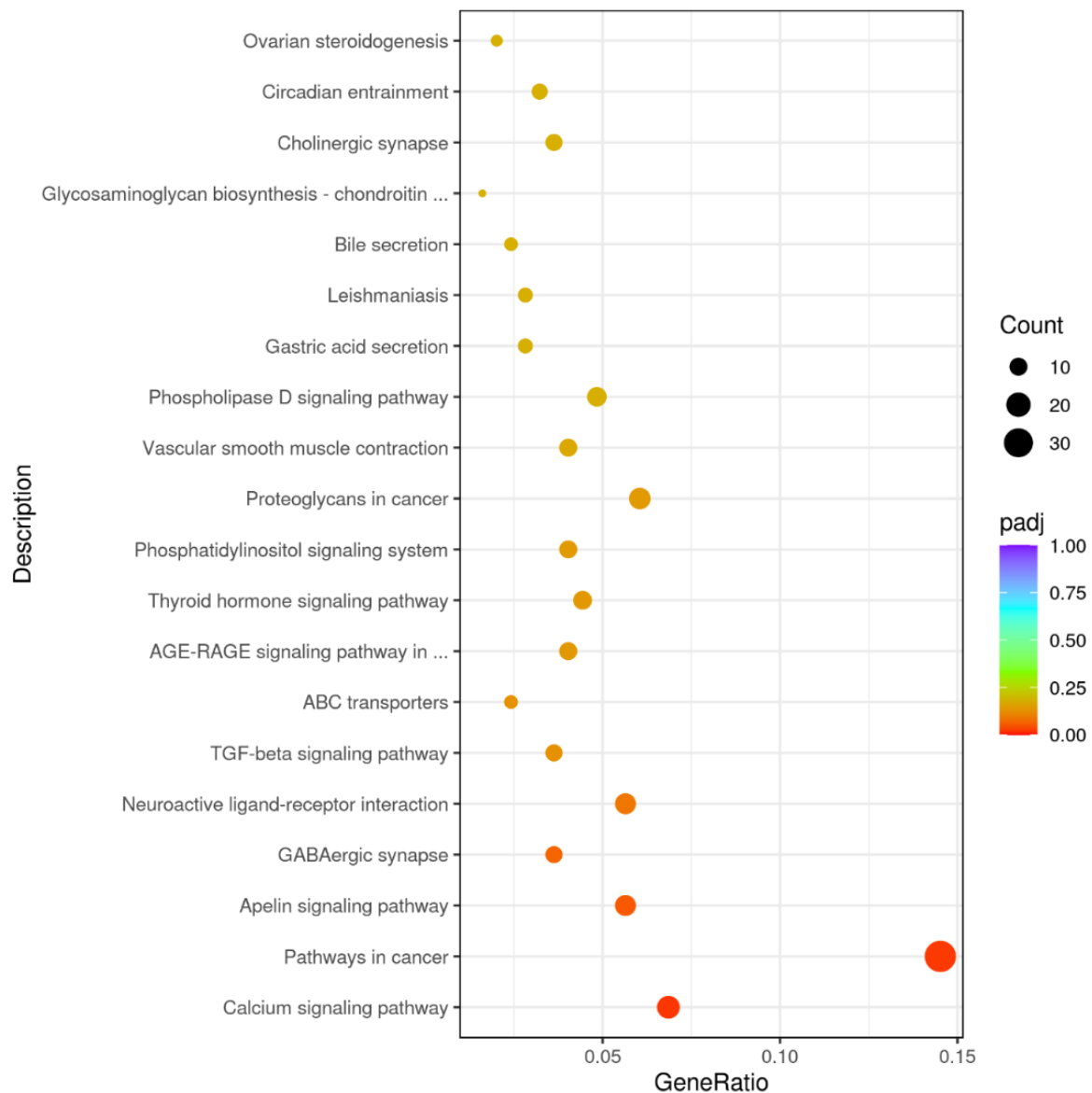
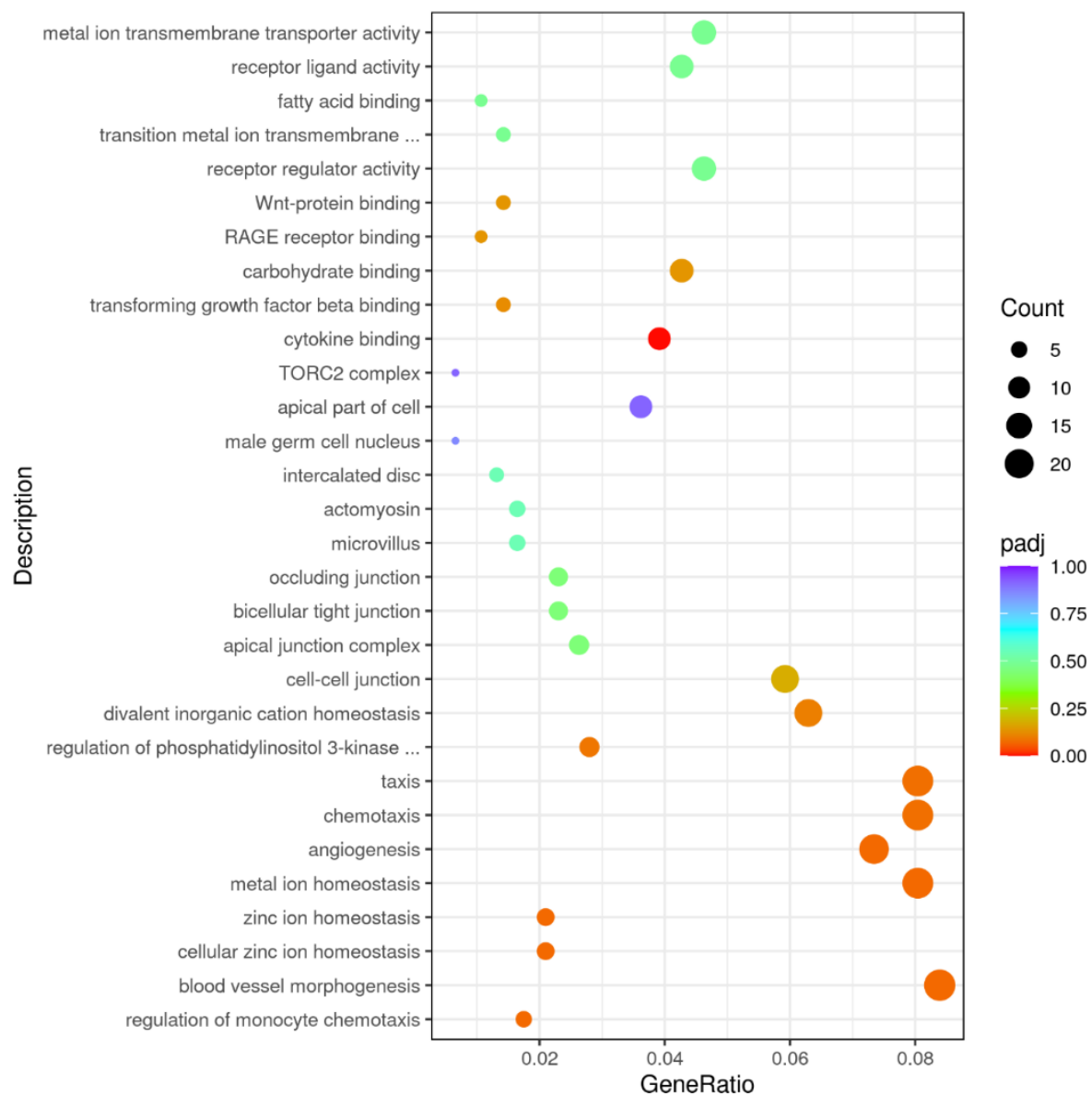


**Figure 16. GO and pathway analysis of DEGs for M2 vs. M2 + rGDF-15 comparison.** A) Dot plot of the top 30 significant GO terms. The Y-axis shows the GO categories, and the X-axis represents the  $-\log_2$  (p-value) of the significant GO terms. B) Histogram of the top 30 significant GO terms classified by GO functional categories. C) Dot plot of the top 30 KEGG pathways. The size of the dots is proportional to the fold enrichment.

Lastly, within the M2+rGDF-15 vs. M2+rGDF-15+LPS comparison, genes were enriched for molecular function GO terms such as cytokine binding and transforming growth factor beta binding. Downregulated GO terms included metal ion homeostasis and zinc ion homeostasis. KEGG analysis did not reveal any statistically significant pathways for this comparison group.



A)



B)

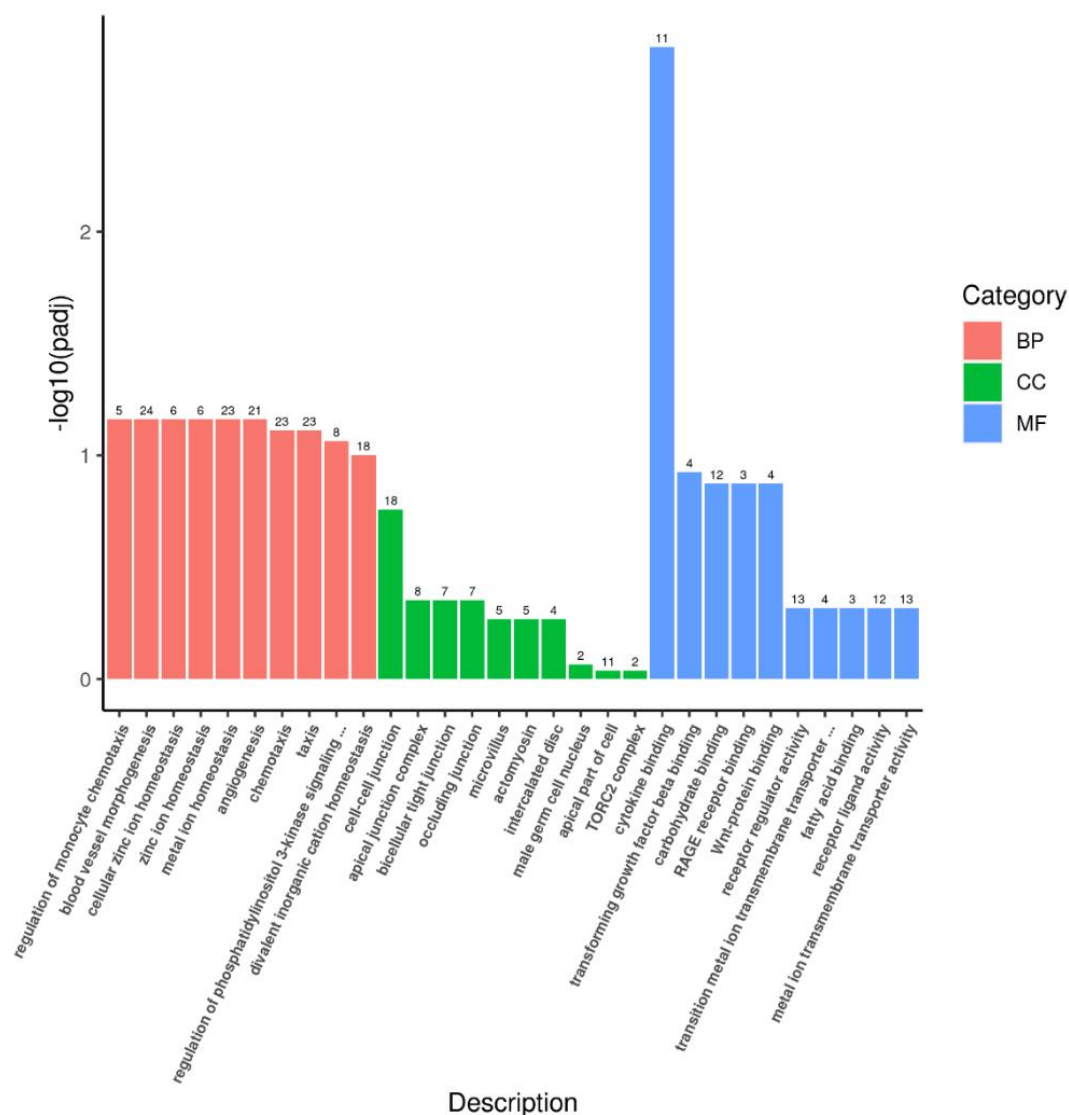


**Figure 17. GO and pathway analysis of DEGs for M2 + rGDF-15 + LPS vs. M2 + LPS comparison.** A) Dot plot of the top 30 significant GO terms. The Y-axis shows the GO categories, and the X-axis represents the  $-\log_2$  (p-value) of the significant GO terms. B) Histogram of the top 30 significant GO terms classified by GO functional categories.

### 3.3.4 Selection of candidate reference genes

To achieve biological reproducibility and following the GO and KEGG analysis, 13 candidate genes were selected further validation, which were among the top significantly up- and downregulated DEGs for the different comparison groups of interest: BCL2L14, CCL15, CLEC12A, GAS7, ID3, IL17RB, KLF2, PALD1, PMEPA1, PROC, PTP4A3, SERPINB2, and SMAD6. All of these genes had FPKM log2-transformed fold changes either greater than 0 or less than 0 within their respective

comparison groups. Table 21 illustrates the top 15 GO terms that were enriched across the conditions of interest, highlighting the DEGs that were selected for further validation. Among them, KLF2 and SMAD6 were shown to be involved in angiogenesis and blood vessel development pathway in the GO analysis (Table 21). KLF2 was significantly altered in macrophages primed with rGDF-15 and then challenged with LPS compared to those challenged with LPS alone. SMAD6 showed significant upregulation in the M2 + rGDF-15 vs. M2 comparison. Other important pathways that were significantly altered involving SMAD6 include “response to transforming growth factor beta” ( $p_{adj}=0,014$ , for the comparison M2 + rGDF-15 vs. M2) and “cellular response to transforming growth factor beta stimulus” ( $p_{adj}=0,04$ , and  $p_{adj}=0,02$ , for the comparison M0 + rGDF-15 vs. M0 and M2 + rGDF-15 vs. M2, respectively), among several others. Similarly, PMEPA1, upregulated in M0 treated with rGDF-15, belongs to pathways involved in the response to TGF- $\beta$ .

**Table 21.** Top 15 GO terms that were enriched for genes differentially expressed across conditions of interest

GO Term	Description	p-value	Genes	Comparison
<b>GO:0001568</b>	blood vessel development	8,55E-06	<i>SMAD6, KLF2</i>	M2+GDFvsM2/M0+GDFvsM0
<b>GO:0071559</b>	response to transforming growth factor beta	6,92E-07	<i>PMEPA1, SMAD6</i>	M2+GDFvsM2/M0+GDFvsM0
<b>GO:0009611</b>	response to wounding	2,17E-08	<i>PROC, SERPINB2, ID3</i>	M2+GDFvsM2/M0+GDFvsM0
<b>GO:0050878</b>	regulation of body fluid levels	2,61E-08	<i>SERPINB2, PROC</i>	M2+GDFvsM2/M0+GDFvsM0
<b>GO:0042060</b>	wound healing	5,87E-08	<i>SERPINB2, PROC</i>	M2+GDFvsM2/M0+GDFvsM0
<b>GO:0061041</b>	regulation of wound healing	2,03E-09	<i>SERPINB2, PROC</i>	M2+GDFvsM2/M0+GDFvsM0
<b>GO:0050900</b>	leukocyte migration	3,44E-09	<i>SERPINB2, PROC, CCL 15</i>	M2+GDFvsM2/M0+GDFvsM0/ M0+GDF+LPSvsM0+LPS
<b>GO:1903034</b>	regulation of response to wounding	7,79E-09	<i>SERPINB2, PROC</i>	M2+GDFvsM2/M0+GDFvsM0
<b>GO:0045596</b>	negative regulation of cell differentiation	0,0001	<i>ID3</i>	M0+GDFvsM0
<b>GO:0060840</b>	artery development	0,0001	<i>SMAD6</i>	M2+GDFvsM2/M0+GDFvsM0
<b>GO:0031589</b>	cell-substrate adhesion	0,0001	<i>SMAD6</i>	M2+GDFvsM2/M0+GDFvsM0
<b>GO:0090101</b>	negative regulation of transmembrane receptor protein serine/threonine kinase signaling pathway	0,0001	<i>PMEPA1, SMAD6</i>	M2+GDFvsM2
<b>GO:0030510</b>	regulation of BMP signaling pathway	0,0002	<i>SMAD6</i>	M0+GDFvsM0
<b>GO:0050729</b>	positive regulation of inflammatory response	0,0002	<i>IL17RB</i>	M2+GDFvsM2/M0+GDFvsM0
<b>GO:0007178</b>	transmembrane receptor protein serine/threonine kinase signaling pathway	0,0002	<i>PMEPA1, SMAD6</i>	M2+GDFvsM2/M0+GDFvsM0

“Response to wounding” was another significantly changed pathway in the GO analysis in both comparisons M0+rGDF-15 vs. M0 and M2+rGDF-15 vs. M2 (padj were 0,004 and 0,001, respectively). Within this pathway PROC, SERPINB2 and ID3 expression was found to be significantly altered (Table 21).

Another pathway significantly upregulated in the comparison M0+rGDF-15 vs. M0 and M2+rGDF-15 vs. M2 was “leukocyte migration”. PROC and CCL15 belong to this pathway and their expression was upregulated in the comparison M0 + rGDF-15 + LPS vs. M0 + LPS. Furthermore, IL17RB upregulated during rGDF-15 treatment in macrophages, belongs to the enriched GO terms involved in the regulation of inflammation and cytokine production.

Finally, for the M0 + rGDF-15 + LPS vs. M0 + LPS and M2 + rGDF-15 + LPS vs. M2 + LPS groups, the top differentially expressed genes were included: PTP4A3, BCL2L14 and PALD1 for M0, and GAS7 and CLEC12A for M2. The fold change for the 13 genes selected by RNA-Seq and their respective RT-PCR validation are shown in the Table 22. The conditions validated by RT-PCR are marked in green as shown below. The functions of the validated genes are described in Table 23.

**Table 22.** RT-PCR validation of RNA-Seq experiments

Gene name	Condition	RNA-Seq		RT-PCR	
		Fold change	p-value	Fold change	p-value
BCL2L14	M0	-	-	na	>0,9999
	M0 + LPS	-3,13	0,003	-0,24	0,164
	M2	-	-	0,00	na
	M2 + LPS	-0,90	0,430	-0,34	0,426
CCL15	M0	-	-	-0,18	0,219
	M0 + LPS	-2,71	0,001	-0,70	0,040
	M2	-	-	-0,05	>0,9999
	M2 + LPS	-0,99	0,068	-0,56	0,059
CLEC12A	M0	0,39	0,524	-0,14	0,538
	M0 + LPS	1,62	0,0001	6,92	0,034
	M2	0,36	0,488	4,17	0,114
	M2 + LPS	2,14	9E-08	11,39	0,108
GAS7	M0	-0,69	3E-04	-0,21	0,244
	M0 + LPS	-1,01	0,041	-0,59	0,005
	M2	-0,56	0,013	0,22	0,607
	M2 + LPS	-1,27	4E-05	-0,85	0,127
ID3	M0	1,47	1E-04	0,49	0,170

	<b>M0 + LPS</b>	3,07	3E-04	0,05	0,901
	<b>M2</b>	0,96	0,190	1,03	0,035
	<b>M2 + LPS</b>	2,51	0,029	2,19	0,012
<b>IL17RB</b>	<b>M0</b>	2,02	0,001	3,25	0,002
	<b>M0 + LPS</b>	1,88	0,08	4,52	0,005
	<b>M2</b>	1,66	0,046	1,25	0,006
	<b>M2 + LPS</b>	1,33	0,212	18,32	0,0002
<b>KLF2</b>	<b>M0</b>	-1,26	4E-05	7,10	0,125
	<b>M0 + LPS</b>	-1,74	2E-08	-0,73	0,625
	<b>M2</b>	-0,76	0,061	-0,26	>0,9999
	<b>M2 + LPS</b>	-1,55	1E-05	-0,92	0,059
<b>PALD1</b>	<b>M0</b>	3,83	1E-09	21,96	0,063
	<b>M0 + LPS</b>	6,57	2E-04	0,39	0,438
	<b>M2</b>	4,23	2E-10	-0,15	0,813
	<b>M2 + LPS</b>	2,41	2,783	1,06	0,313
<b>PMEPA1</b>	<b>M0</b>	3,85	9E-16	28,63	0,005
	<b>M0 + LPS</b>	2,307	2E-02	46,68	0,016
	<b>M2</b>	3,30	2E-03	4,90	0,031
	<b>M2 + LPS</b>	1,99	1E-03	6,74	0,031
<b>PROC</b>	<b>M0</b>	3,17	2E-07	-0,10	0,625
	<b>M0 + LPS</b>	5,24	0,026	1,24	0,447
	<b>M2</b>	3,38	3E-05	4,90	0,375
	<b>M2 + LPS</b>	-1,48	NA	2,76	>0,9999
<b>PTP4A3</b>	<b>M0</b>	-2,52	0,301	-0,73	0,938
	<b>M0 + LPS</b>	-3,99	4E-09	-0,86	0,001
	<b>M2</b>	-0,57	0,753	1,69	0,516
	<b>M2 + LPS</b>	-2,55	2E-04	-0,95	0,007
<b>SERPINB2</b>	<b>M0</b>	-2,76	3E-13	-0,92	0,125
	<b>M0 + LPS</b>	-1,44	0,044	-0,86	0,155
	<b>M2</b>	-2,83	2E-12	-0,87	0,813
	<b>M2 + LPS</b>	-1,44	0,021	-0,75	0,063
<b>SMAD6</b>	<b>M0</b>	4,77	1E-18	17,53	0,004
	<b>M0 + LPS</b>	1,21	0,051	1,57	0,004
	<b>M2</b>	3,49	2E-08	2,64	0,029
	<b>M2 + LPS</b>	1,07	0,102	0,74	0,006

**Table 23.** Selected validated set of genes

Gene annotation	Abbreviation	Function	Condition	Direction of the expression
C-C motif chemokine ligand 15	CCL15	Chemoattractant for monocytes and neutrophils	M0+ LPS	↓
C-type lectin domain family 12 member	CLEC12A	Death cells recognition and negative regulator of inflammation	M0+ LPS	↑
growth arrest specific 7	GAS7	Formation of the phagocytic cup	M0+ LPS	↓
inhibitor of DNA binding 3, HLH protein	ID3	Negative regulator transcription through non-functional dimers	M2	↑
			M2+ LPS	↑
interleukin 17 receptor B	IL17RB	Th2 response and anti-inflammatory mechanisms	M0	↑
			M0+ LPS	↑
			M2	↑
			M2+ LPS	↑
prostate transmembrane protein, androgen induced 1	PMEPA1	Negative feedback mechanism which antagonizes TGF- $\beta$ signaling	M0	↑
			M0+ LPS	↑
			M2	↑
			M2+ LPS	↑
protein tyrosine phosphatase type IVA, member 3	PTP4A3	Cell growth, proliferation, migration and invasion	M0+ LPS	↓
			M2+ LPS	↓
SMAD family member 6	SMAD6	Anti-inflammatory signalling in macrophages	M0	↑
			M0+ LPS	↑
			M2	↑
			M2+ LPS	↑

The expression of these genes was measured in M0, M1 and M2, cultured under the conditions described in the experimental design (Figure 11). The expression levels of the validated genes are shown in the following sections (Sections 3.3.4.1 to 3.3.4.8). The expression profile of the non-validated genes is shown in the Supplementary Material (Supplementary Figures 3 to 7). Moreover, the expression of GDF-15 in the model system was assessed. A significant increase in GDF-15 expression was observed solely in M0 macrophages treated with LPS, as compared to M0 treated with rGDF-15 alone. Furthermore, among M0 and M2 macrophages, those treated with rGDF-15 displayed the lowest GDF-15 expression levels (Supplementary Figure 8).

#### 3.3.4.1 Upregulated CCL15 expression in macrophages driven by LPS treatment is decreased after rGDF-15 priming

CCL15 belongs to the CC chemokine subfamily, and binds to CCR1 and CCR3, and acts as a chemoattractant for monocytes and neutrophils. Its presence in tumor tissue is associated with TAMs infiltration, with angiogenesis, and with metastasis<sup>128</sup>. Increased expression of CCL15 was observed in M0 and M2 challenged by LPS, which was decreased by pre-stimulation with rGDF-15 ( $p=0,0475$  and  $p=0,0591$ , respectively) (Figure 18).

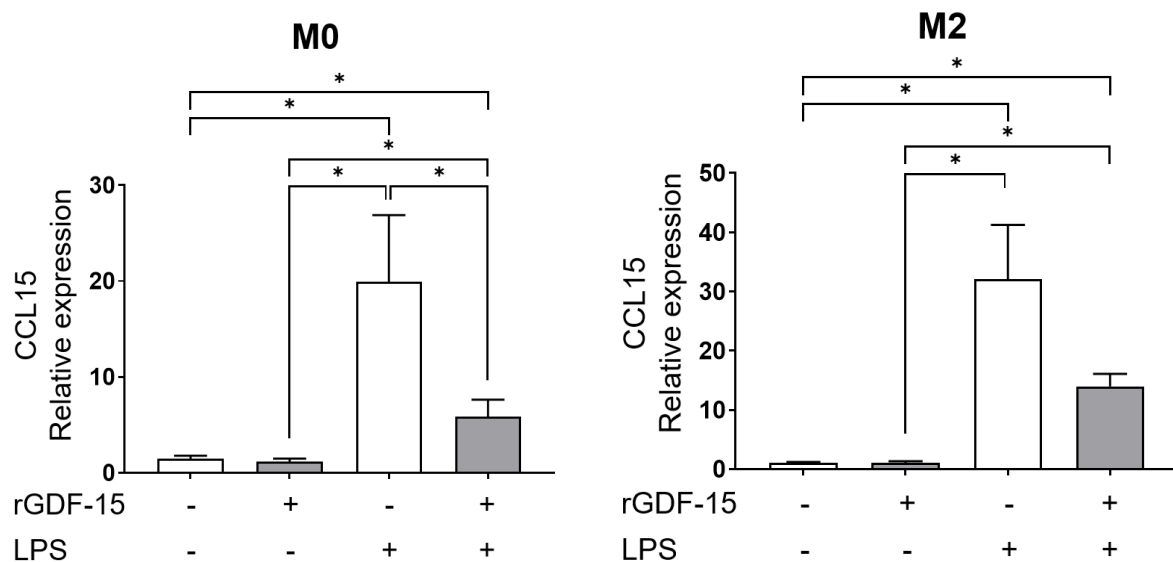


**Figure 18. Effect of rGDF-15 on CCL15 gene expression of CCL15 in macrophages challenged with LPS.** CCL15 mRNA expression was analyzed by RT-PCR in M0 and M2 macrophages cultured for 6 days, primed with rGDF-15 50 ng/mL for 1 hour and challenged with LPS 100 g/mL for 6 hours.  $n=7$  for M0 and  $n=6$  for M2. Data are presented as mean  $\pm$  SEM normalized to 18SrRNA expression levels.  $*p<0.05$ .



### 3.3.4.2 CLEC12A expression is highest in macrophages primed with rGDF-15 and challenged with LPS

C-type lectin domain family 12 member A (CLEC12A) is a receptor highly expressed on myeloid cells and on myeloblasts in patients with acute myeloid leukemia (AML) <sup>129</sup>. CLEC12A recognizes dead cells and seems to be a negative regulator of inflammation<sup>130</sup>. CLEC12A was shown to be predominantly expressed in M0 and M1 macrophages after rGDF-15 priming and LPS challenge compared to LPS challenge alone. In addition, there was a non-significant difference in expression levels in LPS challenged macrophages compared to control or rGDF-15 treated macrophages alone (Figure 19).

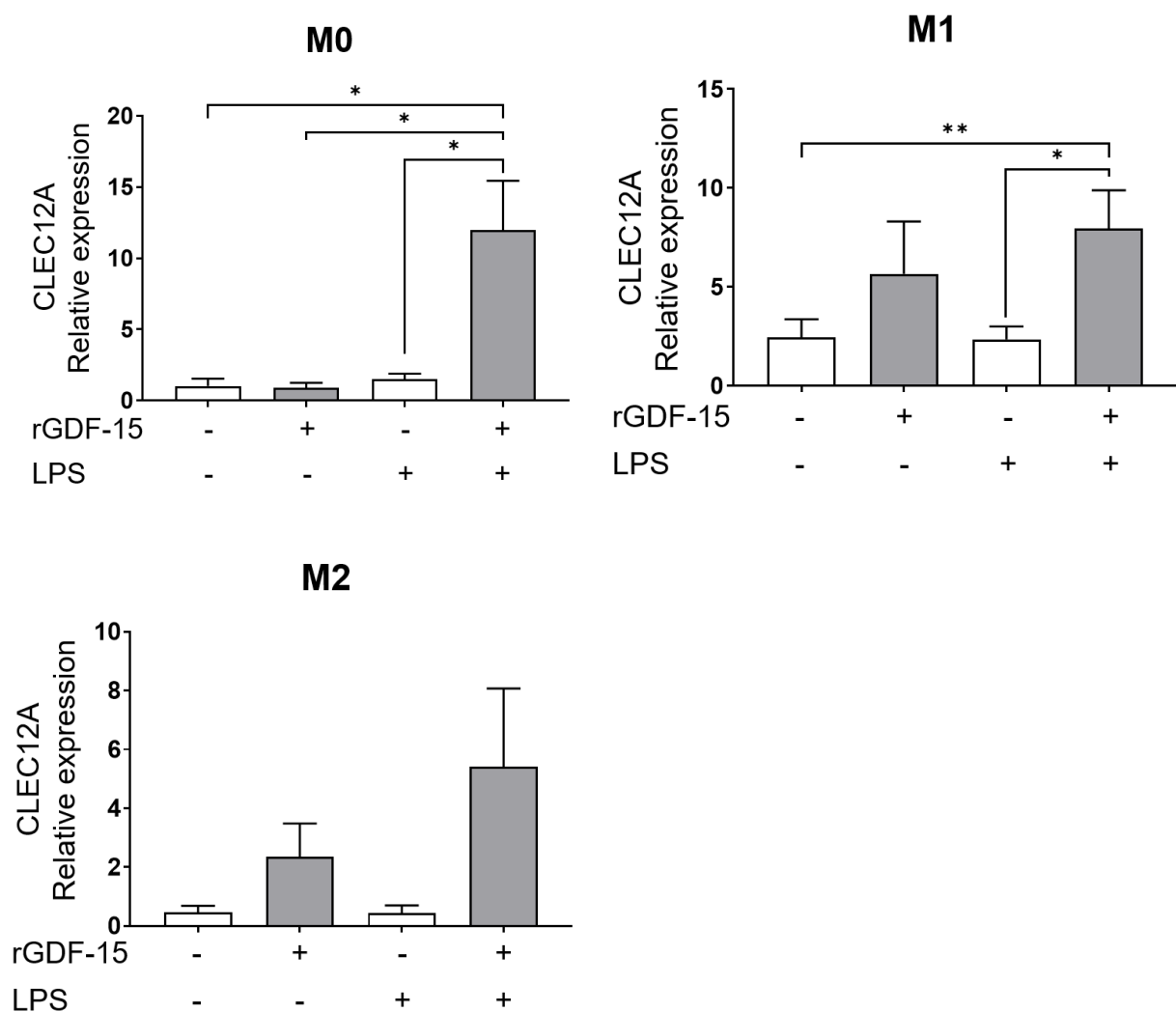


**Figure 19. Effect of rGDF-15 on CLEC12A gene expression in macrophages challenged with LPS.** CLEC12A mRNA expression was analyzed by RT-PCR in M0, M1 and M2 macrophages cultured for 6 days, primed with rGDF-15 50 ng/mL for 1 hour and challenged with LPS 100 g/mL for 6 hours. n=5. Data are presented as mean  $\pm$  SEM normalized to 18S rRNA expression levels. \*p<0.05, \*\*p<0.01.

### 3.3.4.3 GAS7 expression is downregulated by rGDF-15 priming in LPS-challenged macrophages

Growth Arrest-Specific 7 (GAS7) is a transmembrane protein expressed in phagocytes, including macrophages, which is a key factor in the formation of the phagocytic cup<sup>131</sup>. Its expression is induced in macrophages after LPS treatment<sup>132</sup>. In the present project, GAS7 was downregulated in rGDF-15 primed M0 macrophages compared to M0 challenged with LPS alone (Figure 20). The same trend was visible in M1 and M2 macrophages without reaching statistical significance (Figure 20). Interestingly, the lowest GAS7 gene expression was found in macrophages primed with rGDF-15 and challenged with LPS (Figure 20).

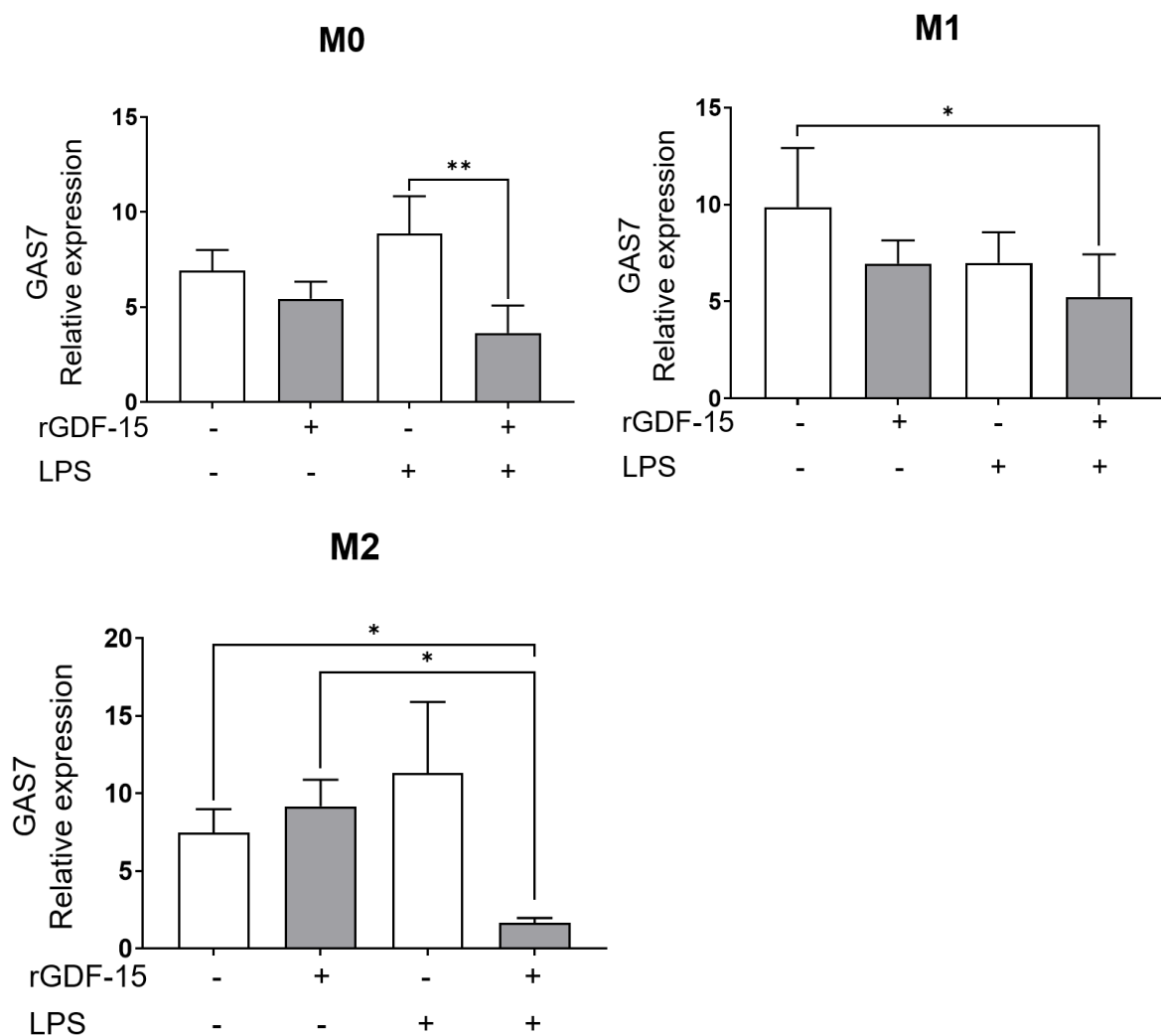


**Figure 20. Effect of rGDF-15 on the gene expression of GAS7 in macrophages challenged with LPS.** GAS7 mRNA expression was analyzed by RT-PCR in M0, M1 and M2 macrophages cultured for 6 days, primed with rGDF-15 50 ng/mL for 1 hour and challenged with LPS 100 g/mL for 6 hours. n=4. Data are presented as mean  $\pm$  SEM normalized to 18SrRNA expression levels. \*p<0.05, \*\*p<0.01.

#### 3.3.4.4 rGDF-15 upregulates ID3 expression in macrophages

Inhibition of differentiation 3 (ID3) is a transcription factor that negatively regulates transcription through non-functional dimers. ID3 expression has been reported to be upregulated in M2 macrophages<sup>133</sup>. In this model, rGDF-15 treatment increased ID3 expression in M1 and M2 macrophages. This increase was particularly evident rGDF-15 treated M1 compared to LPS-challenged macrophages and within M2 + rGDF-15 compared to control and LPS treated macrophages (Figure 21).

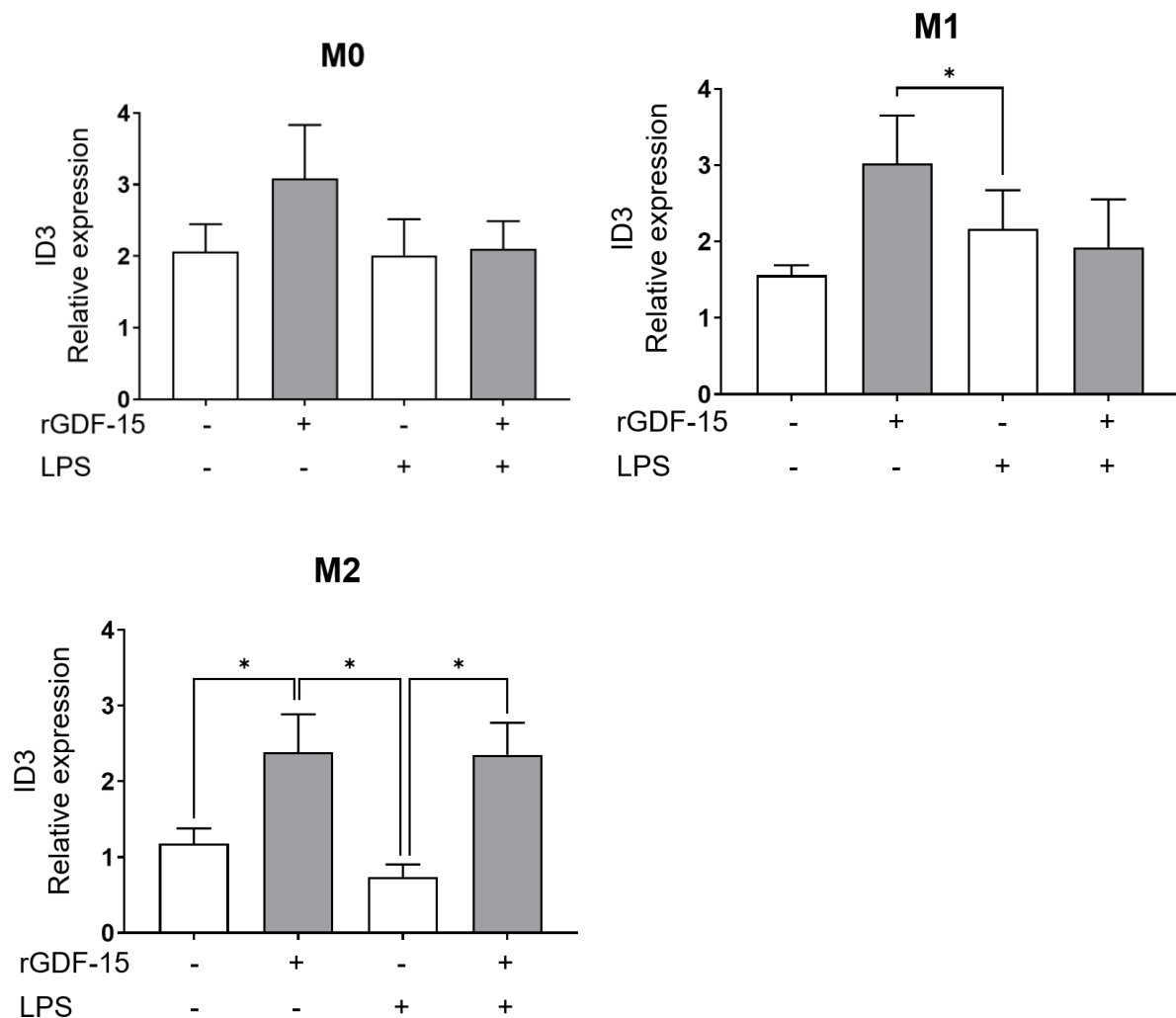


**Figure 21. Effect of rGDF-15 on ID3 gene expression in macrophages challenged with LPS.** ID3 mRNA expression was analyzed by RT-PCR in M0, M1 and M2 macrophages cultured for 6 days, primed with rGDF-15 50 ng/mL for 1 hour and challenged with LPS 100 g/mL for 6 hours. n=6. Data are presented as mean  $\pm$  SEM normalized to 18SrRNA expression levels. \*p<0.05.

#### 3.3.4.5 rGDF-15 upregulates expression of IL17RB in macrophages

IL-17RB is the receptor for IL-17E, also known as IL-25, a member of the IL-17 cytokine family. This cytokine family is predominantly produced by T helper 17 (Th17) cells of the TCD4<sup>+</sup> subset and contributes to the production of pro-inflammatory cytokines such as TNF- $\alpha$  and IL-6. Compared to the other members, IL-17E has a different

functionality, promoting Th2 responses and anti-inflammatory mechanisms. This cytokine is also secreted by macrophages, natural killer (NK) cells and mast cells<sup>134</sup>. The interaction between IL-17RB and its ligand has been implicated in tumor progression and poor prognosis in several cancers<sup>135</sup>. The effect of rGDF-15 on IL17RB expression in macrophages was analyzed in 12 donors in M0, 7 donors in M1 and 13 donors in M2. Figure 22 illustrates a significant upregulation of IL17RB expression on M0 macrophages pretreated with rGDF-15, with and without LPS challenge, compared to those non-treated and those challenged with LPS. Likewise, M2 macrophages showed a significantly increased IL17RB expression with rGDF-15 pre-treatment, which was maintained after LPS challenge. This increased expression was also evident when comparing non-treated M1 and rGDF-15-treated M1 macrophages ( $p=0,0156$ ), but did not reach statistical significance in M1 challenged with LPS.

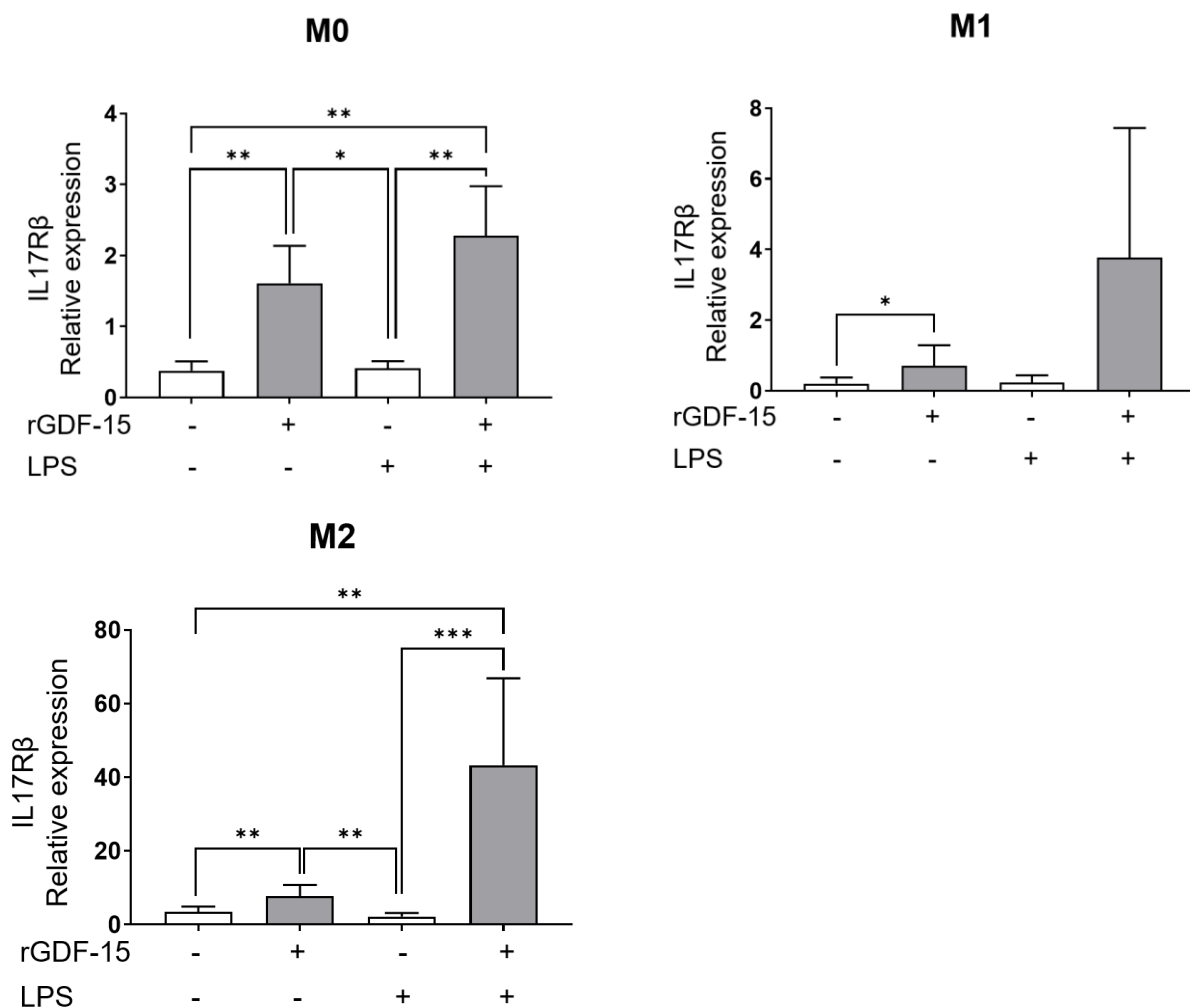


**Figure 22. Effect of rGDF-15 on IL17RB gene expression in macrophages challenged with LPS.** IL17RB mRNA expression was analyzed by RT-PCR in M0, M1 and M2 macrophages cultured for 6 days, primed with rGDF-15 50 ng/mL for 1 hour and challenged

with LPS 100 g/mL for 6 hours. n=12 for M0, n=7 for M1 and n=13 for M2 Data are presented as mean  $\pm$  SEM normalized to 18SrRNA expression levels. \*p<0.05, \*\*p<0.01, \*\*\*p<0.001

### 3.3.4.6 PMEPA1 expression is low in the activated macrophages and it is upregulated after rGDF-15 treatment

Prostate transmembrane protein androgen induced 1 (PMEPA1) is a transmembrane protein with a recently discovered role in tumorigenesis in prostate, cervical, pancreatic, and colorectal cancers. It has also been shown that PMEPA1 activation results in a negative feedback mechanism that antagonizes TGF- $\beta$  signaling<sup>136</sup>.

Upregulated PMEPA1 expression was found in macrophages treated with rGDF-15 in M0 and M2 compared to control (p=0,0048 and p=0,0313, respectively). This upregulated expression was particularly pronounced in macrophages pretreated with rGDF-15 and then challenged with LPS. Interestingly, LPS alone did not upregulate PMEPA1 expression (Figure 23).

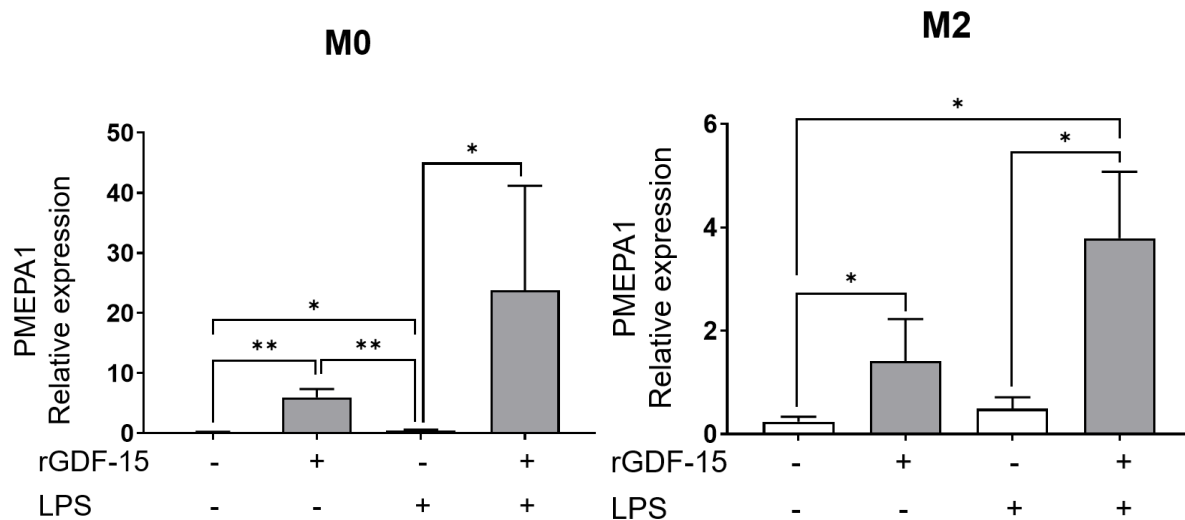


**Figure 23. Effect of rGDF-15 on PMEPA1 gene expression in macrophages challenged with LPS.** PMEPA1 mRNA expression was analyzed by RT-PCR in M0 and M2 macrophages cultured for 6 days, primed with rGDF-15 50 ng/mL for 1 hour and challenged with LPS 100 g/mL for 6 hours. M0 n=6 and M2 n=7. Data are presented as mean  $\pm$  SEM normalized to 18SrRNA expression levels. \*p<0.05, \*\*p<0.01.

### 3.3.4.7 rGDF-15 suppresses PTP4A3 expression in macrophages

Protein tyrosine phosphatase 4A3 (PTP4A3) is a plasma membrane and endosomal phosphatase, that belongs to the phosphatase of regenerative liver (PRL) PTP subfamily, and it is involved in many cellular processes, including cell growth, proliferation, migration and invasion<sup>137</sup>. High expression of this protease has been found in several cancer types including breast, ovarian, and renal cell carcinoma, and it is correlated with metastasis and poor prognosis<sup>138-140</sup>. PTP4A3 expression was evaluated in 11 donors for each macrophage phenotype, M0 and M2 (Figure 24). LPS

treatment significantly increased PTP4A3 expression in M0 and M2 macrophages. However, this increased expression was abolished by pretreatment with rGDF-15. In addition, PTP4A3 expression was almost undetectable in untreated macrophages and in those primed only with rGDF-15 without LPS challenge.

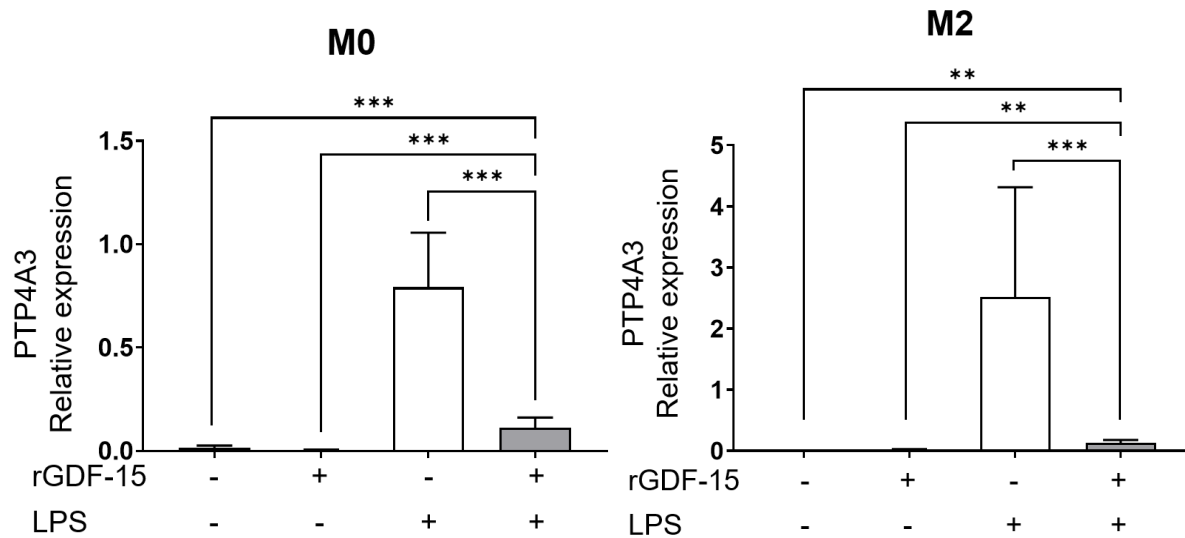


**Figure 24. Effect of rGDF-15 on the gene expression of PTP4A3 in macrophages challenged with LPS.** PTP4A3 mRNA expression was analyzed by RT-PCR in M0 and M2 macrophages cultured for 6 days, primed with rGDF-15 50 ng/mL for 1 hour and challenged with LPS 100 g/mL for 6 hours.  $n=11$ . Data are presented as mean  $\pm$  SEM normalized to 18SrRNA expression levels. \*\* $p<0.01$ , \*\*\* $p<0.001$

3.3.4.8 rGDF-15 upregulates SMAD6 expression in M0 and M2 macrophages  
SMAD6 belongs to the SMAD family, a group of intracellular proteins involved in the TGF- $\beta$  signaling pathway and transcriptional regulation. As inhibitory SMAD proteins, SMAD6 and SMAD7 contribute to repression of the TGF- $\beta$  downstream pathway<sup>141</sup>. When methylated, SMAD6 promotes anti-inflammatory processes in macrophages<sup>142</sup>. Increased expression of SMAD6 was observed in macrophages treated with rGDF-15, as compared to the control. Furthermore, macrophage priming with rGDF-15 also led to an upregulation of SMAD6 expression following LPS challenge, in contrast to macrophages challenged with LPS alone. However, this trend was not apparent among M1 macrophages (Figure 25).

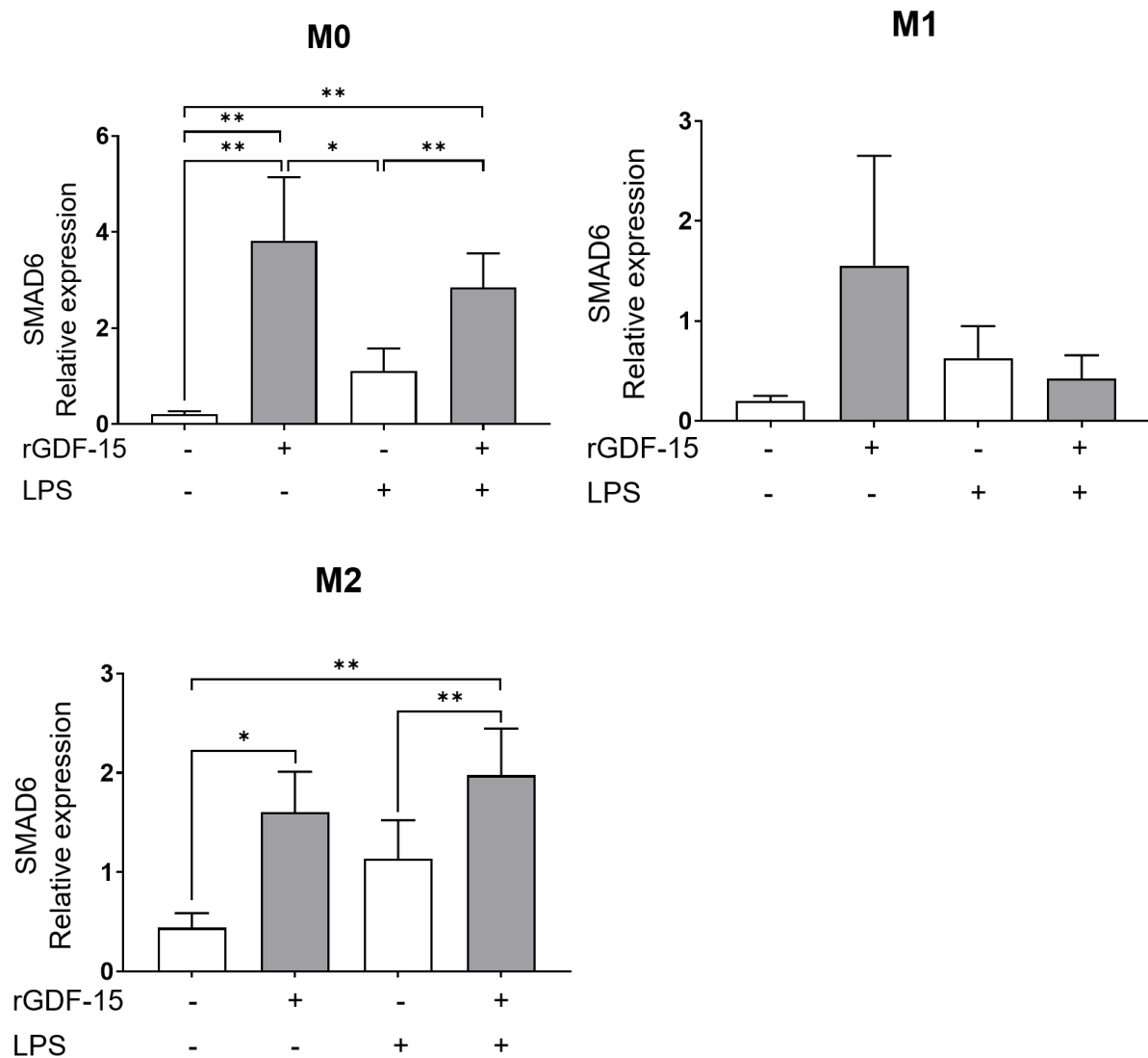


**Figure 25. Effect of rGDF-15 on SMAD6 in macrophages challenged with LPS.** SMAD6 mRNA expression was analyzed by RT-PCR in M0, M1 and M2 macrophages cultured for 6 days, primed with rGDF-15 50 ng/mL for 1 hour and challenged with LPS 100 g/mL for 6 hours.  $n=9$  for M0,  $n=3$  for M1 and  $n=10$ . Data are presented as mean  $\pm$  SEM normalized to 18S rRNA expression levels. \* $p<0.05$ , \*\* $p<0.01$ .

In total, 8 of the 13 genes identified by RNA-Seq were successfully validated by RT-PCR. This set of genes has been extensively referenced in the literature for their involvement in carcinogenesis and metastasis, as mentioned in the previous section. In particular, rGDF-15 showed a significant influence on gene expression related to angiogenesis, a hallmark of cancer. Finally, a bioinformatics analysis was performed using transcriptomic data from The Cancer Genome Atlas (TCGA).

### 3.4 In-silico analysis based on TCGA

For the assessment of gene expression levels in cancer and subsequent analysis, data from TCGA were analyzed using TIMER2.0 and the Xena platform.

### 3.4.1 Abnormal expression of GDF-15 in cancer

The expression level of GDF-15 between tumor and normal tissues in bladder, breast, colon, kidney, lung, prostate and gastric cancer using TIMER2.0. Tumor tissues from breast, colon, lung, prostate and gastric cancer showed a significantly higher GDF-15 expression compared to their adjacent normal counterparts. Interestingly, normal tissue patients with clear cell renal carcinoma (KIRC) showed higher GDF-15 expression than the tumor tissue. In bladder cancer, there was no significant difference in GDF-15 expression between normal and tumor tissues (Figure 26).

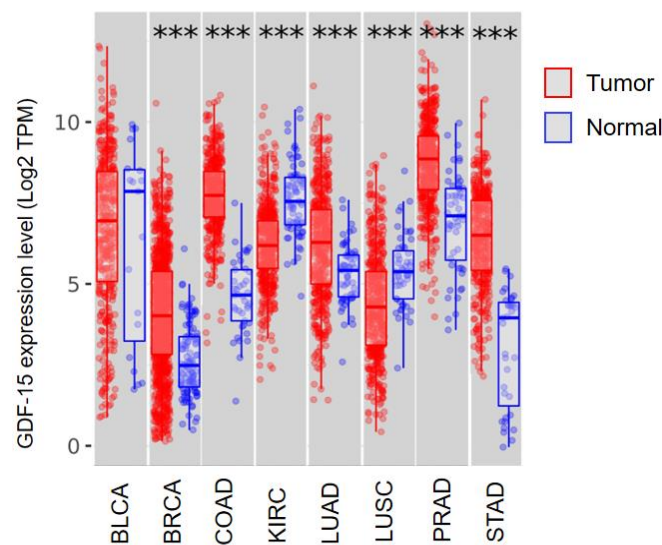


**Figure 26. GDF-15 expression levels in human carcinomas based on pan-cancer analysis.** GDF-15 mRNA expression levels were analyzed by TIMER2.0 using the TCGA database. \*\*\* $p < 0.001$ . BLCA: Bladder Urothelial Carcinoma, BRCA: Breast Invasive Carcinoma, COAD: Colon Adenocarcinoma, KIRC: Kidney Renal Cell Carcinoma, LUAD: Lung Adenocarcinoma, LUSC: Lung Squamous Cell Carcinoma, PRAD: Prostate Adenocarcinoma, STAD: Stomach Adenocarcinoma.

A further analysis was chosen to investigate the influence of GDF-15 expression on KIRC. Using Xena, it was confirmed that GDF-15 expression levels are elevated in normal tissue as compared to tumor tissue in KIRC. Furthermore, within the tumor tissue itself, a significantly higher GDF-15 expression was observed in advanced pathological stages of KIRC (Figure 27A and B). There was no significant difference in GDF-15 levels in terms of Tumor-Node-Metastasis (TNM) staging or disease progression (data not shown). The expression level and prognostic value of GDF-15 and its associations with tumor macrophage infiltration in KIRC were assessed on TIMER2.0 based on cell-type identification by estimating relative subsets of RNA



transcripts (CIBERSORT), as described in Methods. After purity adjustment, M1 infiltration was negatively correlated with GDF-15 expression levels (Figure 27C).

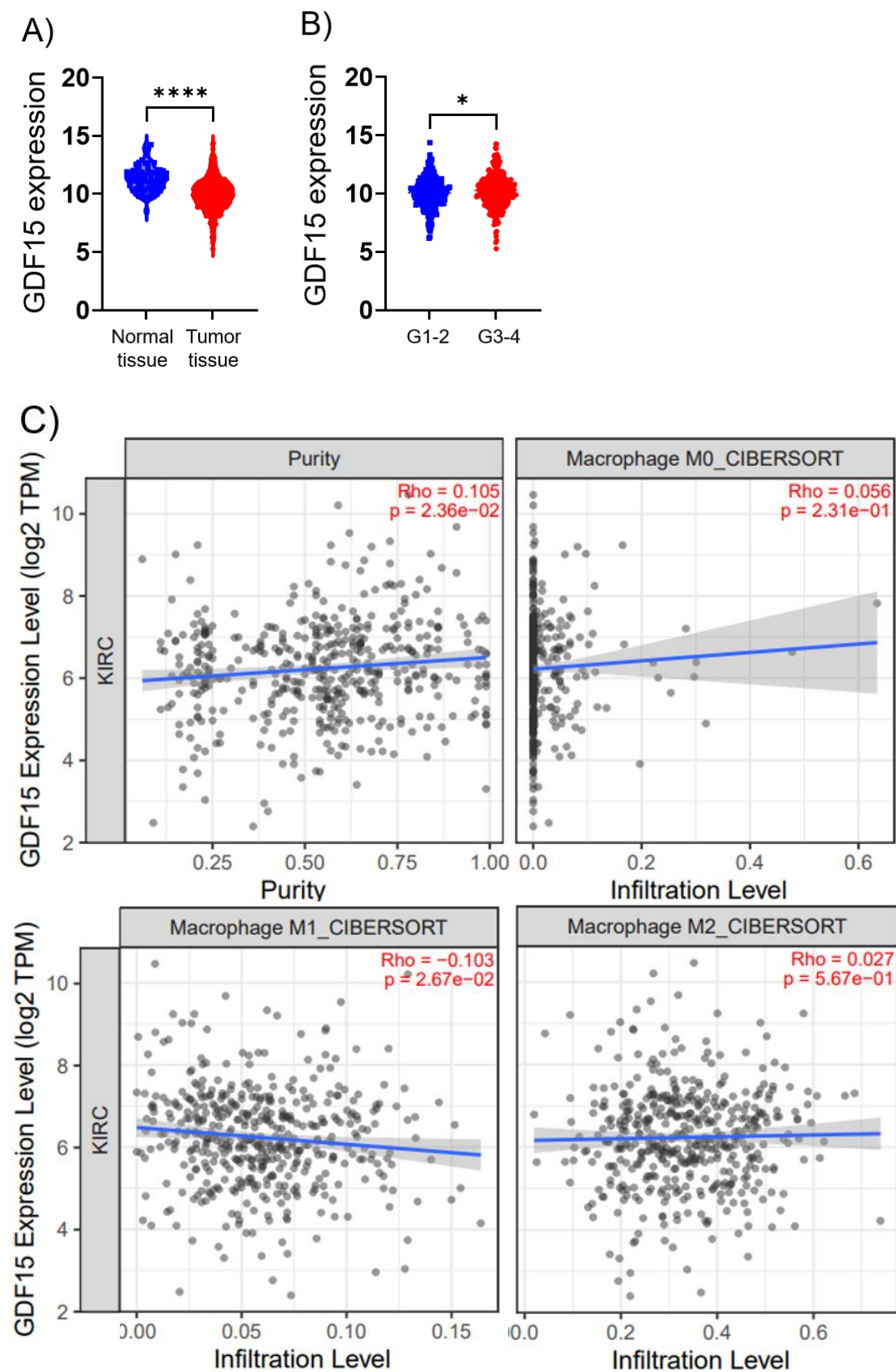


**Figure 27. GDF-15 expression levels in KIRC and its association to histologic stage and macrophage infiltration.** A) GDF-15 mRNA level in KIRC and their paired normal tissues assessed by Xena. B) The level of GDF- in histologic stage. C) Correlation between GDF-15 expression and the level of different macrophage subtypes infiltration in KIRC assessed by CIBERSORT, a bulk expression profile (TIMER 2.0). \* $<0,05$ , \*\*\*\* $<0,0001$ .

### 3.4.2 Abnormal expression of validated set of genes and its association with GDF15 expression in KIRC

Expression of the validated gene set was also evaluated in KIRC tissue compared to adjacent normal tissue using the Xena platform. CCL15, CLEC12A, GAS7, ID3, PMEPA1 and PTP4A3 were significantly higher in tumor tissue compared to normal tissue. In contrast, IL17RB and SMAD6 expression levels were higher in normal tissue compared to tumor tissue (Figure 28).

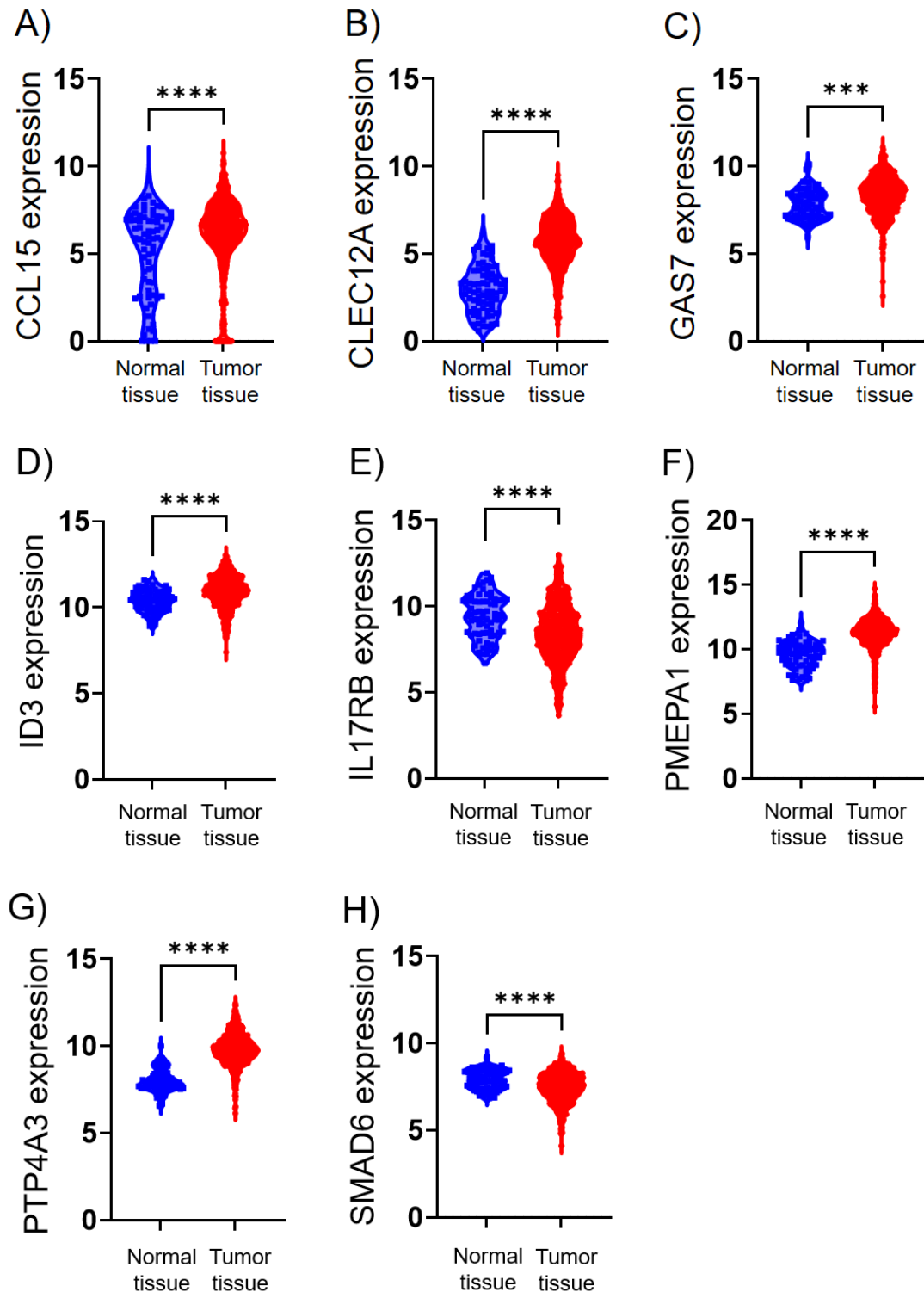


**Figure 28. Tissue-specific gene expression levels in KIRC and adjacent normal tissues** assessed by Xena based on TCGA. A) CCL15, B) CLEC12A, C) GAS7, D) ID3, E) IL17RB, F) PMEPA1, G) PTP4A3 and H) SMAD6. \*\*\* $p < 0.001$ , \*\*\*\* $p < 0.0001$ .

To assess the association between the validated gene set and GDF-15 expression in KIRC tissue, a correlation analysis was conducted using TIMER2.0. All genes showed a statistically significant correlation, except for ID3 and SMAD6 (Figure 29). Notably,

CCL15 and IL17RB showed a positive correlation with high tissue-specific GDF-15 expression levels, whereas CLEC12A, GAS7, PMEPA1 and PTP4A3 displayed a negative correlation. The direction of the correlation was consistent with the effect of rGDF-15 on macrophage gene expression of GAS7, IL17RB, and PTP4A3.

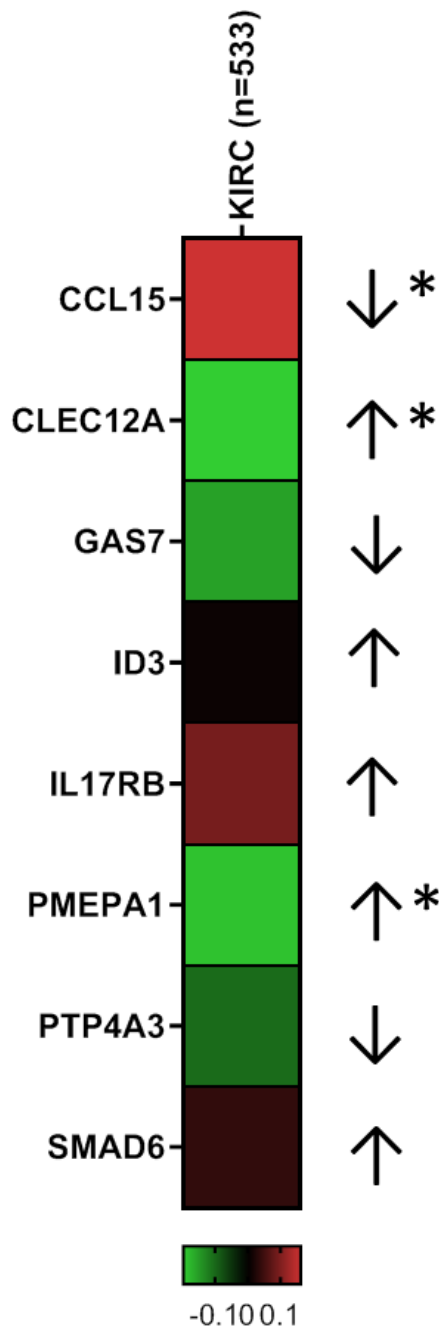
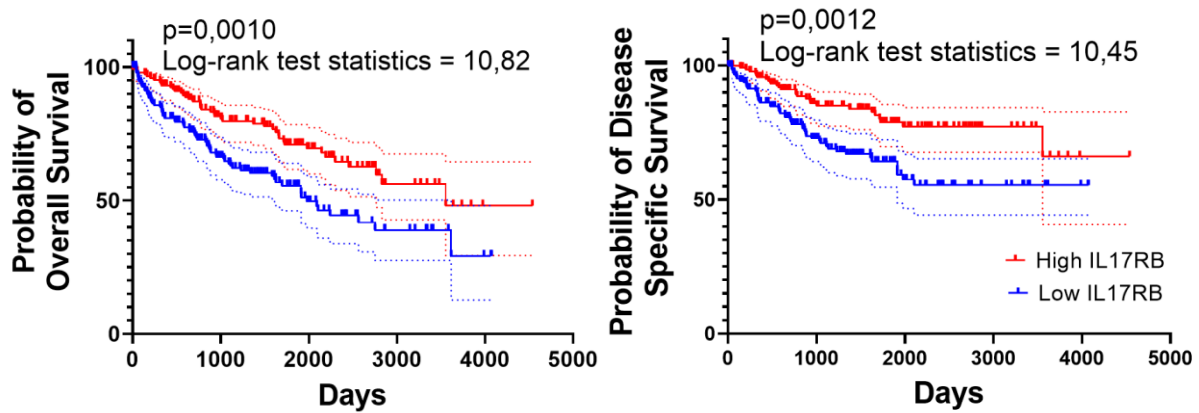


**Figure 29. Heatmap showing the correlation between tissue expression of GDF-15 and the genes validated by RT-PCR.** A negative correlation is indicated by the green color in the squares, while a positive correlation is indicated by red. The expression response to GDF-15 priming in macrophages, as assessed by RT-PCR, is represented by the direction of the arrow. The asterisks indicate genes where the GDF-15 tissue-specific expression direction was opposite to the gene expression validated by RT-PCR.

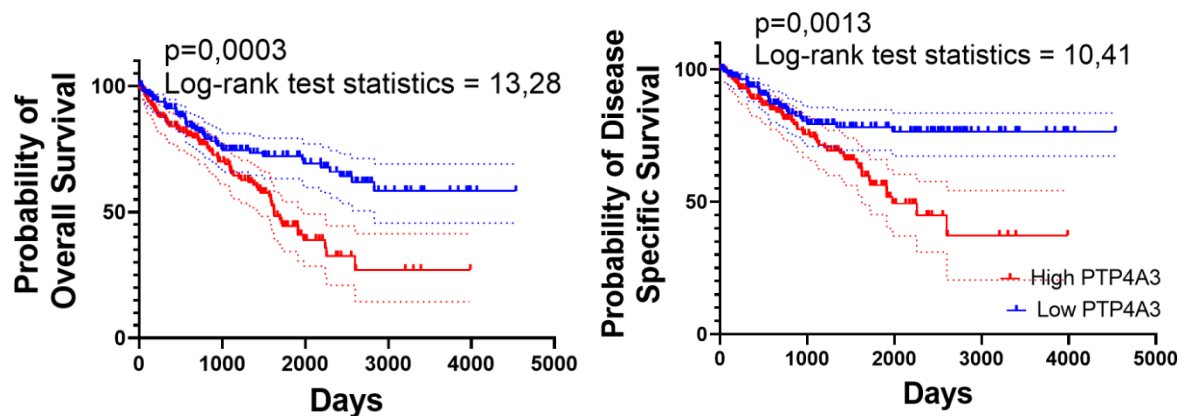
Further Kaplan-Meier curve analysis suggested that a lower IL17RB and SMAD6 expression was associated with poor survival outcomes (Figure 30A and C), whereas high PTP4A3 expression levels were indicative of poor overall survival and disease-

specific survival in patients with KIRC (Figure 30B). The remaining genes in the set showed no association with KIRC outcome (data not shown).

A)



B)



C)

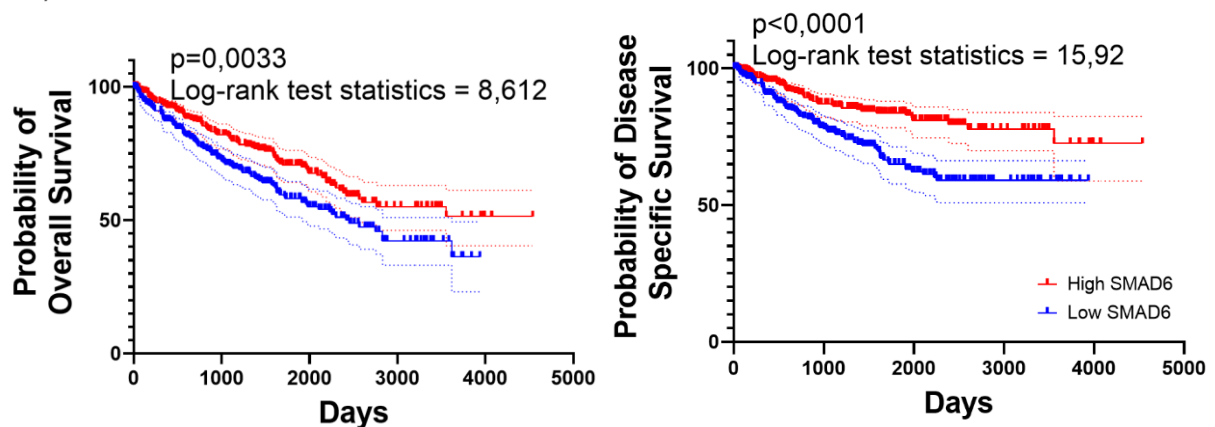


**Figure 30. Kaplan-Meier curves for tissue-specific gene expression levels on overall survival and disease specific survival of KIRC patients. A) IL17RB, B) PTP4A3 and C) SMAD6.**

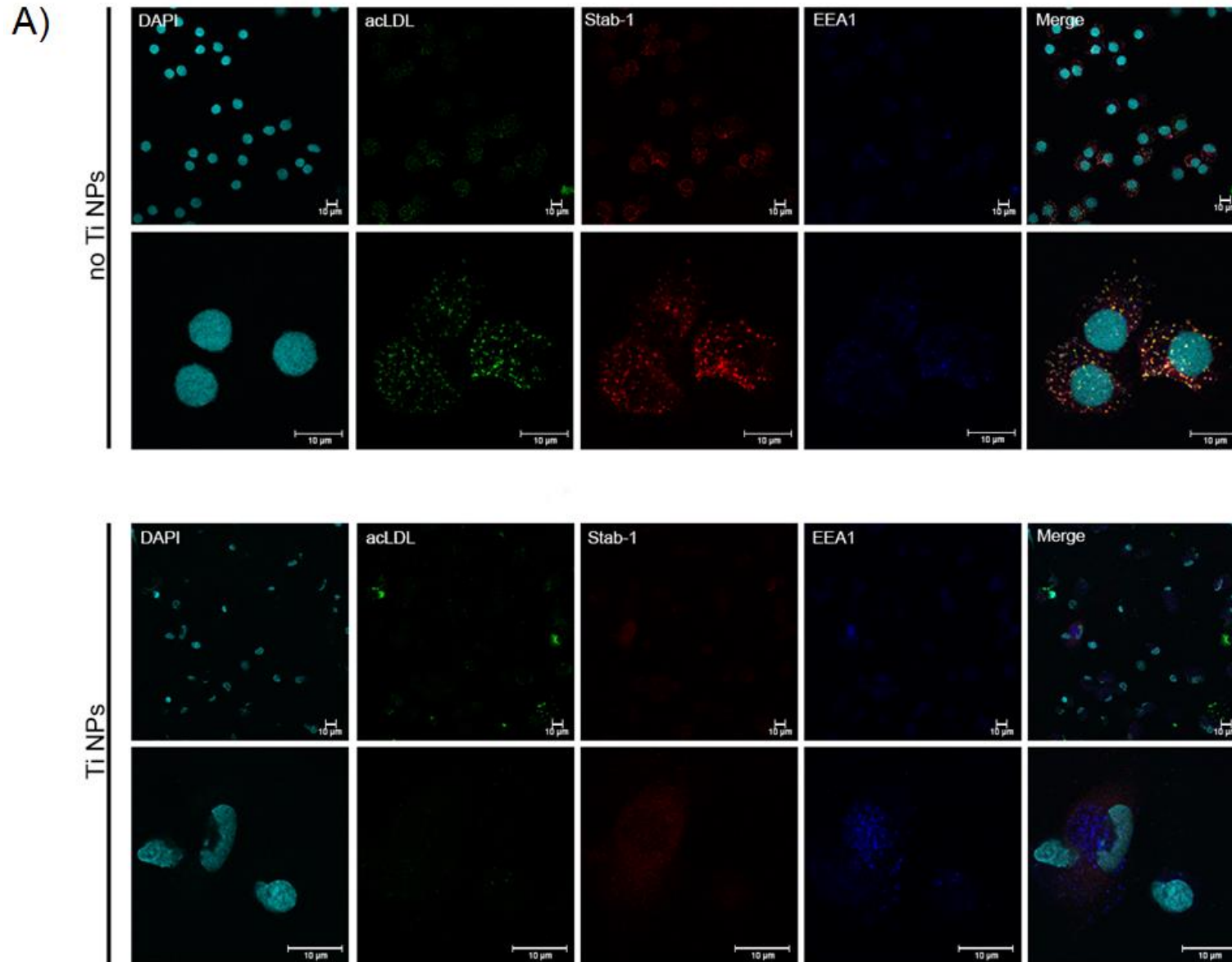
### 3.5 Association between GDF-15 and Stabilin-1

Finally, the role of stabilin-1, a known scavenger receptor for GDF-15, on the macrophage system was evaluated. For this purpose, the disruptive effect of TiNPs

was used to visualize the endocytosis mediated by stabilin-1 using confocal microscopy. The localization of stabilin-1 and its endocytic prototype ligand acLDL-Alexa488 was evaluated in M0, M1 and M2. EEA1-positive early/sorting endosomes is a major vesicular compartment, where stabilin-1 is localized<sup>27</sup>. Therefore, the intracellular localization of stabilin-1 using anti-EEA1 and anti-stabilin-1 rabbit polyclonal RS1 antibody was investigated. In the absence of TiNPs, macrophages expressed high levels of stabilin-1. Additionally, the majority of acLDL-Alexa488 was co-localized with stabilin-1 and was efficiently delivered to EEA1-positive early/sorting endosomes, while EEA1 marked irregularly shaped large endosomes (Figure 31). Treatment with TiNPs resulted in the disruption of endosomal compartment. Only a small amount of remaining EEA1+ endosomes was detected, and internalization of acLDL-Alexa488 was almost abrogated. After TiNPs treatment, stabilin-1 was expressed only in small percentage of macrophages, and only in stabilin-1+cells internalization of acLDL-Alexa488 was still detectable. The same treatment has previously been found in our laboratory to increase extracellular levels of GDF-15 in macrophages, partially due to the impaired ability of stabilin-1 to internalize GDF-15<sup>143</sup>.

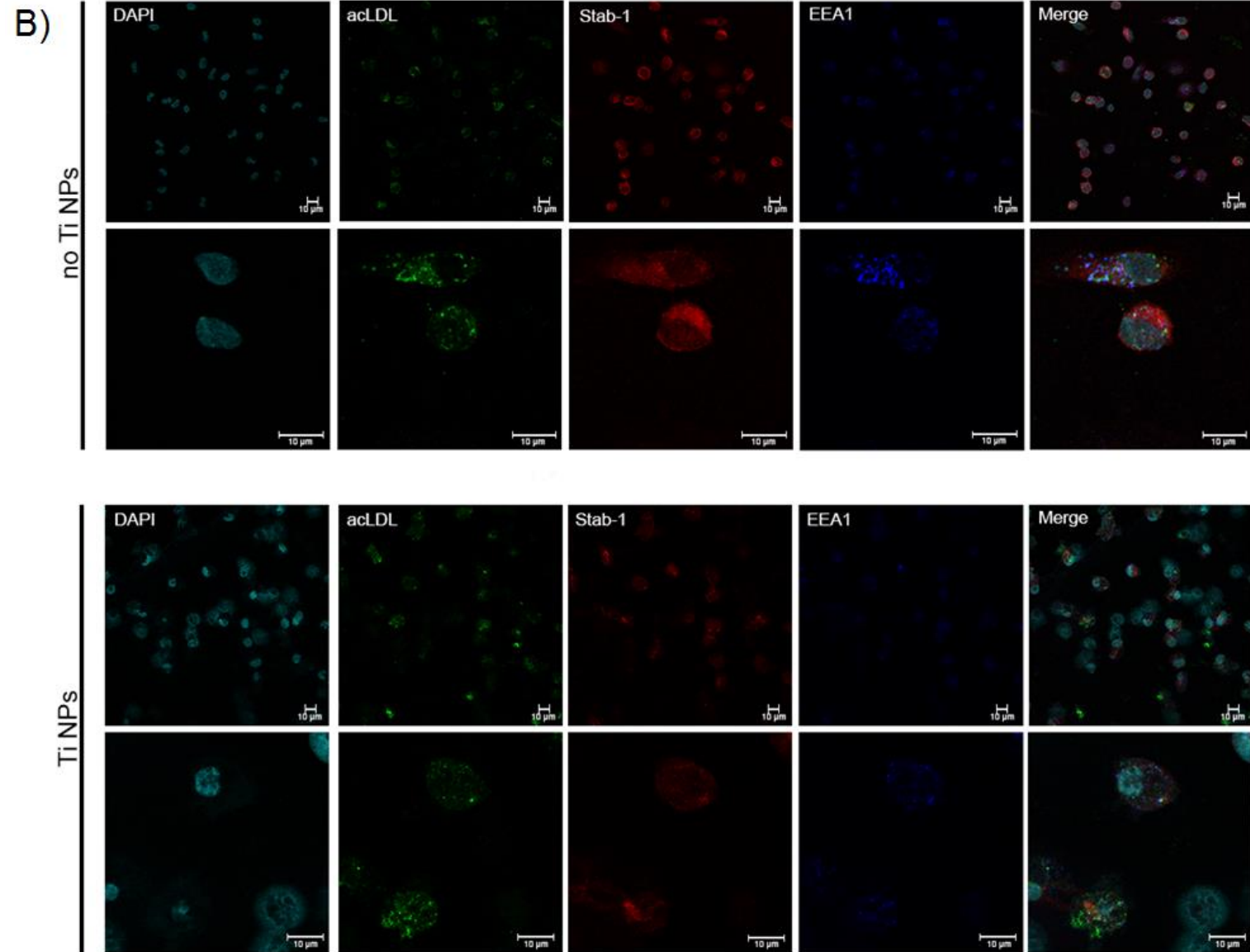
### 3.5.1 Abnormal expression of STAB1 and its association with GDF-15 expression in KIRC

Tissue expression of the stabilin-1 encoding gene STAB1 was next examined in KIRC tissue. Its expression was higher in tumor tissue compared to normal tissue. Furthermore, a negative correlation between GDF-15 and STAB1 expression in KIRC tissue was found. Finally, high levels of STAB1 expression were associated with worse overall and disease-specific survival in patients with KIRC (Figure 32).

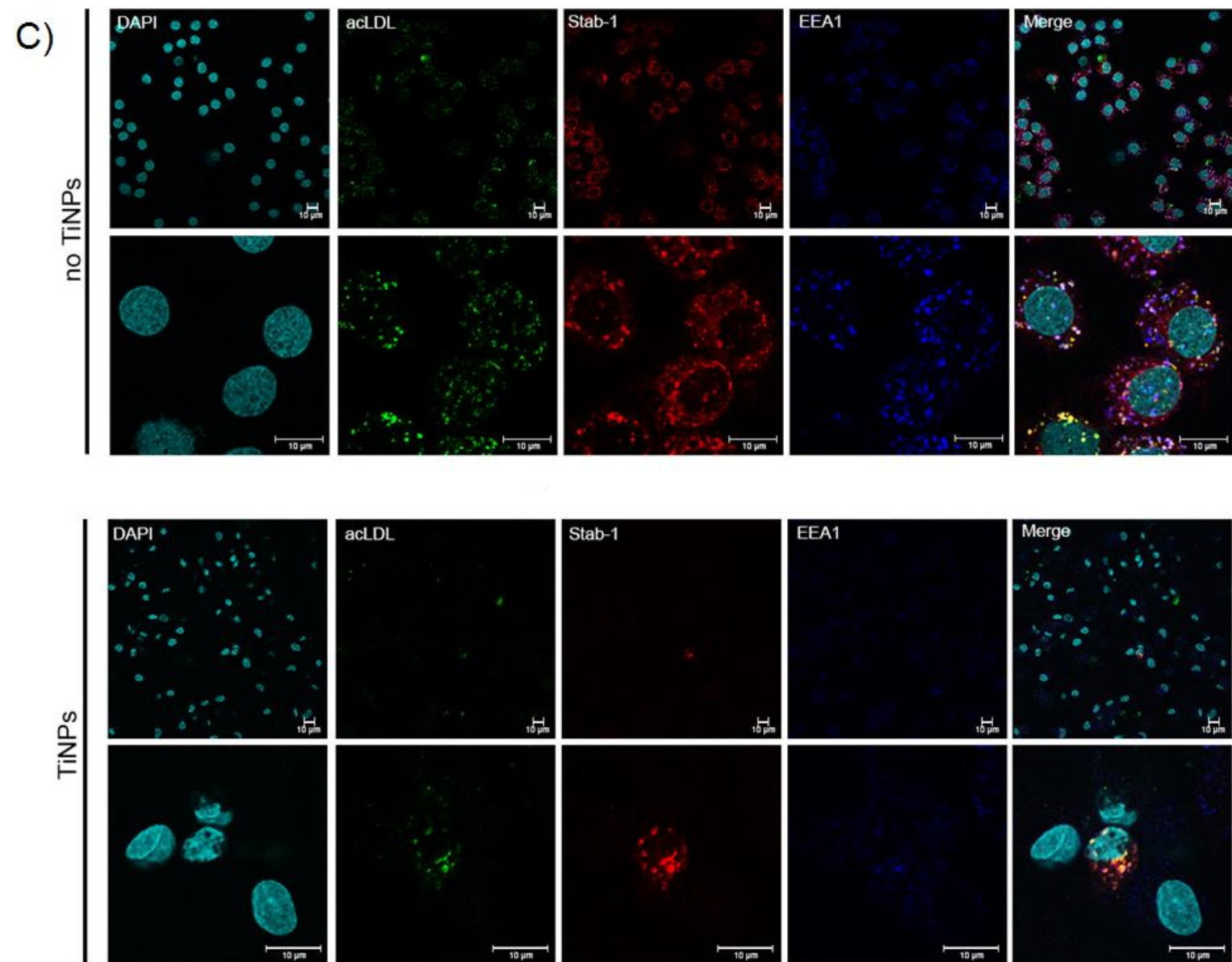


**Figure 31.** Immunofluorescence and confocal microscopy analysis of acLDL endocytosis in cultured M0, M1 and M2 after 6 days in absence or presence of TiNPs. Incubation with acLDL-Alexa488 at a concentration of 5 μg/mL was carried out for 30 minutes. Representative images of A) M0, B) M1 in and C) M2. Visualization of nuclei was performed using Dapi (shown in cyan). acLDL-Alexa488 is shown in green. Stabilin-1 was detected by immunofluorescent staining using RS1 rabbit polyclonal primary antibody and Cy3-conjugated anti-rabbit secondary antibody (shown in red). EEA was detected using anti-EEA mouse primary antibody and Alexa-647 secondary antibody (shown in blue). Representative images of single cells are shown for M2. Scale bars: 10 μm.









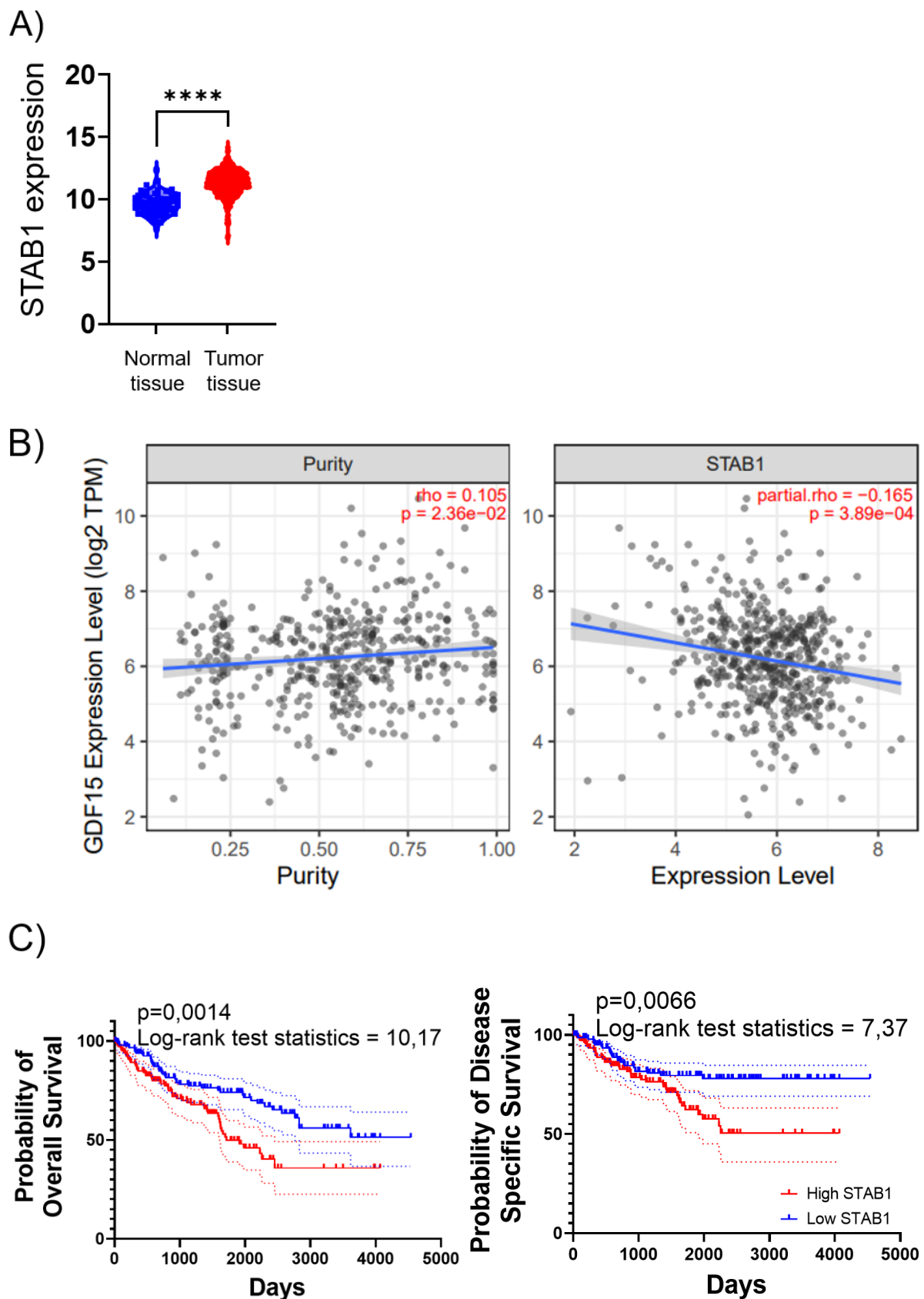


**Figure 32. Tissue-specific STAB1 expression in KIRC and adjacent normal tissues and survival analysis** assessed by Xena based on TCGA. \*\*\*\*<0,0001. A) STAB1 tissue-specific expression. B) Kaplan-Meier curves for tissue-specific STAB1 expression levels on overall survival and disease specific survival of KIRC patients

## 4 DISCUSSION

### 4.1 GDF-15 levels in human serum and in culture media from primary human macrophages

GDF-15 has consistently emerged as a marker of disease progression in various pathologic conditions, including cancer<sup>46, 123, 124</sup>. Previous studies have investigated GDF-15 serum levels in healthy individuals<sup>144</sup>. In this research project, a positive correlation between GDF-15 serum levels and increasing age was observed, which has been reported elsewhere<sup>94</sup>. Likewise, a positive correlation between GDF-15 levels and erythrocyte count was observed, in line with previous studies highlighting the role of GDF-15 in erythropoiesis and its increased expression in response to erythropoietin stimulation<sup>62</sup>. Moreover, GDF-15 secretion levels by differentiated primary human macrophages were assessed after 6 days of cytokine stimulation. The results revealed no significant difference in levels between the different macrophage phenotypes. These concentrations levels are consistent with those reported in the literature from other macrophage model systems, including PBMCs under M-CSF stimulation and TAMs<sup>145</sup>. However, it should be noted that the concentration of GDF-15 in the macrophage conditioned medium was significantly lower than the average in human serum. Nevertheless, as with other cytokines, elevated serum levels of a protein do not necessarily correlate with increased activity in target tissues. In addition, cytokines often have higher levels in tissue than in serum and in culture, especially during inflammation or tissue damage<sup>146</sup>. For example, GDF-15 concentration in placenta can be as high as 54000 pg/mL<sup>50</sup>. Based on this understanding, a wide range of rGDF-15 concentrations, spanning from 10 to 100 ng/mL for the treatment of macrophages in culture, were selected as explained in the results section.

#### 4.2 Effect of rGDF-15 on the macrophage response to LPS-mediated inflammation

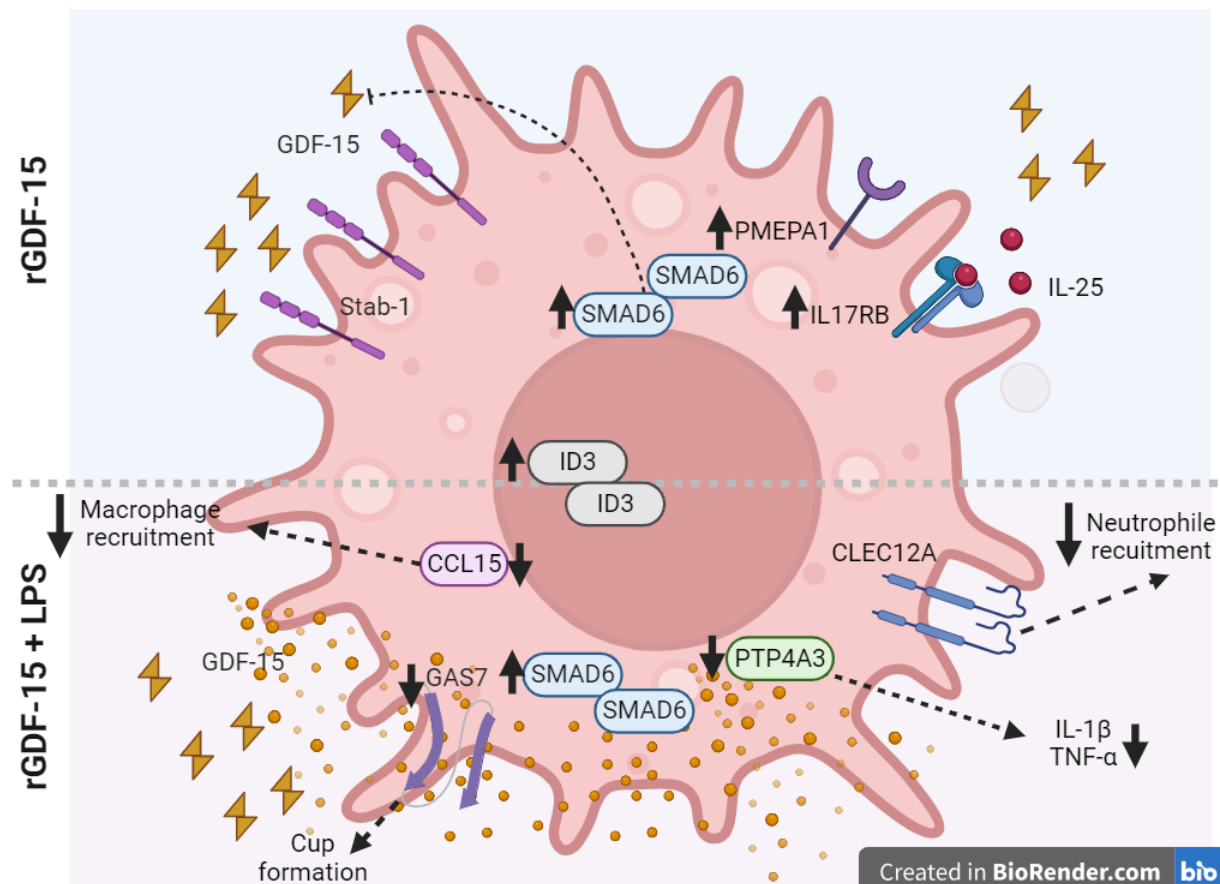


**Figure 33. Schematic representation** of the effects of rGDF-15 on the macrophage system and on macrophage response to inflammation. Created with Biorender.com.

In this project, the impact of varying concentrations of rGDF-15 on M0 (non-stimulated), M1 (pro-inflammatory) and M2 (anti-inflammatory) macrophages was evaluated. In the initial phase of the study, the effect of rGDF-15 pre-stimulation at concentrations of 10, 25, 50 and 100 ng/mL on the expression of the pro-inflammatory cytokines, specifically TNF- $\alpha$  and IL-1 $\beta$ , following exposure to LPS, was assessed using different experimental settings. In all models tested, rGDF-15 significantly reduced the expression of TNF- $\alpha$  after LPS challenge. This effect of GDF-15 has been well known since its discovery. However, this may be different in other macrophage settings, as shown by Li et al., who, in contrast, demonstrated high levels of IL-1 $\beta$  and IL-6 expression after 48 hours of rGDF-15 supplementation in RAW264.7, indicating an induction of M1 polarization by rGDF-15<sup>147</sup>.

Among the experimental models, only the model 3 exhibited a dose-dependent effect. For this reason, the following experiments were performed using this experimental setting. For the upcoming transcriptomic analysis, a concentration of 50 ng/mL rGDF-15 was selected, which was previously shown not to promote an increase in apoptotic

activity in THP-1 cells after 72 hours of incubation<sup>70</sup>. Given the obtained RT-PCR results showing that rGDF-15 has a greater effect on the regulation of the M0 and M2 responses to LPS, the focus was directed to these phenotypes, and M1 was excluded from the RNA-Seq.

Unlike other reported stimulation models, the model used in this study included the identification of the primary effects of rGDF-15 on the pro-inflammatory transcriptome of macrophages after of rGDF-15 priming and without LPS exposure. A similar approach was used by Li et al., who used M2-polarized THP-1 cells and pretreated them with rGDF-15 for 30 minutes prior LPS challenge for 8 hours (2 µg/mL). They found increasing GDF-15 expression and secretion levels with the increasing LPS stimulation and concentration<sup>67</sup>. Conversely, in this project, no change in GDF-15 expression was found after 6 hours of LPS exposure in the different macrophage phenotypes (Supplementary Figure 8). Consistent with the findings reported here, Li et al. also found that the pretreatment with rGDF-15 resulted in a dose-dependent decrease in the expression of pro-inflammatory cytokines, such as TNF-α, IL-6, MCP-1 and IL-10<sup>67</sup>. This trend was also evident here, even at lower doses of rGDF-15 (10 and 25 pg/mL) and lower LPS concentration (100 ng/mL). Similar experiments were conducted by Govaere et al., who showed decreased TNF-α and CCL2 secretion after treatment with rGDF-15 in THP-1 cells challenged with LPS<sup>116</sup>. Possible molecular pathways responsible for the decreased secretion of pro-inflammatory cytokines under GDF-15 exposure have been proposed. Zhang et al. found that rGDF-15 promoted PI3K/Akt phosphorylation in macrophages under LPS-induced inflammation. This effect was reduced by treatment with the PI3K/Akt inhibitor LY294002<sup>148</sup>. Other research groups proposed the decrease in phosphorylation of JAK1/STAT3 and nuclear translocation of NF-κB after rGDF-15 treatment as potential pathways for GDF-15<sup>149</sup>. However, no specific receptor has been proposed to mediate this effect.

To date, this study represents the first investigation of the impact of rGDF-15 on the transcriptome of human macrophages. The experimental model successfully revealed an appropriate clustering pattern among sample repetitions, highlighting the validity of the RNA-Seq. The RNA-Seq results demonstrated that rGDF-15 pretreatment of activated macrophages induces specific transcriptional responses that are distinct from those induced by LPS. Nevertheless, the effect of LPS on macrophage transcriptome

was strong enough that macrophages pretreated with rGDF-15 and subsequently challenge with LPS still clustered with macrophages only challenged with LPS in the PCA.

The GO analysis provided a more detailed insight into the significant genes related to functional groups. The results of the thesis project revealed that the enriched GO terms in M0 and M2 pretreated with rGDF-15 were mainly associated to angiogenesis, immune regulation and cell adhesion. Interestingly, there was little difference in the altered GO terms between M0 and M2. In the groups challenged with LPS, the most upregulated GO terms were associated with TGF- $\beta$  interaction and to receptor complex formation, whereas pathways associated with nucleic acid metabolism and inflammatory response were downregulated. Regarding the KEEG analysis, both M0 and M2 exhibited “Pathways in cancer” as the most significant term after rGDF-15 treatment. Taken together, the GO terms highlighted altered molecular processes relevant to cancer pathogenesis that contribute to cancer progression and metastasis. Therefore, the final steps of the project focused on assessing GDF-15 expression in the most prevalent cancer types, as elaborated in the following sections.

A total of 13 genes that were differentially expressed and displayed maximum fold change in the comparison groups, were selected for further evaluation. All of the selected DEGs were found to be common to at least two of the comparison groups. 8 genes, namely CCL15, CLEC12A, GAS7, ID3, IL17RB, PMEPA1, PTP4A3 and SMAD6, passed the validation analysis in at least one of the comparison groups (see Table 22). Figure 33 summarizes the results of the effects of rGDF-15 in the macrophage system and its possible implications.

The transcriptomic analysis revealed for the first time, the significant upregulation of IL17RB as a downstream protein following rGDF-15 supplementation. IL17RB expression levels have been reported to rise in M2-activated macrophages and after the treatment with IL-4 and TGF- $\beta$ <sup>150</sup>. IL17RB serves as a receptor for IL-25, also called IL-17E, a Th2 cell-derived cytokine. Interestingly, both IL-25 and GDF-15 have been associated with increased thermogenesis in adipose tissue and increased mitochondrial respiratory capacity in macrophages during high-fat diet-induced obesity in mouse models. In this context, IL-25 promotes M2 polarization, decreases pro-inflammatory cytokine release by macrophages and increases catecholamine release in adipose tissue<sup>97, 151</sup>.

In the here presented model system, the supplementation with rGDF-15 leads to a significant increase in IL17RB expression across all macrophage phenotypes (Figure 22). However, there was no significant difference in IL-25 expression after rGDF-15 treatment on RNA-Seq results (data not shown). Nevertheless, an increased surface presence of IL17RB can potentially enhance the effect of IL-25 on macrophages, thereby contributing to increased macrophage activation and recruitment within tissues. Therefore, the effects of IL-25, such as increased thermogenesis, may be enhanced after rGDF-15 priming. To date, there are no reports available linking GDF-15 and IL-25/IL17RB pathways. Although the effect of GDF-15 on metabolic pathways has been studied and explained by binding to its receptor GFRAL/RET in neurons in the area postrema and nucleus of the solitary tract, it remains uncertain whether GDF-15-mediated effects on thermogenesis can result from heightened sensitivity to IL-25 due to increased availability of IL-17RB<sup>83</sup>. This hypothesis may provide insight into the peripheral effects of GDF-15 observed during its supplementation in vitro, independent of GFRAL/RET activation. In addition, GDF-15 supplementation activates downstream pathways that are also activated by IL25/IL17RB binding, including NF- $\kappa$ B, MAPK, JAK and STAT3<sup>46, 152</sup>.

The increased IL17RB expression after rGDF-15 treatment aligns with the recognized effect of GDF-15 on macrophage polarization towards the M2 phenotype<sup>66</sup>. Regarding the influence of rGDF-15 after LPS challenge, increased IL17RB expression was observed in M0 and M2 primed with rGDF-15 and then challenged with LPS. In contrast, LPS challenge alone had little to no effect on IL17RB expression in macrophages. No other authors have investigated this scenario before, but since IL17RB is predominantly expressed by tolerogenic macrophages, it is reasonable to expect that its expression levels would remain low after LPS challenge. Supporting this perspective, IL17RB expression did not exhibit significant differences in M1 macrophages primed with rGDF15 and challenged with LPS compared to those challenged with LPS alone. Contrastingly, studies involving other cell lines, such as human nasal epithelial cells and atopic dendritic cells, showed an increase in IL17RB protein expression after LPS treatment<sup>153, 154</sup>. Other authors have shown that the supplementation with rIL-25 after LPS treatment led to an increased tolerogenic response in adipocytes and M1 polarized macrophages, which showed decreased expression of IL-6, IL-23, TNF- $\alpha$ , IL-1 $\beta$  and CCL15<sup>155, 156</sup>. This mechanism may explain

the known anti-inflammatory effects of rGDF-15 on the macrophage system during LPS treatment. In this context, rGDF-15 may increase the availability of IL17RB, thereby facilitating the binding of IL-25, which may contribute to the anti-inflammatory effects during low-grade inflammation. The data presented here provide evidence for a sustained effect of rGDF-15 on IL17RB expression even after 6 hours of LPS challenge.

Likewise, CLEC12A is highly expressed throughout the monocyte/macrophage system. It is well documented that CLEC12A expression is downregulated during inflammation. CLEC12A decreases neutrophil recruitment, ROS production and IL-8 secretion, serving as a regulator of hyperinflammation<sup>157</sup>. This study demonstrated that CLEC12A is upregulated in rGDF-15-primed M0 and M1 macrophages following exposure to LPS. This finding strengthens the hypothesis that rGDF-15 has an anti-inflammatory role during macrophage inflammation. Another noteworthy finding contributing to this hypothesis is the increased ID3 expression in M2 primed with rGDF-15, regardless of LPS challenge. Previous research has shown that ID3 expression decreases after IFN/LPS treatment but increases after exposure to IL-10, dexamethasone, TGF- $\beta$ , and CD5L, all of which are known drivers of M2 polarization<sup>133, 158</sup>. SMAD6 is another downstream gene of TGF- $\beta$ , and it is recognized that SMAD6 acts as an inhibitor of TGF- $\beta$  in a negative feedback mechanism through various molecular pathways<sup>141</sup>. Here, it was reported that rGDF-15 treatment significantly increased SMAD6 expression levels in M0 and M2 phenotypes. This is consistent with the literature reporting an increase in SMAD6 levels upon TGF- $\beta$  treatment<sup>159</sup>. Other researchers have also demonstrated that LPS treatment increases SMAD6 expression in murine macrophages, with SMAD6 playing a role in promoting M2 polarization and accelerating wound healing in mouse models<sup>160</sup>.

Expression PMEPA1, a transmembrane protein that contains a Smad interacting motif, has been associated with the M2 phenotype and TAMs, particularly within a distinct macrophage subset expressing Arg-1B that has been found to be localized to the tumor periphery in cervical cancer mouse models<sup>161, 162</sup>. Here, PMEPA1 expression was found to be minimal in unstimulated macrophages, while the addition of rGDF-15 to culture in M0 and M2 phenotypes significantly promoted its upregulation. These results highlight PMEPA1 as a marker of M2 differentiation following rGDF-15 treatment.



Additionally, rGDF-15 was effective in maintaining increased PMEPA1 expression even after LPS challenge in both M0 and M2 phenotypes, emphasizing the acute and stable effect of rGDF-15 on the macrophage transcriptome.

This analysis showed for the first time an increased PMEPA1 expression level in macrophages primed with rGDF-15 and challenged with LPS compared to those challenged with LPS alone. PMEPA1 expression levels in M0 were higher after LPS challenge compared to control, which was also previously unknown. These results suggest that the rGDF-15/PMEPA1 axis may be relevant in low-grade inflammation.

PTP4A3 (protein-tyrosine phosphatase) and CCL15 (chemotactic factor for neutrophils, monocytes, and lymphocytes) expression levels were increased only after LPS challenge in the macrophage system and were almost undetectable in differentiated macrophages treated and non-treated with rGDF-15. Therefore, the inhibitory effect of rGDF-15 was only visible in macrophages challenged with LPS, highlighting that CCL15 and PTP4A3 expression may be only detectable in the macrophage system during low-grade inflammation. Interestingly, in triple-negative breast cancer cells, PTP4A3 expression was shown to be positively regulated by NF- $\kappa$ B pathway, a pathway that is downregulated in macrophages upon exposure to rGDF-15<sup>138, 149</sup>. This shared mechanism may explain the downregulatory effect of rGDF-15 on PTP4A3 expression. In addition, PTP4A3 has been shown to promote dephosphorylation of p38 MAPK in LPS-treated macrophages, resulting in decreased expression of pro-inflammatory cytokines such as TNF- $\alpha$  and IL-1 $\beta$ <sup>163</sup>. In the presented setting, a decreased PTP4A3 expression upon rGDF-15 priming may help to explain the low levels of TNF- $\alpha$  and IL-1 $\beta$  evidenced in the first part of the project.

Another candidate gene found to be downregulated upon rGDF-15 exposure was GAS7. This was particularly evident in M0 during LPS challenge. In the M1 setting, GAS7 expression was similar among the different M1-comparison groups, except in M1 primed with rGDF-15 and challenged with LPS, where its expression was decreased. It was already published that GAS7 expression increases during M1 polarization, a process that depends on NF- $\kappa$ B activation. Additionally, its expression levels have been evidenced to be higher in M1 compared to M0 and M2<sup>132</sup>. Furthermore, the decreased expression of GAS7 could be translated into a decreased phagocytosis capacity, as it was demonstrated that GAS7 is involved in the membrane cup formation during phagocytosis in macrophages<sup>131</sup>. Among all macrophage

phenotypes, the condition with the lowest GAS7 levels was rGDF-15 + LPS. However, a statistical significance was not reached between all the comparison groups, probably due to the lack of sufficient replicates (n=4).

#### 4.3 GDF-15 expression patterns and implications in cancer: focus on kidney renal clear cell carcinoma (KIRC) and tumor microenvironment

In this study, a differential expression of GDF-15 was observed in the most prevalent cancers. In most of them GDF-15 expression levels were elevated in tumor tissue compared to normal tissue, except for KIRC, in which GDF-15 levels were higher in normal tissue. KIRC is the most common type of renal cancer and the leading cause of death among renal cancers due to its high metastatic potential and late diagnosis. There is an urgent need to better understand the molecular mechanisms involved in KIRC progression and metastasis<sup>164</sup>. To date, the role of GDF-15 in KIRC has not been explored. However, KIRC is known to have an important immunogenic component and one of the main therapies against it is immunotherapy<sup>164</sup>.

Collectively, GDF-15 has been reported to exert pleiotropic effects on carcinogenesis. Regarding primary tumor growth, rGDF-15 has been shown to promote proliferation of esophagus carcinoma cells<sup>145</sup>. In contrast, in bladder cancer, GDF-15 has been demonstrated to decrease cell proliferation and invasion<sup>54</sup>. Additionally, GDF-15 promotes angiogenesis by activating the hypoxia-inducible factor-1 $\alpha$  (HIF-1 $\alpha$ )/VEGF signaling pathway in colorectal cancer<sup>124, 165</sup>. This is supported by the observation that rGDF-15 promotes p53 degradation, increased HIF-1 $\alpha$  accumulation and vessel formation in human umbilical vein endothelial cells<sup>166</sup>.

GDF-15 also plays a role in the tumor microenvironment. Recently, YKL-40 produced by macrophages was shown to promote GDF-15 expression in tumor cells<sup>167</sup>. The interaction of YKL-40 and GDF-15 leads to tumor invasion and suppression of the immune answer from CD8+ T lymphocytes through the induction of PD-L1 in gallbladder tumor cells<sup>167</sup>. This was also evidenced in glioblastoma cells<sup>168</sup>. In support of this observation, patients with low plasmatic levels of GDF-15 show better response rates to anti-PD-1/PD-L1 inhibitors in advanced non-small-cell lung cancer<sup>169</sup>. The use of GDF-15 as a marker for patients who would benefit from such therapy may be a valuable option in KIRC, where anti-PD-1/PD-L1 inhibitors are used as first-line therapy in intermediate- and poor-risk metastatic tumors<sup>164</sup>.

Elevated GDF-15 has been strongly associated with metastasis in prostate cancer, esophageal, hepatocellular colorectal cancer, pancreatic, gastric and endometrial cancers<sup>170</sup>. Esophageal, breast and colon cancer models show that GDF-15 correlates with the loss of E-cadherin and that the inhibition of GDF-15 expression decreases cell migration and invasion ability<sup>87, 171, 172</sup>. In contrast, in A549 lung cancer cells, an overexpression of GDF-15 reduces cell growth and migration and decreases the spread of lung and bone metastases<sup>173</sup>. The exact effects and mechanisms explaining GDF-15 behavior in cancer are still controversial and often paradoxical. This may be explained by epigenetic modifications. For example, in bladder cancer, hypermethylation of the GDF-15 promoter has been detected and the level of hypermethylation diminishes with tumor progression<sup>174</sup>. N-glycosylation of GDF-15, an additional epigenetic modification, has been evidenced during prolonged treatment with androgen receptor inhibitors in PRAD<sup>175</sup>.

A logical approach to understand the effects of GDF-15 in cancer, and in KIRC, is to examine its downstream activated genes in one of the most important members of the tumor microenvironment, macrophages. An overview of the effects of the GDF-15-induced genes on carcinogenesis is shown in Figure 34. Among them, only IL17RB, PTP4A3 and SMAD6 showed a significant association with KIRC clinical outcomes in the bioinformatics analysis.

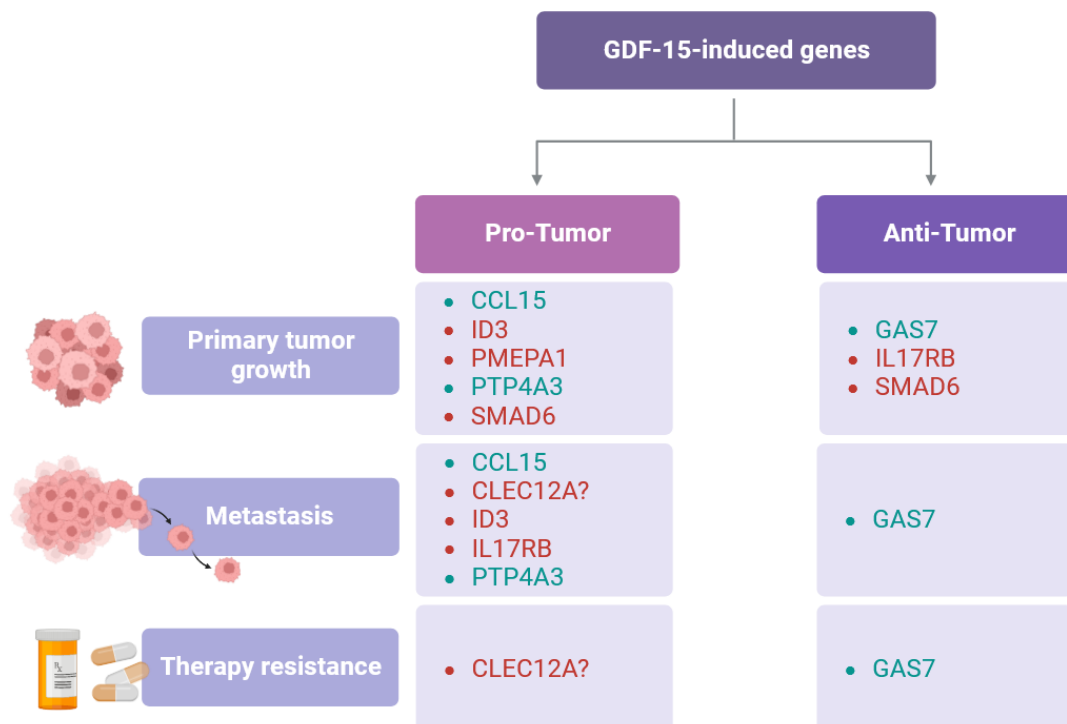


**Figure 34. Overview of the effect of GDF-15-induced genes in carcinogenesis.** Genes in red represent those genes that were upregulated and in green those that were downregulated after the rGDF-15 treatment in the in vitro model. Created with Biorender.com.

A positive correlation was found between GDF-15 and IL17RB expression levels in KIRC. Accordingly, both genes showed low expression levels in KIRC compared to normal tissue. In addition, low IL17RB was associated with worse overall and disease-specific survival in patients with KIRC. In contrast, in pancreatic cancer, IL17RB has been found to inversely correlate with progression-free survival, and its elevated expression levels were associated with metastasis<sup>176</sup>. Low expression of IL17RB may result in reduced availability of IL17RB on the cell surface and consequently reduced IL-25 binding. Some authors have suggested that IL-25 promotes metastasis and others have demonstrated anti-tumor properties by inducing tumor apoptosis<sup>177, 178</sup>. SMAD6 was also found to be upregulated in normal tissue compared to KIRC tissue and its high expression levels correlated with better overall and disease-specific survival in KIRC patients<sup>179</sup>. The same finding was previously reported in KIRC tissue and was associated with aberrant hypermethylation of promoter regions within the SMAD6 genes<sup>180</sup>. Accordingly, in the in vitro experiments presented here, rGDF-15 treatment increased SMAD6 expression, which is consistent with the observation that GDF-15 and SMAD6 expression levels are also elevated in normal tissue compared to KIRC tissue. Although GDF-15 expression levels in KIRC were not associated with the clinical outcomes analyzed, SMAD6 and IL17RB expression levels were. This highlights a downstream mechanism by which GDF-15 may exert its effects in carcinogenesis and tumor progression. In contrast to the transcriptome signature of KIRC, other cancers, such as colon and lung cancer, show high levels of SMAD6 in tumor tissue, which is associated with poor prognosis<sup>181</sup>.

PTP4A3 has been consistently implicated in increased tumor proliferation and metastasis through apoptosis prevention, angiogenesis, and genome instability in several cancer types<sup>182</sup>. PTP4A3 expression in the macrophage system is low in most body tissues, except for the kidney<sup>183</sup>. As reported here in KIRC, Song et al. showed increased PTP4A3 expression levels in papillary renal cell carcinoma tissue compared to normal tissue, which was also associated with poor prognosis and with proliferation, migration and invasion<sup>140</sup>. In the in vitro experiments, rGDF-15 priming significantly decreased PTP4A3 expression in macrophages challenged with LPS. This is consistent with the gene expression correlation in KIRC tissue showing that GDF-15 negatively correlates with PTP4A3 expression.

In the bioinformatic analysis, CCL15, CLEC12A, GAS7, ID3 and PMEPA1 were significantly upregulated in KIRC tissue compared to normal tissue. However, their expression was not associated with the evaluated clinical outcomes. High expression of CCL15, ID3 and PMEPA1 has been associated with progression and invasion in several tumors<sup>128, 184, 185</sup>. CLEC12A is highly expressed in leukemic blasts and negatively correlated with survival and treatment response in acute myeloid leukemia<sup>186</sup>. As a modulator of the exuberant inflammatory response, CLEC12A may contribute to cancer progression, metastasis and immune escape<sup>157</sup>. However, this hypothesis has not yet been tested. GAS7 is predominantly expressed by macrophages in the kidney; this increased GAS7 expression may indicate a higher macrophage infiltration, particularly M1, for which GAS7 is a marker<sup>132, 183</sup>. GAS7 negatively correlated with GDF-15 expression levels in tumor tissue, which is consistent with the in vitro results showing that rGDF-15 decreases GAS7 expression. This is also consistent with the negative correlation of GDF-15 and M1 infiltration in KIRC tissue found in the bioinformatics analysis. GAS7 has been proposed as a metastasis suppressor in breast cancer, non-small cell lung cancer and in neuroblastoma, and its increased expression has been associated with an increased sensitivity to therapy<sup>187-189</sup>.

In conclusion, the bioinformatics approaches used here provide an essential tool to link the most relevant downstream GDF-15-regulated genes in the macrophage system to pathology. These genes were associated with angiogenesis, leukocyte migration, tissue remodeling and wound response, pathways that are implicated in carcinogenesis. Taken together, it is difficult to identify a single effect of GDF-15 in cancer, which, as explained above, is rather pleiotropic. However, GDF-15-induced genes with an impact on KIRC survival tend to show that supplementation with rGDF-15 may have a beneficial effect on KIRC by increasing the expression of IL17RB and SMAD6 and by decreasing PTP4A3. Further studies are needed to further elucidate the role of GDF-15 in KIRC.

#### 4.3.1 Stabilin-1 expression in the macrophage system and its implications in GDF-15-mediated processes with a focus on KIRC

Our previous experiments have shown that macrophages exposed to TiNPs respond by increasing the expression and secretion of GDF-15. We also found that TiNPs decreased the expression of stabilin-1, a clearance receptor of GDF-15, in macrophages<sup>143</sup>. Here, the effect of TiNPs on the presence of stabilin-1 in the different

macrophage phenotypes was evaluated using confocal microscopy. Overall, immunofluorescence analysis confirmed the suppressive effect of TiNPs on Stabilin-1 expression at the protein level and stabilin-1 mediated endocytosis. This effect was particularly evident in M0 and M2, which were positive for stabilin-1 in the endocytic compartment. In contrast, M1 expressed stabilin-1 mainly peripherally on the plasma membrane. A decreased presence of stabilin-1 could further increase the local levels of GDF-15 and contribute to inadequate implant osseointegration and aseptic loosening, as it has been shown by others that GDF-15 can induce osteoclastogenesis-related genes expression in osteoclasts<sup>74</sup>.

Stabilin-1 is highly expressed in TAMs and has pro-tumoral functions, including the clearance of anti-tumor factor SPARC and intracellular targeting for secretion of YKL39, which induces angiogenesis<sup>190-192</sup>. In overall, the presence of stabilin-1 in tumor tends to be associated to a poorer prognosis<sup>18</sup>.

In the bioinformatics analysis, STAB1 was highly expressed in KIRC tissue compared to normal tissue and this elevation is inversely associated with GDF-15 expression. Interestingly, high STAB1 expression levels correlated with worse survival in KIRC patients. One intriguing possibility is that an increased presence of STAB1 might contribute to an increased clearance of GDF-15 in tumor tissues, resulting in decreased expression of GDF-15-induced genes in tumor tissues, such as IL17RB and SMAD6, while promoting an increased expression of PTP4A3, which is downregulated by rGDF-15 in the macrophage system, as demonstrated here. This hypothesis remains to be tested and could partially explain the transcriptomic signature of KIRC shown in this study. The combination of increased GDF-15 transcription and impaired clearance via stabilin-1 may represent a mechanism by which macrophages maintain their capacity to restrain tumor growth.

The current study provides new insights to better understand GDF-15 function in the macrophage system. A limitation of this work is that the stimulation model used is inherently limited in examining the spectrum of macrophage activation beyond the M1 and M2 states. Recent research has shown that macrophage plasticity extends beyond these two states to include a more diverse and complex spectrum of macrophages with overlapping functions<sup>6</sup>. Thus, the understanding of macrophage activation and function is far from complete, and future studies should consider exploring a broader range of activation states and their functions. Another limitation is that there are still inconsistencies in the literature regarding the mechanism by which GDF-15 mediates

its peripheral effects, in this case its effects on the macrophage system. In particular, no definitive rGDF-15 receptor has been identified on macrophages. It is likely that GDF-15 uses TGF- $\beta$  receptors to be internalized by macrophages, as described above. Other authors have suggested an upregulation of GFRAL/RET under stress conditions and in tumors in osteoblast and prostate carcinoma cells, which could explain the effect of GDF-15 beyond the central nervous system<sup>74, 193</sup>. However, in the transcriptomic analysis, neither GFRAL nor RET expression was significantly altered in the different comparison groups (data not shown), making this hypothesis unlikely in this context.

## 5 SUMMARY

GDF-15 is a multifunctional cytokine involved in immune tolerance that is elevated in stress conditions, correlating with disease severity and survival. GDF-15 is expressed by macrophages and can be endocytosed by the scavenger receptor stabilin-1. The role of GDF-15 in macrophages and its effects on the macrophage transcriptional program have been studied to only a limited extent. The aims of this study were: 1) to develop a model system to study the effect of recombinant human GDF-15 (rGDF-15) on macrophages; 2) to identify the transcriptional program induced by GDF-15 in macrophages by RNA-Seq and validate differentially expressed genes using RT-PCR; 3) to bioinformatically analyze the role of GDF-15, stabilin-1, and GDF-15-mediated pathways in most relevant cancers, particularly in kidney renal clear cell carcinoma (KIRC). Human monocytes were isolated from buffy coats by CD14<sup>+</sup> positive selection and differentiated into M0 (non-stimulated), M1 (IFN- $\gamma$  stimulated) and M2 (IL-4 stimulated) macrophages for 6 days. The selected protocol was as follows: on the day 6 of macrophage differentiation, a pretreatment with 50 ng/mL rGDF15 was performed for 1 hour, followed by a 6 hour challenge with 100 ng/mL LPS. RNA was isolated and total RNA Seq was performed in M0 and M2, revealing that rGDF15 altered the expression of 210 genes in M0 and of 372 in M2. rGDF15 and LPS in M0 and M2 exhibited changes in 230 and 295 genes, respectively. Top upregulated Gene Ontology (GO) terms, in both M0 and M2 treated with rGDF15 were associated with blood vessel morphogenesis and angiogenesis. In M0 and M2 under rGDF-15 and LPS, top upregulated GO terms belonged to TGF- $\beta$  receptor and cytokine signaling pathways. Thirteen genes were selected for validation by RT-PCR. M1 phenotype was also included for validation. RT-PCR showed that rGDF-15 increased expression of CLEC12A in M0+LPS and M1+LPS, ID3 in M2 and M2+LPS, SMAD6 in M0, M2  $\pm$  LPS, and of IL17RB and PMEPA1 in all groups. rGDF-15 suppressed expression of CCL15 in M0+LPS and M2+LPS, GAS7 in M0+LPS and PTP4A3 in M0 and M2 + LPS. This pattern of gene expression suggests an anti-inflammatory effect of rGDF-15 in macrophages. Based on the TCGA database and using TIMER2.0 and the Xena platform, GDF-15 expression in cancer tissues was investigated. Contrary to the pattern seen in other cancers, GDF-15 expression was found to be lower in KIRC compared to normal tissue. Genes induced by GDF-15 (IL17RB and SMAD6) exhibited low expression levels in KIRC compared to normal tissue. Conversely, PTP4A3,



downregulated by GDF-15, showed elevated levels in KIRC. High levels of IL17RB and SMAD6, along with the low levels of PTP4A3, correlated with better patient outcomes in KIRC. Stabilin-1 is the only known scavenger receptor for GDF-15. Functional endocytosis assay and confocal microscopy revealed that titanium nanoparticles, previously shown to enhance GDF-15 production by macrophages, can suppress the scavenging function of stabilin-1 encoded by the STAB1 gene. STAB1 expression was elevated in KIRC tissue and correlated with worse survival outcomes. Impairment of the stabilin-1 scavenging function may additionally increase the bioavailability of GDF-15 in KIRC, influencing patient outcomes. In summary, GDF-15 can program human macrophages into a tolerogenic phenotype, support angiogenesis and modify TGF- $\beta$  signaling. Increased GDF-15 transcription, together with impaired stabilin-1-mediated clearance, can be suggested as a mechanism by which macrophages retain their ability to limit tumor growth.

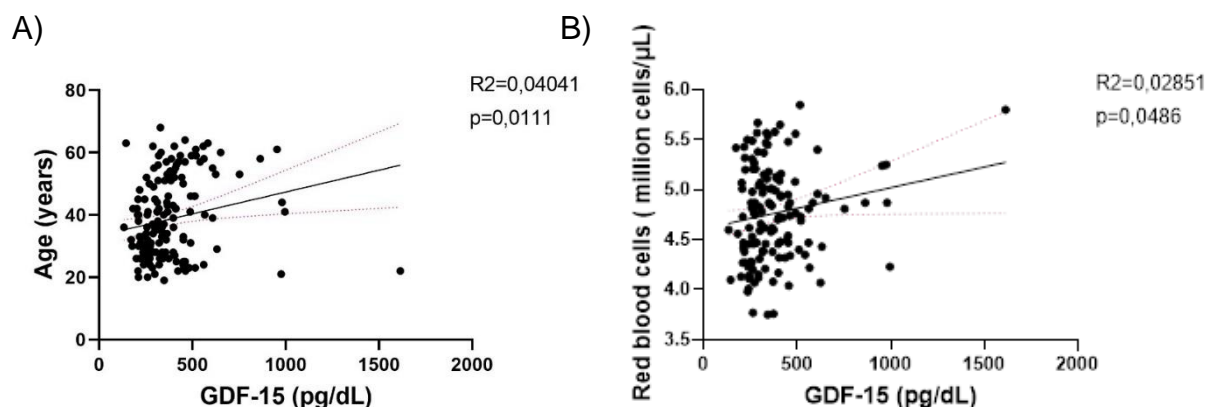
## 6 SUPPLEMENTARY DATA

### 6.1 GDF-15 serum levels in healthy plasma donors

**Supplementary Table 1.** Characteristics of participants  
n=68

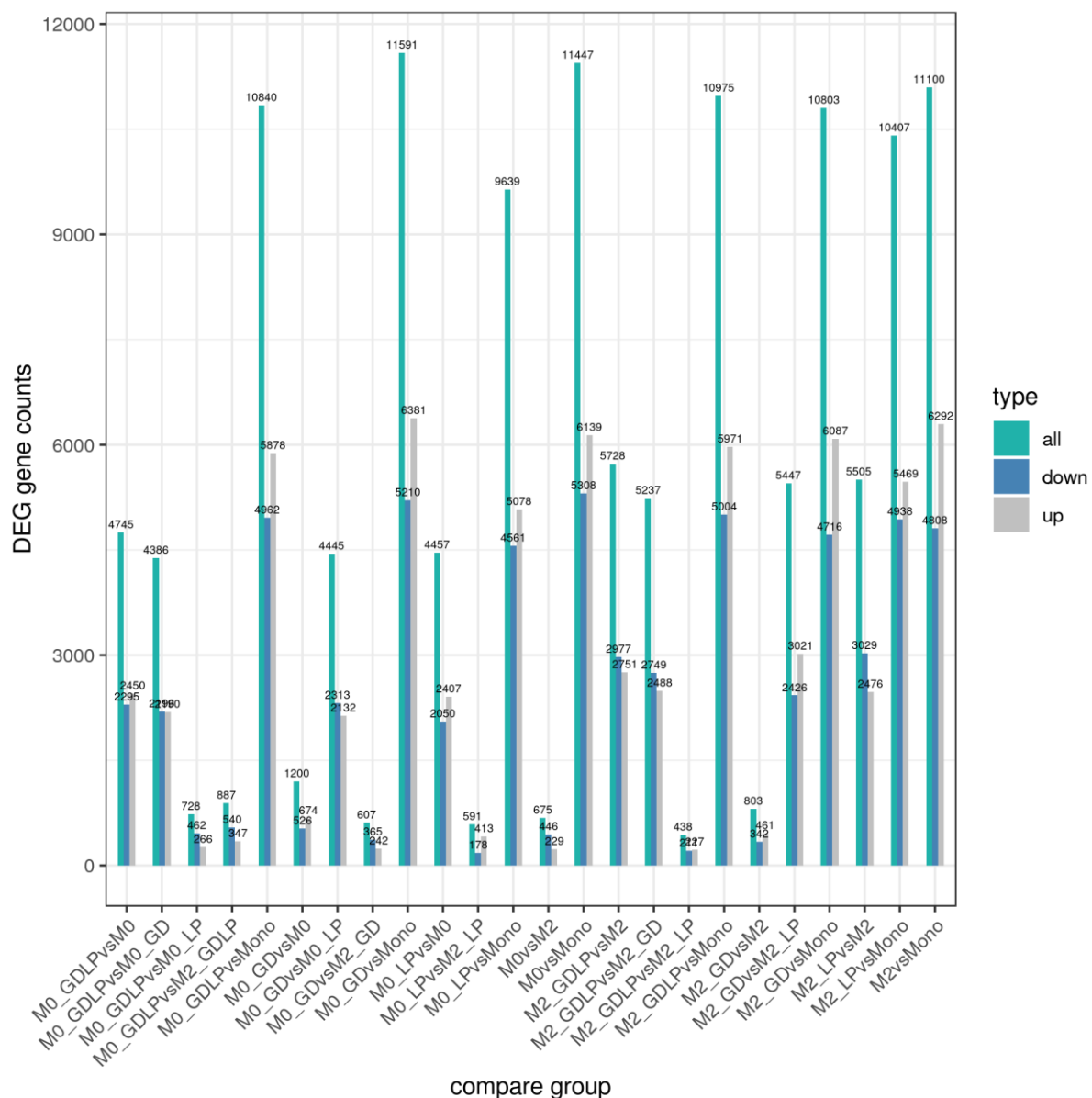
Age	36 (19-68)
Weight (kg)	76,6 (25-143)
Body-mass index (kg/m <sup>2</sup> )	25,7 (19,1-45,6)
Systolic blood pressure (mmHg)	130,6 (106-177)
Diastolic blood pressure (mmHg)	79 (55-99)
Heart rate (bpm)	78,1 (53-105)
Body temperature (°C)	36,3 (36-37)
Leukocytes (10 <sup>9</sup> /L)	6 (3,6-12,7)
RBCs (T/L)	4,7 (3,8-5,8)
Hemoglobin (g/L)	140,1 (110-172)
Haematocrit (%)	40,8 (31,9-48)
MCV	86,3 (80,8-97,6)
Platelets (10 <sup>9</sup> /L)	254,4 (142-430)
Basal GDF-15 (pg/dL)	382,7 (85,3-1830)

Serum levels of GDF-15 were measured in healthy plasma donors. Sixty-five participants (49% men, 57% women), aged 19 to 68 years were included. The mean BMI was 25,7 kg/m<sup>2</sup>. The lost to follow-up rate was 24,6%. Mean GDF-15 levels were 382,7 pg/mL (SD=11,94). Spearman correlation of different baseline characteristics showed a significant positive correlation between mean GDF-15 serum levels and age, as well as with red cell count (Supplementary Figure 1).



**Supplementary Figure 1. Correlation of serum GDF-15 levels with clinical characteristics.** A) Spearman correlation of mean GDF-15 serum levels with age and B) red blood cell count. Lines show the linear regression and the dashed lines show the 95% confidence limits.

## 6.2 DEG count for all the comparison groups

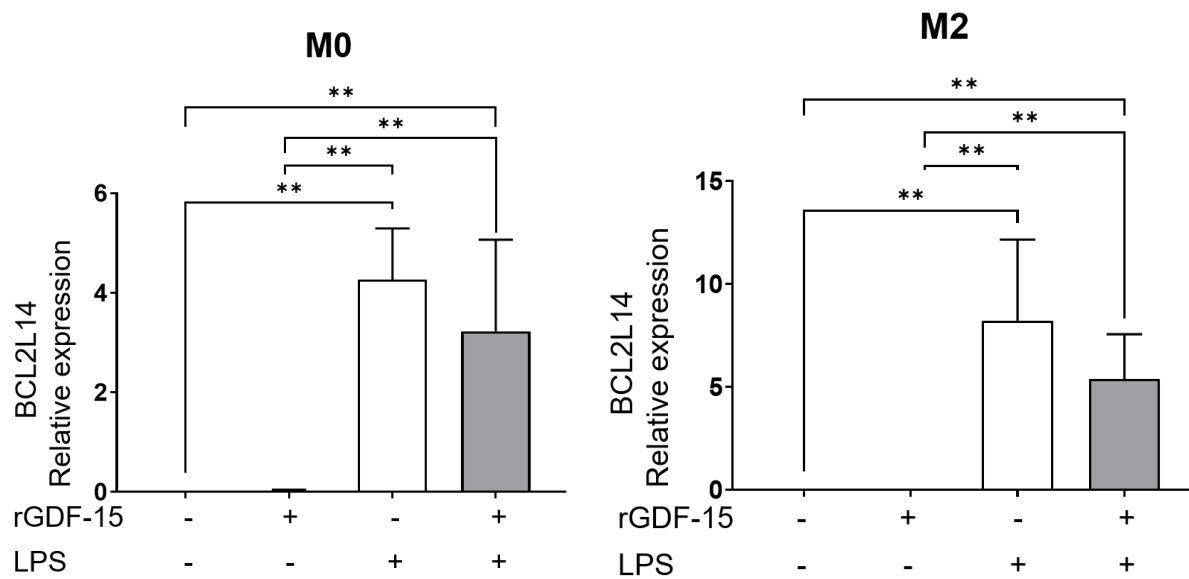


**Supplementary Figure 2.** Histogram of the number of DEGs statistics

## 6.3 BCL2L14 expression is increased after LPS challenge in macrophages

The expression of the apoptosis facilitator Bcl-2-like protein 14 (BCL2L14) was evaluated in the proposed macrophage model. BCL2L14 is a member of the Bcl-2 family that has been shown to promote apoptosis in macrophages during LPS challenge<sup>194</sup>. Additionally, BCL2L14 is highly expressed in the gastrointestinal tract and it has been found to be mutated, amplified or deleted, in several cancers. Within 9 donors, a low BCL2L14 expression was found in M0 and M2, and in rGDF-15 primed macrophages. In contrast, LPS-stimulated macrophages show a significantly increased expression of BCL2L14 compared to control and to rGDF-15 treated

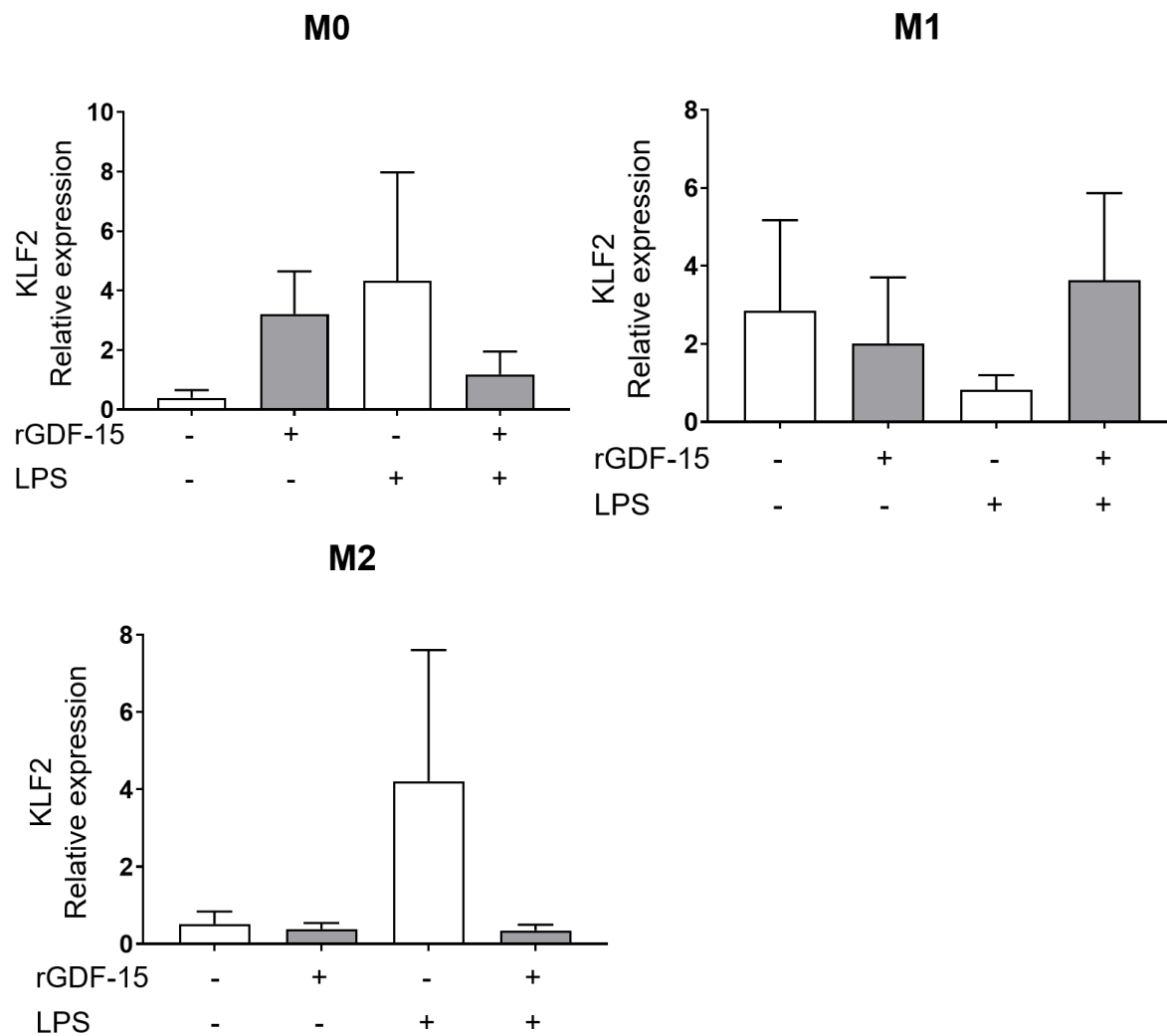
macrophages. Moreover, rGDF-15 priming did not significantly alter the effect of LPS on BCL2L14 expression (Supplementary Figure 3).



**Supplementary Figure 3.** Effect of rGDF-15 on BCL2L14 gene expression in macrophages challenged with LPS. mRNA expression was analyzed by RT-PCR in M0 and M2 cultured for 6 days, primed with rGDF-15 50 ng/mL for 1 hour and challenged with LPS 100 g/mL for 6 hours. n=9. Data are presented as mean  $\pm$  SEM normalized to 18SrRNA expression levels. \*\*p<0.01.

#### 6.4 rGDF-15 treatment does not significantly change KLF2 expression in macrophages

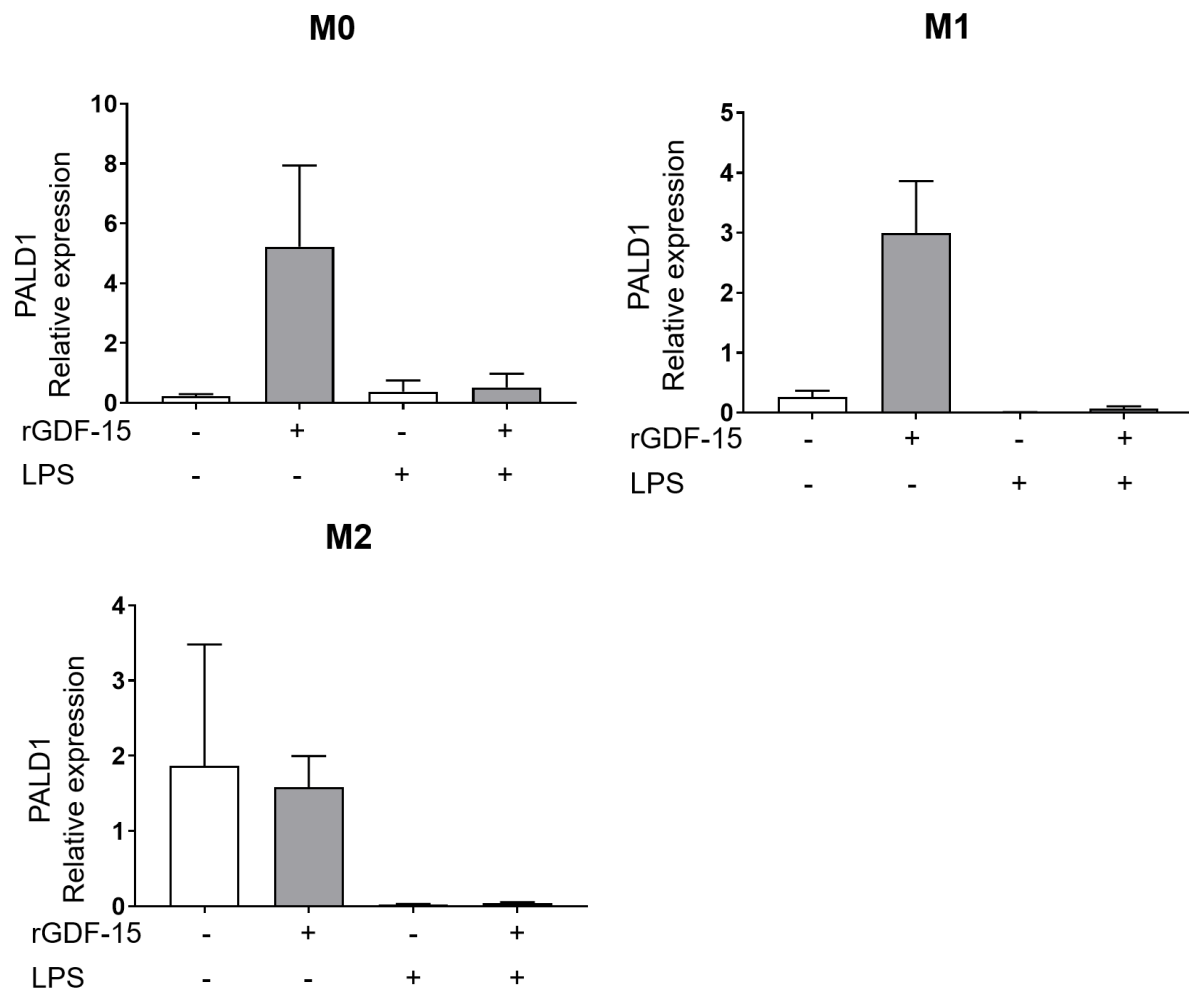
Kruppel-like transcription factor 2 (KLF2) is involved in cell differentiation, such as erythropoiesis and osteoblastogenesis, and regulatory processes in the immune and vascular systems. KLF2 has been shown to decrease the expression of proinflammatory genes such as TNF- $\alpha$  and IL-1 $\beta$  in LPS-treated macrophages. Conversely, TNF- $\alpha$  and IL-1 $\beta$  decrease KLF2 expression in endothelial cells<sup>195</sup>. In overall, an increased but not statistically significant KLF2 expression was found in M0 and M2 macrophages challenged with LPS. This trend was less evident in the M1 phenotype (Supplementary Figure 4).



**Supplementary Figure 4. Effect of rGDF-15 on KLF2 expression of in macrophages challenged with LPS.** mRNA expression was analyzed by RT-PCR in M0, M1 and M2 cultured for 6 days, primed with rGDF-15 50 ng/mL for 1 hour and challenged with LPS 100 g/mL for 6 hours.  $n=5$ . Data are presented as mean  $\pm$  SEM normalized to 18SrRNA expression levels.

## 6.5 PALD1 expression is not altered in activated macrophages

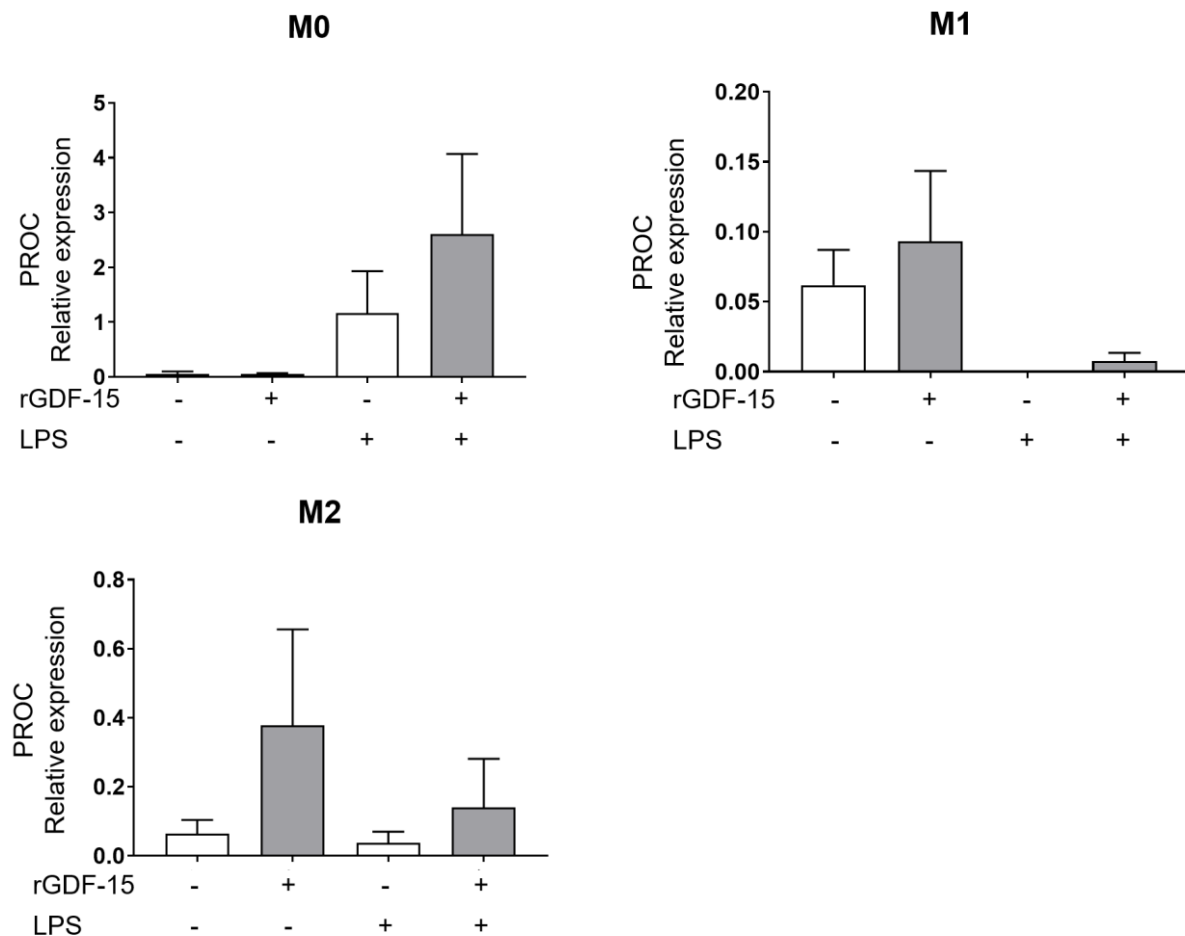
Paladin is a vascular PI(4,5)P2 phosphatase encoded by the gene PALD1, which is involved in VEGFR2 endosomal signaling and angiogenesis. PALD1 has been shown to be involved in endosomal trafficking via VEGFR2 interaction in endothelial cells<sup>196</sup>. The role of paladin in inflammation and macrophage activation is unknown. No significant difference in PALD1 gene expression was observed among the different macrophage phenotypes within 5 donors. Notably, the lowest PALD1 expression levels were found in macrophages challenged with LPS with and without rGDF-15 priming (Supplementary Figure 5).



**Supplementary Figure 5. Effect of rGDF-15 on PALD1 expression of in macrophages challenged with LPS.** mRNA expression was analyzed by RT-PCR in M0, M1 and M2 cultured for 6 days, primed with rGDF-15 50 ng/mL for 1 hour and challenged with LPS 100 g/mL for 6 hours.  $n=5$ . Data are presented as mean  $\pm$  SEM normalized to 18SrRNA expression levels.

#### 6.6 PROC expression does not change within activated macrophages challenged with LPS

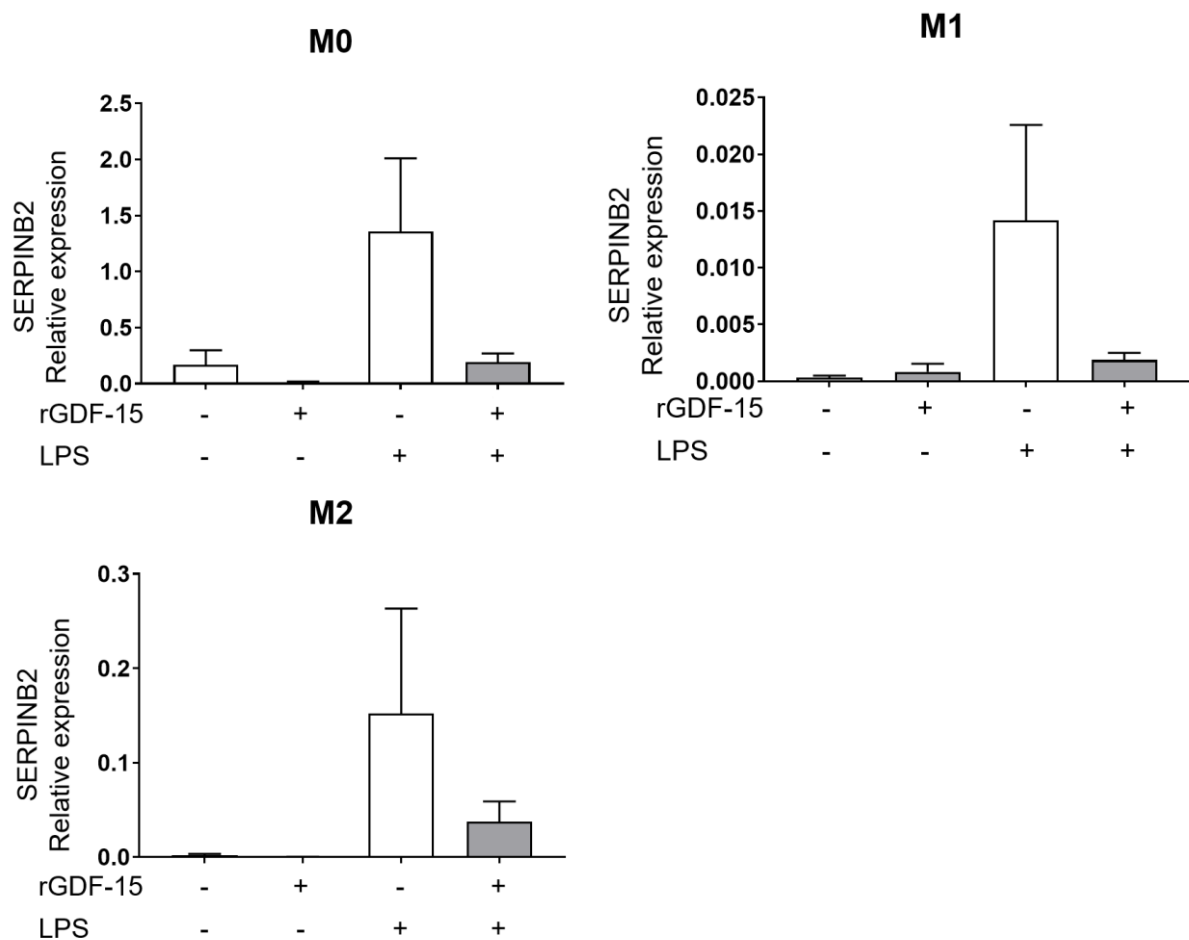
Protein C (PROC) is a well-known vitamin K-dependent anticoagulant factor that in its active form (activated protein C or APC), inactivates factors Va and VIIIa. In addition to its hemostatic function, protein C is also involved in the modulation of inflammation<sup>197</sup>. Specifically, PROC reduces inflammasome activity in LPS-treated<sup>198</sup>. Five donors were examined and no difference was found in PROC expression in M0, M1 and M2 under the conditions studied. PROC expression was nearly absent in all conditions, especially in LPS-challenged macrophages (Supplementary Figure 6).



**Supplementary Figure 6. Effect of rGDF-15 on PROC expression in macrophages challenged with LPS.** mRNA expression was analyzed by RT-PCR in M0, M1 and M2 cultured for 6 days, primed with rGDF-15 50 ng/mL for 1 hour and challenged with LPS 100 g/mL for 6 hours.  $n=5$ . Data are presented as mean  $\pm$  SEM normalized to 18SrRNA expression levels.

#### 6.7 SERPINB2 expression levels remain unchanged in macrophages after rGDF-15 treatment

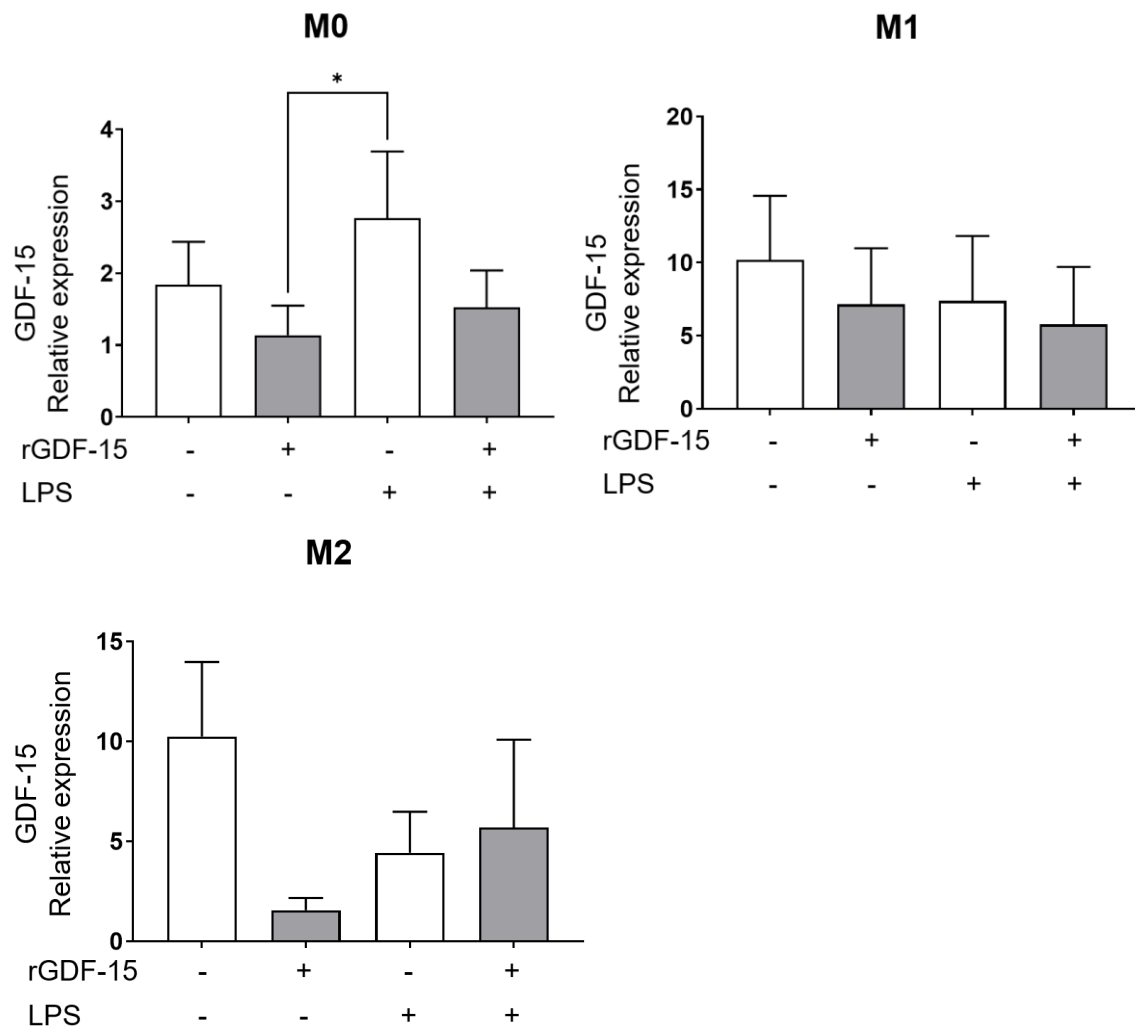
SERPINB2 is a member of the serine protease inhibitor (serpin) superfamily that mediates the inhibition of urokinase plasminogen formation, thereby preventing processes such as fibrinolysis, immune cell migration and extracellular matrix remodeling. In the macrophage system, SERPINB2 gene expression is upregulated during M1 polarization in response to LPS<sup>199</sup>. No statistical difference was observed between the different conditions. However, an upregulation of SERPIN2 in response to LPS challenge is evident, which was reduced in macrophages pretreated with rGDF-15 (Supplementary Figure 7).



**Supplementary Figure 7. Effect of rGDF-15 on SERPINB2 expression in macrophages challenged with LPS.** mRNA expression was analyzed by RT-PCR in M0, M1 and M2 cultured for 6 days, primed with rGDF-15 50 ng/mL for 1 hour and challenged with LPS 100 g/mL for 6 hours. n=5. Data are presented as mean  $\pm$  SEM normalized to 18SrRNA expression levels. \*p<0.05, \*\*p<0.01.



## 6.8 rGDF-treatment does not change the GDF-15 expression in macrophages



**Supplementary Figure 8.** Effect of rGDF-15 priming on GDF-15 expression of in M0, M1 and M2 challenged with LPS. mRNA expression was analyzed by RT-PCR in macrophages cultured for 6 days, primed for 1 hour with rGDF-15 50 ng/mL and challenged with LPS (100 ng/mL) for 6 hours. n=5. Data are presented as mean  $\pm$  SEM normalized to 18SrRNA expression levels. \*p<0.05, \*\*p<0.01.

## 7 REFERENCES

1. Lawrence T, Natoli G. Transcriptional regulation of macrophage polarization: enabling diversity with identity. *Nat Rev Immunol*. 2011 Oct 25;11(11):750-61.
2. Jha AK, Huang SC, Sergushichev A, Lampropoulou V, Ivanova Y, Loginicheva E, et al. Network integration of parallel metabolic and transcriptional data reveals metabolic modules that regulate macrophage polarization. *Immunity*. 2015 Mar 17;42(3):419-30.
3. Orecchioni M, Ghosheh Y, Pramod AB, Ley K. Macrophage Polarization: Different Gene Signatures in M1(LPS+) vs. Classically and M2(LPS-) vs. Alternatively Activated Macrophages. *Front Immunol*. 2019;10:1084.
4. Kim SY, Nair MG. Macrophages in wound healing: activation and plasticity. *Immunol Cell Biol*. 2019 Mar;97(3):258-67.
5. Xue J, Schmidt SV, Sander J, Draffehn A, Krebs W, Quester I, et al. Transcriptome-based network analysis reveals a spectrum model of human macrophage activation. *Immunity*. 2014 Feb 20;40(2):274-88.
6. Shapouri-Moghaddam A, Mohammadian S, Vazini H, Taghadosi M, Esmaili SA, Mardani F, et al. Macrophage plasticity, polarization, and function in health and disease. *J Cell Physiol*. 2018 Sep;233(9):6425-40.
7. Mosser DM, Hamidzadeh K, Goncalves R. Macrophages and the maintenance of homeostasis. *Cell Mol Immunol*. 2021 Mar;18(3):579-87.
8. Bryan BA, Walshe TE, Mitchell DC, Havumaki JS, Saint-Geniez M, Maharaj AS, et al. Coordinated vascular endothelial growth factor expression and signaling during skeletal myogenic differentiation. *Mol Biol Cell*. 2008 Mar;19(3):994-1006.
9. Oishi Y, Manabe I. Macrophages in inflammation, repair and regeneration. *Int Immunol*. 2018 Oct 29;30(11):511-28.
10. Milich LM, Ryan CB, Lee JK. The origin, fate, and contribution of macrophages to spinal cord injury pathology. *Acta Neuropathol*. 2019 May;137(5):785-97.
11. Torres-Castro I, Arroyo-Camarena UD, Martinez-Reyes CP, Gomez-Arauz AY, Duenas-Andrade Y, Hernandez-Ruiz J, et al. Human monocytes and macrophages undergo M1-type inflammatory polarization in response to high levels of glucose. *Immunol Lett*. 2016 Aug;176:81-9.
12. Rendra E, Riabov V, Mossel DM, Sevastyanova T, Harmsen MC, Kzhyshkowska J. Reactive oxygen species (ROS) in macrophage activation and function in diabetes. *Immunobiology*. 2019 Mar;224(2):242-53.
13. Li A, Zhao F, Zhao Y, Liu H, Wang Z. ATF4-mediated GDF15 suppresses LPS-induced inflammation and MUC5AC in human nasal epithelial cells through the PI3K/Akt pathway. *Life Sci*. 2021 Jun 15;275:119356.
14. de Castro Bras LE, Frangogiannis NG. Extracellular matrix-derived peptides in tissue remodeling and fibrosis. *Matrix Biol*. 2020 Sep;91-92:176-87.
15. Wynn TA, Chawla A, Pollard JW. Macrophage biology in development, homeostasis and disease. *Nature*. 2013 Apr 25;496(7446):445-55.
16. Riabov V, Gudima A, Wang N, Mickley A, Orekhov A, Kzhyshkowska J. Role of tumor associated macrophages in tumor angiogenesis and lymphangiogenesis. *Front Physiol*. 2014;5:75.
17. Larionova I, Kazakova E, Gerashchenko T, Kzhyshkowska J. New Angiogenic Regulators Produced by TAMs: Perspective for Targeting Tumor Angiogenesis. *Cancers (Basel)*. 2021 Jun 29;13(13).

18. Kazakova E, Iamshchikov P, Larionova I, Kzhyshkowska J. Macrophage scavenger receptors: Tumor support and tumor inhibition. *Front Oncol.* 2022;12:1096897.
19. Kzhyshkowska J. Multifunctional receptor stabilin-1 in homeostasis and disease. *ScientificWorldJournal.* 2010 Oct 12;10:2039-53.
20. Kzhyshkowska J, Gratchev A, Goerdts S. Stabilin-1, a homeostatic scavenger receptor with multiple functions. *J Cell Mol Med.* 2006 Jul-Sep;10(3):635-49.
21. Adachi H, Tsujimoto M. FEEL-1, a novel scavenger receptor with in vitro bacteria-binding and angiogenesis-modulating activities. *J Biol Chem.* 2002 Sep 13;277(37):34264-70.
22. Larionova I, Tuguzbaeva G, Ponomaryova A, Stakheyeva M, Cherdyntseva N, Pavlov V, et al. Tumor-Associated Macrophages in Human Breast, Colorectal, Lung, Ovarian and Prostate Cancers. *Front Oncol.* 2020;10:566511.
23. Palani S, Elima K, Ekholm E, Jalkanen S, Salmi M. Monocyte Stabilin-1 Suppresses the Activation of Th1 Lymphocytes. *J Immunol.* 2016 Jan 1;196(1):115-23.
24. Tamura Y, Adachi H, Osuga J, Ohashi K, Yahagi N, Sekiya M, et al. FEEL-1 and FEEL-2 are endocytic receptors for advanced glycation end products. *J Biol Chem.* 2003 Apr 11;278(15):12613-7.
25. Zhang J, Gratchev A, Riabov V, Mamidi S, Schmuttermayr C, Krusell L, et al. A novel GGA-binding site is required for intracellular sorting mediated by stabilin-1. *Mol Cell Biol.* 2009 Nov;29(22):6097-105.
26. Penberthy KK, Ravichandran KS. Apoptotic cell recognition receptors and scavenger receptors. *Immunol Rev.* 2016 Jan;269(1):44-59.
27. Kzhyshkowska J, Gratchev A, Martens JH, Pervushina O, Mamidi S, Johansson S, et al. Stabilin-1 localizes to endosomes and the trans-Golgi network in human macrophages and interacts with GGA adaptors. *J Leukoc Biol.* 2004 Dec;76(6):1151-61.
28. Irjala H, Elima K, Johansson EL, Merinen M, Kontula K, Alanen K, et al. The same endothelial receptor controls lymphocyte traffic both in vascular and lymphatic vessels. *Eur J Immunol.* 2003 Mar;33(3):815-24.
29. Karikoski M, Marttila-Ichihara F, Elima K, Rantakari P, Hollmen M, Kelkka T, et al. Clever-1/stabilin-1 controls cancer growth and metastasis. *Clin Cancer Res.* 2014 Dec 15;20(24):6452-64.
30. Tzavlaki K, Moustakas A. TGF-beta Signaling. *Biomolecules.* 2020 Mar 23;10(3).
31. Ren LL, Li XJ, Duan TT, Li ZH, Yang JZ, Zhang YM, et al. Transforming growth factor-beta signaling: From tissue fibrosis to therapeutic opportunities. *Chem Biol Interact.* 2023 Jan 5;369:110289.
32. Shi X, Yang J, Deng S, Xu H, Wu D, Zeng Q, et al. TGF-beta signaling in the tumor metabolic microenvironment and targeted therapies. *J Hematol Oncol.* 2022 Sep 17;15(1):135.
33. Tian M, Schiemann WP. The TGF-beta paradox in human cancer: an update. *Future Oncol.* 2009 Mar;5(2):259-71.
34. Bal Z, Kushioka J, Kodama J, Kaito T, Yoshikawa H, Korkusuz P, et al. BMP and TGFbeta use and release in bone regeneration. *Turk J Med Sci.* 2020 Nov 3;50(SI-2):1707-22.
35. Machelak W, Szczepaniak A, Jacenik D, Zielinska M. The role of GDF11 during inflammation - An overview. *Life Sci.* 2023 Jun 1;322:121650.

36. Bootcov MR, Bauskin AR, Valenzuela SM, Moore AG, Bansal M, He XY, et al. MIC-1, a novel macrophage inhibitory cytokine, is a divergent member of the TGF-beta superfamily. *Proc Natl Acad Sci U S A*. 1997 Oct 14;94(21):11514-9.
37. Strelau J, Bottner M, Lingor P, Suter-Crazzolara C, Galter D, Jaszai J, et al. GDF-15/MIC-1 a novel member of the TGF-beta superfamily. *J Neural Transm Suppl*. 2000 (60):273-6.
38. Hsu JY, Crawley S, Chen M, Ayupova DA, Lindhout DA, Higbee J, et al. Non-homeostatic body weight regulation through a brainstem-restricted receptor for GDF15. *Nature*. 2017 Oct 12;550(7675):255-59.
39. Lawton LN, Bonaldo MF, Jelenc PC, Qiu L, Baumes SA, Marcelino RA, et al. Identification of a novel member of the TGF-beta superfamily highly expressed in human placenta. *Gene*. 1997 Dec 5;203(1):17-26.
40. Paralkar VM, Vail AL, Grasser WA, Brown TA, Xu H, Vukicevic S, et al. Cloning and characterization of a novel member of the transforming growth factor-beta/bone morphogenetic protein family. *J Biol Chem*. 1998 May 29;273(22):13760-7.
41. Baek SJ, Kim KS, Nixon JB, Wilson LC, Eling TE. Cyclooxygenase inhibitors regulate the expression of a TGF-beta superfamily member that has proapoptotic and antitumorigenic activities. *Mol Pharmacol*. 2001 Apr;59(4):901-8.
42. Schreiber F, Patricio M, Muffato M, Pignatelli M, Bateman A. TreeFam v9: a new website, more species and orthology-on-the-fly. *Nucleic Acids Res*. 2014 Jan;42(Database issue):D922-5.
43. Pereiro P, Libran-Perez M, Figueras A, Novoa B. Conserved function of zebrafish (*Danio rerio*) Gdf15 as a sepsis tolerance mediator. *Dev Comp Immunol*. 2020 Aug;109:103698.
44. Li S, Wang Y, Cao B, Wu Y, Ji L, Li YX, et al. Maturation of growth differentiation factor 15 in human placental trophoblast cells depends on the interaction with Matrix Metalloproteinase-26. *J Clin Endocrinol Metab*. 2014 Nov;99(11):E2277-87.
45. Li JJ, Liu J, Lupino K, Liu X, Zhang L, Pei L. Growth Differentiation Factor 15 Maturation Requires Proteolytic Cleavage by PCSK3, -5, and -6. *Mol Cell Biol*. 2018 Nov 1;38(21).
46. Wischhusen J, Melero I, Fridman WH. Growth/Differentiation Factor-15 (GDF-15): From Biomarker to Novel Targetable Immune Checkpoint. *Front Immunol*. 2020;11:951.
47. Fairlie WD, Zhang HP, Wu WM, Pankhurst SL, Bauskin AR, Russell PK, et al. The propeptide of the transforming growth factor-beta superfamily member, macrophage inhibitory cytokine-1 (MIC-1), is a multifunctional domain that can facilitate protein folding and secretion. *J Biol Chem*. 2001 May 18;276(20):16911-8.
48. Bauskin AR, Brown DA, Junankar S, Rasiah KK, Eggleton S, Hunter M, et al. The propeptide mediates formation of stromal stores of PROMIC-1: role in determining prostate cancer outcome. *Cancer Res*. 2005 Mar 15;65(6):2330-6.
49. Bauskin AR, Jiang L, Luo XW, Wu L, Brown DA, Breit SN. The TGF-beta superfamily cytokine MIC-1/GDF15: secretory mechanisms facilitate creation of latent stromal stores. *J Interferon Cytokine Res*. 2010 Jun;30(6):389-97.
50. Moore AG, Brown DA, Fairlie WD, Bauskin AR, Brown PK, Munier ML, et al. The transforming growth factor-ss superfamily cytokine macrophage inhibitory cytokine-1 is present in high concentrations in the serum of pregnant women. *J Clin Endocrinol Metab*. 2000 Dec;85(12):4781-8.
51. Laurens C, Parmar A, Murphy E, Carper D, Lair B, Maes P, et al. Growth and differentiation factor 15 is secreted by skeletal muscle during exercise and promotes lipolysis in humans. *JCI Insight*. 2020 Mar 26;5(6).

52. Abulizi P, Loganathan N, Zhao D, Mele T, Zhang Y, Zwiep T, et al. Growth Differentiation Factor-15 Deficiency Augments Inflammatory Response and Exacerbates Septic Heart and Renal Injury Induced by Lipopolysaccharide. *Sci Rep*. 2017 Apr 21;7(1):1037.
53. Cheung PK, Woolcock B, Adomat H, Sutcliffe M, Bainbridge TC, Jones EC, et al. Protein profiling of microdissected prostate tissue links growth differentiation factor 15 to prostate carcinogenesis. *Cancer Res*. 2004 Sep 1;64(17):5929-33.
54. Tsui KH, Hsu SY, Chung LC, Lin YH, Feng TH, Lee TY, et al. Growth differentiation factor-15: a p53- and demethylation-upregulating gene represses cell proliferation, invasion, and tumorigenesis in bladder carcinoma cells. *Sci Rep*. 2015 Aug 7;5:12870.
55. Perez-Gomez MV, Pizarro-Sanchez S, Gracia-Iguacel C, Cano S, Cannata-Ortiz P, Sanchez-Rodriguez J, et al. Urinary Growth Differentiation Factor-15 (GDF15) levels as a biomarker of adverse outcomes and biopsy findings in chronic kidney disease. *J Nephrol*. 2021 Dec;34(6):1819-32.
56. Wu Q, Jiang D, Chu HW. Cigarette smoke induces growth differentiation factor 15 production in human lung epithelial cells: implication in mucin over-expression. *Innate Immun*. 2012 Aug;18(4):617-26.
57. Shnaper S, Desbaillets I, Brown DA, Murat A, Migliavacca E, Schluep M, et al. Elevated levels of MIC-1/GDF15 in the cerebrospinal fluid of patients are associated with glioblastoma and worse outcome. *Int J Cancer*. 2009 Dec 1;125(11):2624-30.
58. Sramkova V, Koc M, Krauzova E, Kracmerova J, Siklova M, Elkalaf M, et al. Expression of lipogenic markers is decreased in subcutaneous adipose tissue and adipocytes of older women and is negatively linked to GDF15 expression. *J Physiol Biochem*. 2019 Aug;75(3):253-62.
59. Takenouchi Y, Kitakaze K, Tsuboi K, Okamoto Y. Growth differentiation factor 15 facilitates lung fibrosis by activating macrophages and fibroblasts. *Exp Cell Res*. 2020 Jun 15;391(2):112010.
60. Miyake M, Zhang J, Yasue A, Hisanaga S, Tsugawa K, Sakaue H, et al. Integrated stress response regulates GDF15 secretion from adipocytes, preferentially suppresses appetite for a high-fat diet and improves obesity. *iScience*. 2021 Dec 17;24(12):103448.
61. Kim J, Kim SH, Kang H, Lee S, Park SY, Cho Y, et al. TFEB-GDF15 axis protects against obesity and insulin resistance as a lysosomal stress response. *Nat Metab*. 2021 Mar;3(3):410-27.
62. Ramirez JM, Schaad O, Durual S, Cossali D, Docquier M, Beris P, et al. Growth differentiation factor 15 production is necessary for normal erythroid differentiation and is increased in refractory anaemia with ring-sideroblasts. *Br J Haematol*. 2009 Jan;144(2):251-62.
63. Tanno T, Bhanu NV, Oneal PA, Goh SH, Staker P, Lee YT, et al. High levels of GDF15 in thalassemia suppress expression of the iron regulatory protein hepcidin. *Nat Med*. 2007 Sep;13(9):1096-101.
64. Uchiyama T, Kawabata H, Miura Y, Yoshioka S, Iwasa M, Yao H, et al. The role of growth differentiation factor 15 in the pathogenesis of primary myelofibrosis. *Cancer Med*. 2015 Oct;4(10):1558-72.
65. Blum M, Chang HY, Chuguransky S, Grego T, Kandasaamy S, Mitchell A, et al. The InterPro protein families and domains database: 20 years on. *Nucleic Acids Res*. 2021 Jan 8;49(D1):D344-D54.
66. Jung SB, Choi MJ, Ryu D, Yi HS, Lee SE, Chang JY, et al. Reduced oxidative capacity in macrophages results in systemic insulin resistance. *Nat Commun*. 2018 Apr 19;9(1):1551.

67. Li H, Tang D, Chen J, Hu Y, Cai X, Zhang P. The Clinical Value of GDF15 and Its Prospective Mechanism in Sepsis. *Front Immunol*. 2021;12:710977.
68. Ha G, De Torres F, Arouche N, Benzoubir N, Ferratge S, Hatem E, et al. GDF15 secreted by senescent endothelial cells improves vascular progenitor cell functions. *PLoS One*. 2019;14(5):e0216602.
69. Lambrecht S, Smith V, De Wilde K, Coudenys J, Decuman S, Deforce D, et al. Growth differentiation factor 15, a marker of lung involvement in systemic sclerosis, is involved in fibrosis development but is not indispensable for fibrosis development. *Arthritis Rheumatol*. 2014 Feb;66(2):418-27.
70. Ranjbaran R, Abbasi M, Rahimian E, Dehbidi GR, Seyyedi N, Zare F, et al. GDF-15 negatively regulates excess erythropoiesis and its overexpression is involved in erythroid hyperplasia. *Exp Cell Res*. 2020 Dec 15;397(2):112346.
71. Frank D, Kuhn C, Brors B, Hanselmann C, Ludde M, Katus HA, et al. Gene expression pattern in biomechanically stretched cardiomyocytes: evidence for a stretch-specific gene program. *Hypertension*. 2008 Feb;51(2):309-18.
72. Lee SE, Kang SG, Choi MJ, Jung SB, Ryu MJ, Chung HK, et al. Growth Differentiation Factor 15 Mediates Systemic Glucose Regulatory Action of T-Helper Type 2 Cytokines. *Diabetes*. 2017 Nov;66(11):2774-88.
73. Kim Y, Noren Hooten N, Evans MK. CRP Stimulates GDF15 Expression in Endothelial Cells through p53. *Mediators Inflamm*. 2018;2018:8278039.
74. Siddiqui JA, Seshacharyulu P, Muniyan S, Pothuraju R, Khan P, Vengoji R, et al. GDF15 promotes prostate cancer bone metastasis and colonization through osteoblastic CCL2 and RANKL activation. *Bone Res*. 2022 Jan 20;10(1):6.
75. Chung HK, Ryu D, Kim KS, Chang JY, Kim YK, Yi HS, et al. Growth differentiation factor 15 is a myomitokine governing systemic energy homeostasis. *J Cell Biol*. 2017 Jan 2;216(1):149-65.
76. Jin Y, Jung SN, Lim MA, Oh C, Piao Y, Kim HJ, et al. Transcriptional Regulation of GDF15 by EGR1 Promotes Head and Neck Cancer Progression through a Positive Feedback Loop. *Int J Mol Sci*. 2021 Oct 15;22(20).
77. Day EA, Ford RJ, Smith BK, Mohammadi-Shemirani P, Morrow MR, Gutgesell RM, et al. Metformin-induced increases in GDF15 are important for suppressing appetite and promoting weight loss. *Nat Metab*. 2019 Dec;1(12):1202-08.
78. Zhao C, Li Y, Qiu W, He F, Zhang W, Zhao D, et al. C5a induces A549 cell proliferation of non-small cell lung cancer via GDF15 gene activation mediated by GCN5-dependent KLF5 acetylation. *Oncogene*. 2018 Aug;37(35):4821-37.
79. Choi HJ, Kim HG, Kim J, Park SH, Park J, Oh CG, et al. Pro-apoptotic action of macrophage inhibitory cytokine 1 and counteraction of activating transcription factor 3 in carrageenan-exposed enterocytes. *Toxicol Lett*. 2014 Nov 18;231(1):1-8.
80. Lee SH, Krisanapun C, Baek SJ. NSAID-activated gene-1 as a molecular target for capsaicin-induced apoptosis through a novel molecular mechanism involving GSK3beta, C/EBPbeta and ATF3. *Carcinogenesis*. 2010 Apr;31(4):719-28.
81. L'Homme L, Sermikli BP, Staels B, Piette J, Legrand-Poels S, Dombrowicz D. Saturated Fatty Acids Promote GDF15 Expression in Human Macrophages through the PERK/eIF2/CHOP Signaling Pathway. *Nutrients*. 2020 Dec 8;12(12).
82. Wang T, Mao B, Cheng C, Zou Z, Gao J, Yang Y, et al. YAP promotes breast cancer metastasis by repressing growth differentiation factor-15. *Biochim Biophys Acta Mol Basis Dis*. 2018 May;1864(5 Pt A):1744-53.
83. Emmerson PJ, Wang F, Du Y, Liu Q, Pickard RT, Gonciarz MD, et al. The metabolic effects of GDF15 are mediated by the orphan receptor GFRAL. *Nat Med*. 2017 Oct;23(10):1215-19.

84. Mullican SE, Lin-Schmidt X, Chin CN, Chavez JA, Furman JL, Armstrong AA, et al. GFRAL is the receptor for GDF15 and the ligand promotes weight loss in mice and nonhuman primates. *Nat Med*. 2017 Oct;23(10):1150-57.
85. Yang L, Chang CC, Sun Z, Madsen D, Zhu H, Padkjaer SB, et al. GFRAL is the receptor for GDF15 and is required for the anti-obesity effects of the ligand. *Nat Med*. 2017 Oct;23(10):1158-66.
86. Moon JS, Goeminne LJE, Kim JT, Tian JW, Kim SH, Nga HT, et al. Growth differentiation factor 15 protects against the aging-mediated systemic inflammatory response in humans and mice. *Aging Cell*. 2020 Aug;19(8):e13195.
87. Artz A, Butz S, Vestweber D. GDF-15 inhibits integrin activation and mouse neutrophil recruitment through the ALK-5/TGF-betaRII heterodimer. *Blood*. 2016 Jul 28;128(4):529-41.
88. Li C, Wang J, Kong J, Tang J, Wu Y, Xu E, et al. GDF15 promotes EMT and metastasis in colorectal cancer. *Oncotarget*. 2016 Jan 5;7(1):860-72.
89. Olsen OE, Skjaervik A, Stordal BF, Sundan A, Holien T. TGF-beta contamination of purified recombinant GDF15. *PLoS One*. 2017;12(11):e0187349.
90. Tsai VWW, Husaini Y, Sainsbury A, Brown DA, Breit SN. The MIC-1/GDF15-GFRAL Pathway in Energy Homeostasis: Implications for Obesity, Cachexia, and Other Associated Diseases. *Cell Metab*. 2018 Sep 4;28(3):353-68.
91. Schledzewski K, Geraud C, Arnold B, Wang S, Grone HJ, Kempf T, et al. Deficiency of liver sinusoidal scavenger receptors stabilin-1 and -2 in mice causes glomerulofibrotic nephropathy via impaired hepatic clearance of noxious blood factors. *J Clin Invest*. 2011 Feb;121(2):703-14.
92. Ho JE, Mahajan A, Chen MH, Larson MG, McCabe EL, Ghorbani A, et al. Clinical and genetic correlates of growth differentiation factor 15 in the community. *Clin Chem*. 2012 Nov;58(11):1582-91.
93. Diaz M, Campderros L, Guimaraes MP, Lopez-Bermejo A, de Zegher F, Villarroya F, et al. Circulating growth-and-differentiation factor-15 in early life: relation to prenatal and postnatal growth and adiposity measurements. *Pediatr Res*. 2020 Apr;87(5):897-902.
94. Pence BD, Yarbrow JR, Emmons RS. Growth differentiation factor-15 is associated with age-related monocyte dysfunction. *Aging Med (Milton)*. 2021 Mar;4(1):47-52.
95. Patel AR, Frikke-Schmidt H, Bezy O, Sabatini PV, Rittig N, Jessen N, et al. LPS induces rapid increase in GDF15 levels in mice, rats, and humans but is not required for anorexia in mice. *Am J Physiol Gastrointest Liver Physiol*. 2022 Feb 1;322(2):G247-G55.
96. Ackermann K, Bonaterra GA, Kinscherf R, Schwarz A. Growth differentiation factor-15 regulates oxLDL-induced lipid homeostasis and autophagy in human macrophages. *Atherosclerosis*. 2019 Feb;281:128-36.
97. Campderros L, Moure R, Cairo M, Gavalda-Navarro A, Quesada-Lopez T, Cereijo R, et al. Brown Adipocytes Secrete GDF15 in Response to Thermogenic Activation. *Obesity (Silver Spring)*. 2019 Oct;27(10):1606-16.
98. Park H, Nam KS, Lee HJ, Kim KS. Ionizing Radiation-Induced GDF15 Promotes Angiogenesis in Human Glioblastoma Models by Promoting VEGFA Expression Through p-MAPK1/SP1 Signaling. *Front Oncol*. 2022;12:801230.
99. Deng M, Su D, Xiao N, Zhang Z, Wang Y, Zong F, et al. Gdf15 deletion exacerbates acute lung injuries induced by intratracheal inoculation of aerosolized ricin in mice. *Toxicology*. 2022 Mar 15;469:153135.
100. Brown DA, Stephan C, Ward RL, Law M, Hunter M, Bauskin AR, et al. Measurement of serum levels of macrophage inhibitory cytokine 1 combined with

- prostate-specific antigen improves prostate cancer diagnosis. *Clin Cancer Res.* 2006 Jan 1;12(1):89-96.
101. Koopmann J, Rosenzweig CN, Zhang Z, Canto MI, Brown DA, Hunter M, et al. Serum markers in patients with resectable pancreatic adenocarcinoma: macrophage inhibitory cytokine 1 versus CA19-9. *Clin Cancer Res.* 2006 Jan 15;12(2):442-6.
102. Brown DA, Ward RL, Buckhaults P, Liu T, Romans KE, Hawkins NJ, et al. MIC-1 serum level and genotype: associations with progress and prognosis of colorectal carcinoma. *Clin Cancer Res.* 2003 Jul;9(7):2642-50.
103. Notz Q, Schmalzing M, Wedekink F, Schlesinger T, Gernert M, Herrmann J, et al. Pro- and Anti-Inflammatory Responses in Severe COVID-19-Induced Acute Respiratory Distress Syndrome-An Observational Pilot Study. *Front Immunol.* 2020;11:581338.
104. Staff AC, Trovik J, Eriksson AG, Wik E, Wollert KC, Kempf T, et al. Elevated plasma growth differentiation factor-15 correlates with lymph node metastases and poor survival in endometrial cancer. *Clin Cancer Res.* 2011 Jul 15;17(14):4825-33.
105. Kempf T, Horn-Wichmann R, Brabant G, Peter T, Allhoff T, Klein G, et al. Circulating concentrations of growth-differentiation factor 15 in apparently healthy elderly individuals and patients with chronic heart failure as assessed by a new immunoradiometric sandwich assay. *Clin Chem.* 2007 Feb;53(2):284-91.
106. Yatsuga S, Fujita Y, Ishii A, Fukumoto Y, Arahata H, Kakuma T, et al. Growth differentiation factor 15 as a useful biomarker for mitochondrial disorders. *Ann Neurol.* 2015 Nov;78(5):814-23.
107. Staff AC, Bock AJ, Becker C, Kempf T, Wollert KC, Davidson B. Growth differentiation factor-15 as a prognostic biomarker in ovarian cancer. *Gynecol Oncol.* 2010 Sep;118(3):237-43.
108. Hagstrom E, Held C, Stewart RA, Aylward PE, Budaj A, Cannon CP, et al. Growth Differentiation Factor 15 Predicts All-Cause Morbidity and Mortality in Stable Coronary Heart Disease. *Clin Chem.* 2017 Jan;63(1):325-33.
109. Xiong Y, Walker K, Min X, Hale C, Tran T, Komorowski R, et al. Long-acting MIC-1/GDF15 molecules to treat obesity: Evidence from mice to monkeys. *Sci Transl Med.* 2017 Oct 18;9(412).
110. Breen DM, Jagarlapudi S, Patel A, Zou C, Joaquim S, Li X, et al. Growth differentiation factor 15 neutralization does not impact anorexia or survival in lipopolysaccharide-induced inflammation. *iScience.* 2021 Jun 25;24(6):102554.
111. Breit SN, Brown DA, Tsai VW. The GDF15-GFRAL Pathway in Health and Metabolic Disease: Friend or Foe? *Annu Rev Physiol.* 2021 Feb 10;83:127-51.
112. Wang D, Day EA, Townsend LK, Djordjevic D, Jorgensen SB, Steinberg GR. GDF15: emerging biology and therapeutic applications for obesity and cardiometabolic disease. *Nat Rev Endocrinol.* 2021 Oct;17(10):592-607.
113. Wang Y, Zhen C, Wang R, Wang G. Growth-differentiation factor-15 predicts adverse cardiac events in patients with acute coronary syndrome: A meta-analysis. *Am J Emerg Med.* 2019 Jul;37(7):1346-52.
114. Xie S, Lu L, Liu L. Growth differentiation factor-15 and the risk of cardiovascular diseases and all-cause mortality: A meta-analysis of prospective studies. *Clin Cardiol.* 2019 May;42(5):513-23.
115. Kempf T, Zarbock A, Widera C, Butz S, Stadtmann A, Rossaint J, et al. GDF-15 is an inhibitor of leukocyte integrin activation required for survival after myocardial infarction in mice. *Nat Med.* 2011 May;17(5):581-8.
116. Govaere O, Cockell S, Tiniakos D, Queen R, Younes R, Vacca M, et al. Transcriptomic profiling across the nonalcoholic fatty liver disease spectrum reveals gene signatures for steatohepatitis and fibrosis. *Sci Transl Med.* 2020 Dec 2;12(572).



117. Li X, Huai Q, Zhu C, Zhang X, Xu W, Dai H, et al. GDF15 Ameliorates Liver Fibrosis by Metabolic Reprogramming of Macrophages to Acquire Anti-Inflammatory Properties. *Cell Mol Gastroenterol Hepatol*. 2023 Jul 25.
118. Buendgens L, Yagmur E, Bruensing J, Herbers U, Baeck C, Trautwein C, et al. Growth Differentiation Factor-15 Is a Predictor of Mortality in Critically Ill Patients with Sepsis. *Dis Markers*. 2017;2017:5271203.
119. Santos I, Colaco HG, Neves-Costa A, Seixas E, Velho TR, Pedroso D, et al. CXCL5-mediated recruitment of neutrophils into the peritoneal cavity of Gdf15-deficient mice protects against abdominal sepsis. *Proc Natl Acad Sci U S A*. 2020 Jun 2;117(22):12281-87.
120. Ebihara T, Matsumoto H, Matsubara T, Togami Y, Nakao S, Matsuura H, et al. Cytokine Elevation in Severe COVID-19 From Longitudinal Proteomics Analysis: Comparison With Sepsis. *Front Immunol*. 2021;12:798338.
121. Luan HH, Wang A, Hilliard BK, Carvalho F, Rosen CE, Ahasic AM, et al. GDF15 Is an Inflammation-Induced Central Mediator of Tissue Tolerance. *Cell*. 2019 Aug 22;178(5):1231-44 e11.
122. Wang D, Townsend LK, DesOrmeaux GJ, Frangos SM, Batchuluun B, Dumont L, et al. GDF15 promotes weight loss by enhancing energy expenditure in muscle. *Nature*. 2023 Jul;619(7968):143-50.
123. Wang Y, Jiang T, Jiang M, Gu S. Appraising growth differentiation factor 15 as a promising biomarker in digestive system tumors: a meta-analysis. *BMC Cancer*. 2019 Feb 26;19(1):177.
124. Traeger L, Ellermann I, Wiethoff H, Ihbe J, Gallitz I, Eveslage M, et al. Serum Hepcidin and GDF-15 levels as prognostic markers in urothelial carcinoma of the upper urinary tract and renal cell carcinoma. *BMC Cancer*. 2019 Jan 15;19(1):74.
125. Rochette L, Meloux A, Zeller M, Cottin Y, Vergely C. Functional roles of GDF15 in modulating microenvironment to promote carcinogenesis. *Biochim Biophys Acta Mol Basis Dis*. 2020 Aug 1;1866(8):165798.
126. Muniyan S, Pothuraju R, Seshacharyulu P, Batra SK. Macrophage inhibitory cytokine-1 in cancer: Beyond the cellular phenotype. *Cancer Lett*. 2022 Jun 28;536:215664.
127. Spanopoulou A, Gkretsi V. Growth differentiation factor 15 (GDF15) in cancer cell metastasis: from the cells to the patients. *Clin Exp Metastasis*. 2020 Aug;37(4):451-64.
128. Qin R, Ren W, Ya G, Wang B, He J, Ren S, et al. Role of chemokines in the crosstalk between tumor and tumor-associated macrophages. *Clin Exp Med*. 2023 Sep;23(5):1359-73.
129. Willier S, Rothamel P, Hastreiter M, Wilhelm J, Stenger D, Blaesche F, et al. CLEC12A and CD33 coexpression as a preferential target for pediatric AML combinatorial immunotherapy. *Blood*. 2021 Feb 25;137(8):1037-49.
130. Neumann K, Castineiras-Vilarino M, Hockendorf U, Hanneschlager N, Lemeer S, Kupka D, et al. Clec12a is an inhibitory receptor for uric acid crystals that regulates inflammation in response to cell death. *Immunity*. 2014 Mar 20;40(3):389-99.
131. Hanawa-Suetsugu K, Itoh Y, Ab Fatah M, Nishimura T, Takemura K, Takeshita K, et al. Phagocytosis is mediated by two-dimensional assemblies of the F-BAR protein GAS7. *Nat Commun*. 2019 Oct 18;10(1):4763.
132. Xu Q, Liu X, Wang X, Hua Y, Wang X, Chen J, et al. Growth arrest-specific protein 7 regulates the murine M1 alveolar macrophage polarization. *Immunol Res*. 2017 Oct;65(5):1065-73.

133. Sanjurjo L, Aran G, Tellez E, Amezaga N, Armengol C, Lopez D, et al. CD5L Promotes M2 Macrophage Polarization through Autophagy-Mediated Upregulation of ID3. *Front Immunol.* 2018;9:480.
134. Yuan Q, Peng N, Xiao F, Shi X, Zhu B, Rui K, et al. New insights into the function of Interleukin-25 in disease pathogenesis. *Biomark Res.* 2023 Apr 1;11(1):36.
135. Bastid J, Dejoux C, Docquier A, Bonnefoy N. The Emerging Role of the IL-17B/IL-17RB Pathway in Cancer. *Front Immunol.* 2020;11:718.
136. Sharad S, Dobi A, Srivastava S, Srinivasan A, Li H. PMEPA1 Gene Isoforms: A Potential Biomarker and Therapeutic Target in Prostate Cancer. *Biomolecules.* 2020 Aug 22;10(9).
137. Basak S, Jacobs SB, Krieg AJ, Pathak N, Zeng Q, Kaldis P, et al. The metastasis-associated gene Prl-3 is a p53 target involved in cell-cycle regulation. *Mol Cell.* 2008 May 9;30(3):303-14.
138. Gari HH, DeGala GD, Lucia MS, Lambert JR. Loss of the oncogenic phosphatase PRL-3 promotes a TNF-R1 feedback loop that mediates triple-negative breast cancer growth. *Oncogenesis.* 2016 Aug 15;5(8):e255.
139. McQueeney KE, Salamoun JM, Burnett JC, Barabutis N, Pekic P, Lewandowski SL, et al. Targeting ovarian cancer and endothelium with an allosteric PTP4A3 phosphatase inhibitor. *Oncotarget.* 2018 Feb 2;9(9):8223-40.
140. Song Q, Zheng Y, Wu J, Wang S, Meng L, Yao Q, et al. PTP4A3 Is a Prognostic Biomarker Correlated With Immune Infiltrates in Papillary Renal Cell Carcinoma. *Front Immunol.* 2021;12:717688.
141. Miyazawa K, Miyazono K. Regulation of TGF-beta Family Signaling by Inhibitory Smads. *Cold Spring Harb Perspect Biol.* 2017 Mar 1;9(3).
142. Zhang T, Wu J, Ungvijanpunya N, Jackson-Weaver O, Gou Y, Feng J, et al. Smad6 Methylation Represses NFkappaB Activation and Periodontal Inflammation. *J Dent Res.* 2018 Jul;97(7):810-19.
143. Silva-Bermudez LS, Sevastyanova TN, Schmuttermayer C, De La Torre C, Schumacher L, Kluter H, et al. Titanium Nanoparticles Enhance Production and Suppress Stabilin-1-Mediated Clearance of GDF-15 in Human Primary Macrophages. *Front Immunol.* 2021;12:760577.
144. Mattia L, Gossiel F, Walsh JS, Eastell R. Effect of age and gender on serum growth differentiation factor 15 and its relationship to bone density and bone turnover. *Bone Rep.* 2023 Jun;18:101676.
145. Urakawa N, Utsunomiya S, Nishio M, Shigeoka M, Takase N, Arai N, et al. GDF15 derived from both tumor-associated macrophages and esophageal squamous cell carcinomas contributes to tumor progression via Akt and Erk pathways. *Lab Invest.* 2015 May;95(5):491-503.
146. Tanaka T, Narazaki M, Kishimoto T. IL-6 in inflammation, immunity, and disease. *Cold Spring Harb Perspect Biol.* 2014 Sep 4;6(10):a016295.
147. Li S, Li Q, Zhu Y, Hu W. GDF15 induced by compressive force contributes to osteoclast differentiation in human periodontal ligament cells. *Exp Cell Res.* 2020 Feb 1;387(1):111745.
148. Zhang X, Dong S. Protective effect of growth differentiation factor 15 in sepsis by regulating macrophage polarization and its mechanism. *Bioengineered.* 2022 Apr;13(4):9687-707.
149. Li M, Song K, Huang X, Fu S, Zeng Q. GDF-15 prevents LPS and D-galactosamine-induced inflammation and acute liver injury in mice. *Int J Mol Med.* 2018 Sep;42(3):1756-64.

150. Gratchev A, Kzhyshkowska J, Duperrier K, Utikal J, Velten FW, Goerdts S. The receptor for interleukin-17E is induced by Th2 cytokines in antigen-presenting cells. *Scand J Immunol*. 2004 Sep;60(3):233-7.
151. Li L, Ma L, Zhao Z, Luo S, Gong B, Li J, et al. IL-25-induced shifts in macrophage polarization promote development of beige fat and improve metabolic homeostasis in mice. *PLoS Biol*. 2021 Aug;19(8):e3001348.
152. Borowczyk J, Shutova M, Brembilla NC, Boehncke WH. IL-25 (IL-17E) in epithelial immunology and pathophysiology. *J Allergy Clin Immunol*. 2021 Jul;148(1):40-52.
153. Zheng R, Chen FH, Gao WX, Wang D, Yang QT, Wang K, et al. The T(H)2-polarizing function of atopic interleukin 17 receptor B-positive dendritic cells up-regulated by lipopolysaccharide. *Ann Allergy Asthma Immunol*. 2017 Apr;118(4):474-82 e1.
154. He F, Liu H, Luo W. The PI3K-Akt-HIF-1alpha Pathway Reducing Nasal Airway Inflammation and Remodeling in Nasal Polyposis. *Ear Nose Throat J*. 2021 Jan;100(1):NP43-NP49.
155. Liu J, Zhou X, Zhan Z, Meng Q, Han Y, Shi Q, et al. IL-25 regulates the polarization of macrophages and attenuates obliterative bronchiolitis in murine trachea transplantation models. *Int Immunopharmacol*. 2015 Apr;25(2):383-92.
156. Jeerawattanawart S, Siripurkpong P, Roytrakul S, Angkasekwinai P. IL-25 directly modulates adipocyte function and inflammation through the regulation of adiponectin. *Inflamm Res*. 2022 Nov;71(10-11):1229-44.
157. Drouin M, Saenz J, Chiffolleau E. C-Type Lectin-Like Receptors: Head or Tail in Cell Death Immunity. *Front Immunol*. 2020;11:251.
158. Gratchev A, Kzhyshkowska J, Kannookadan S, Ochsenreiter M, Popova A, Yu X, et al. Activation of a TGF-beta-specific multistep gene expression program in mature macrophages requires glucocorticoid-mediated surface expression of TGF-beta receptor II. *J Immunol*. 2008 May 15;180(10):6553-65.
159. Xu J, Kimball TR, Lorenz JN, Brown DA, Bauskin AR, Klevitsky R, et al. GDF15/MIC-1 functions as a protective and antihypertrophic factor released from the myocardium in association with SMAD protein activation. *Circ Res*. 2006 Feb 17;98(3):342-50.
160. Ma Y, Hu J, Xue X, Gu J, Pan Y, Yang J. SENP3 deletion promotes M2 macrophage polarization and accelerates wound healing through smad6/IkappaB/p65 signaling pathway. *Heliyon*. 2023 May;9(5):e15584.
161. Arlauckas SP, Garren SB, Garriss CS, Kohler RH, Oh J, Pittet MJ, et al. Arg1 expression defines immunosuppressive subsets of tumor-associated macrophages. *Theranostics*. 2018;8(21):5842-54.
162. Li J, Kong WM. PMEPA1 Serves as a Prognostic Biomarker and Correlates with Immune Infiltrates in Cervical Cancer. *J Immunol Res*. 2022;2022:4510462.
163. Tang X, Woodward T, Amar S. A PTP4A3 peptide PIMAP39 modulates TNF-alpha levels and endotoxic shock. *J Innate Immun*. 2010;2(1):43-55.
164. Diaz-Montero CM, Rini BI, Finke JH. The immunology of renal cell carcinoma. *Nat Rev Nephrol*. 2020 Dec;16(12):721-35.
165. Mielcarska S, Stopinska K, Dawidowicz M, Kula A, Kiczmer P, Senkowska AP, et al. GDF-15 Level Correlates with CMKLR1 and VEGF-A in Tumor-free Margin in Colorectal Cancer. *Curr Med Sci*. 2021 Jun;41(3):522-28.
166. Song H, Yin D, Liu Z. GDF-15 promotes angiogenesis through modulating p53/HIF-1alpha signaling pathway in hypoxic human umbilical vein endothelial cells. *Mol Biol Rep*. 2012 Apr;39(4):4017-22.

167. Wang Z, Wang S, Jia Z, Hu Y, Cao D, Yang M, et al. YKL-40 derived from infiltrating macrophages cooperates with GDF15 to establish an immune suppressive microenvironment in gallbladder cancer. *Cancer Lett.* 2023 Jun 1;563:216184.
168. Peng H, Li Z, Fu J, Zhou R. Growth and differentiation factor 15 regulates PD-L1 expression in glioblastoma. *Cancer Manag Res.* 2019;11:2653-61.
169. Hong G, Sun P, Chung C, Park D, Lee SI, Kim N, et al. Plasma GDF15 levels associated with circulating immune cells predict the efficacy of PD-1/PD-L1 inhibitor treatment and prognosis in patients with advanced non-small cell lung cancer. *J Cancer Res Clin Oncol.* 2023 Jan;149(1):159-71.
170. Joo M, Kim D, Lee MW, Lee HJ, Kim JM. GDF15 Promotes Cell Growth, Migration, and Invasion in Gastric Cancer by Inducing STAT3 Activation. *Int J Mol Sci.* 2023 Feb 2;24(3).
171. Peake BF, Eze SM, Yang L, Castellino RC, Nahta R. Growth differentiation factor 15 mediates epithelial mesenchymal transition and invasion of breast cancers through IGF-1R-FoxM1 signaling. *Oncotarget.* 2017 Nov 7;8(55):94393-406.
172. Dong G, Huang X, Jiang S, Ni L, Ma L, Zhu C, et al. SCAP Mediated GDF15-Induced Invasion and EMT of Esophageal Cancer. *Front Oncol.* 2020;10:564785.
173. Duan L, Pang HL, Chen WJ, Shen WW, Cao PP, Wang SM, et al. The role of GDF15 in bone metastasis of lung adenocarcinoma cells. *Oncol Rep.* 2019 Apr;41(4):2379-88.
174. Costa VL, Henrique R, Danielsen SA, Duarte-Pereira S, Eknaes M, Skotheim RI, et al. Three epigenetic biomarkers, GDF15, TMEFF2, and VIM, accurately predict bladder cancer from DNA-based analyses of urine samples. *Clin Cancer Res.* 2010 Dec 1;16(23):5842-51.
175. Wang R, Wen P, Yang G, Feng Y, Mi Y, Wang X, et al. N-glycosylation of GDF15 abolishes its inhibitory effect on EGFR in AR inhibitor-resistant prostate cancer cells. *Cell Death Dis.* 2022 Jul 19;13(7):626.
176. Wu HH, Hwang-Verslues WW, Lee WH, Huang CK, Wei PC, Chen CL, et al. Targeting IL-17B-IL-17RB signaling with an anti-IL-17RB antibody blocks pancreatic cancer metastasis by silencing multiple chemokines. *J Exp Med.* 2015 Mar 9;212(3):333-49.
177. Furuta S, Jeng YM, Zhou L, Huang L, Kuhn I, Bissell MJ, et al. IL-25 causes apoptosis of IL-25R-expressing breast cancer cells without toxicity to nonmalignant cells. *Sci Transl Med.* 2011 Apr 13;3(78):78ra31.
178. Yin SY, Jian FY, Chen YH, Chien SC, Hsieh MC, Hsiao PW, et al. Induction of IL-25 secretion from tumour-associated fibroblasts suppresses mammary tumour metastasis. *Nat Commun.* 2016 Apr 18;7:11311.
179. Zhang S, Liu Z, Xiao M, Liu H. The prognostic value and immunological role of the small mother against decapentaplegic proteins in kidney renal clear cell carcinoma. *Transl Cancer Res.* 2021 Jun;10(6):2678-93.
180. Hu CY, Mohtat D, Yu Y, Ko YA, Shenoy N, Bhattacharya S, et al. Kidney cancer is characterized by aberrant methylation of tissue-specific enhancers that are prognostic for overall survival. *Clin Cancer Res.* 2014 Aug 15;20(16):4349-60.
181. Ding N, Luo H, Zhang T, Peng T, Yao Y, He Y. Correlation between SMADs and Colorectal Cancer Expression, Prognosis, and Immune Infiltrates. *Int J Anal Chem.* 2023;2023:8414040.
182. Chia PL, Ang KH, Thura M, Zeng Q. PRL3 as a therapeutic target for novel cancer immunotherapy in multiple cancer types. *Theranostics.* 2023;13(6):1876-91.
183. Karlsson M, Zhang C, Mear L, Zhong W, Digre A, Katona B, et al. A single-cell type transcriptomics map of human tissues. *Sci Adv.* 2021 Jul;7(31).

184. Zhang X, Ai F, Li X, She X, Li N, Tang A, et al. Inflammation-induced S100A8 activates Id3 and promotes colorectal tumorigenesis. *Int J Cancer*. 2015 Dec 15;137(12):2803-14.
185. Qiu D, Hu J, Hu J, Yu A, Othmane B, He T, et al. PMEPA1 Is a Prognostic Biomarker That Correlates With Cell Malignancy and the Tumor Microenvironment in Bladder Cancer. *Front Immunol*. 2021;12:705086.
186. Morsink LM, Walter RB, Ossenkoppele GJ. Prognostic and therapeutic role of CLEC12A in acute myeloid leukemia. *Blood Rev*. 2019 Mar;34:26-33.
187. Chang JW, Kuo WH, Lin CM, Chen WL, Chan SH, Chiu MF, et al. Wild-type p53 upregulates an early onset breast cancer-associated gene GAS7 to suppress metastasis via GAS7-CYFIP1-mediated signaling pathway. *Oncogene*. 2018 Jul;37(30):4137-50.
188. Ping W, Gao Y, Fan X, Li W, Deng Y, Fu X. MiR-181a contributes gefitinib resistance in non-small cell lung cancer cells by targeting GAS7. *Biochem Biophys Res Commun*. 2018 Jan 22;495(4):2482-89.
189. Dong Z, Yeo KS, Lopez G, Zhang C, Dankert Eggum EN, Rokita JL, et al. GAS7 Deficiency Promotes Metastasis in MYCN-Driven Neuroblastoma. *Cancer Res*. 2021 Jun 1;81(11):2995-3007.
190. Kzhyshkowska J, Gratchev A, Schmuttermayr C, Brundiers H, Krusell L, Mamidi S, et al. Alternatively activated macrophages regulate extracellular levels of the hormone placental lactogen via receptor-mediated uptake and transcytosis. *J Immunol*. 2008 Mar 1;180(5):3028-37.
191. Riabov V, Yin S, Song B, Avdic A, Schledzewski K, Ovsy I, et al. Stabilin-1 is expressed in human breast cancer and supports tumor growth in mammary adenocarcinoma mouse model. *Oncotarget*. 2016 May 24;7(21):31097-110.
192. Liu T, Larionova I, Litviakov N, Riabov V, Zavyalova M, Tsyganov M, et al. Tumor-associated macrophages in human breast cancer produce new monocyte attracting and pro-angiogenic factor YKL-39 indicative for increased metastasis after neoadjuvant chemotherapy. *Oncoimmunology*. 2018;7(6):e1436922.
193. Wang W, Yang X, Dai J, Lu Y, Zhang J, Keller ET. Prostate cancer promotes a vicious cycle of bone metastasis progression through inducing osteocytes to secrete GDF15 that stimulates prostate cancer growth and invasion. *Oncogene*. 2019 Jun;38(23):4540-59.
194. Watanabe J, Nakagawa M, Watanabe N, Nakamura M. Ubiquitin-like protein MNSFbeta covalently binds to Bcl-G and enhances lipopolysaccharide/interferon gamma-induced apoptosis in macrophages. *FEBS J*. 2013 Mar;280(5):1281-93.
195. Rolph D, Das H. Transcriptional Regulation of Osteoclastogenesis: The Emerging Role of KLF2. *Front Immunol*. 2020;11:937.
196. Nitzsche A, Pietila R, Love DT, Testini C, Ninchoji T, Smith RO, et al. Paladin is a phosphoinositide phosphatase regulating endosomal VEGFR2 signalling and angiogenesis. *EMBO Rep*. 2021 Feb 3;22(2):e50218.
197. Oto J, Fernandez-Pardo A, Miralles M, Plana E, Espana F, Navarro S, et al. Activated protein C assays: A review. *Clin Chim Acta*. 2020 Mar;502:227-32.
198. Healy LD, Fernandez JA, Mosnier LO, Griffin JH. Activated protein C and PAR1-derived and PAR3-derived peptides are anti-inflammatory by suppressing macrophage NLRP3 inflammasomes. *J Thromb Haemost*. 2021 Jan;19(1):269-80.
199. Shea-Donohue T, Zhao A, Antalis TM. SerpinB2 mediated regulation of macrophage function during enteric infection. *Gut Microbes*. 2014 Mar-Apr;5(2):254-8.

## 8 CURRICULUM VITAE

### PERSONAL

Name: Silva Bermúdez, Lina Susana  
Date of birth: 09.11.1994  
Place of Birth: Neiva, Colombia

### SCHOOL COURSE

01.2003 – 11.2011      Gymnasium  
Colombus American School  
Neiva, Colombia

### EDUCATIONAL EXPERIENCE

SS 2012 – WS 2018      Medical doctor  
Faculty of Medicine  
Universidad de los Andes, Bogotá, Colombia  
  
24.01.2019              Staatsexamen  
Universidad de los Andes, Bogotá, Colombia  
  
2019 – 2020              Master of Science in Translational Medical Research  
Titel: Effect of Titanium Nanoparticles on Healing  
Functions of Human Primary Macrophages  
Medizinische Fakultät Mannheim  
Universität Heidelberg  
Mannheim, Germany  
  
09.03.2021              Approbation als Ärztin  
Regierungspräsidium Stuttgart

### PUBLICATIONS

1. Silva-Bermúdez, L. S., Vargas-Villanueva, A., Sánchez-Vallejo, C. A., Palacio, A. C., Buitrago, A. F., & Mendivil, C. O. (2022). Peri-event plasma PCSK9 and hsCRP after an acute myocardial infarction correlate with early deterioration of left ventricular ejection fraction: a cohort study. *Lipids in Health and Disease*, 21(1), 61.
2. Silva-Bermudez, L. S., Sevastyanova, T. N., Schmuttermayr, C., De La Torre, C., Schumacher, L., Klüter, H., & Kzhyshkowska, J. (2021). Titanium Nanoparticles Enhance Production and Suppress Stabilin-1-Mediated Clearance of GDF-15 in Human Primary Macrophages. *Frontiers in immunology*, 5310.

3. Silva-Bermudez, L.S., Toloza, F.J.K., Perez-Matos, M.C., de Souza, R.J., Banfield, L., Vargas-Villanueva, A & Mendivil C.O. (2020). Effects of oral contraceptives on metabolic parameters in adult premenopausal women. *Endocrine Connections*.
4. Amaya-Montoya, M., Pinzón-Cortés, J. A., Silva-Bermúdez, L. S., Ruiz-Manco, D., Pérez-Matos, M. C., Jiménez-Mora, M. A., & Mendivil, C. O. (2020). ApoE and apoC-III-defined HDL subtypes: a descriptive study of their lecithin cholesterol acyl transferase and cholesteryl ester transfer protein content and activity. *Lipids in Health and Disease*, 19(1), 1-11.
5. Makke, M., Martinez, M. M., Gaya, S., Schwarz, Y., Frisch, W., Silva-Bermudez, L., ... & Bruns, D. (2018). A mechanism for exocytotic arrest by the Complexin C-terminus. *Elife*, 7, e38981

## 9 ACKNOWLEDGEMENTS

I am very grateful to my principal investigator and supervisor, Prof. Dr. Julia Kzhyshkowska, for her constant support and advice during the course of my doctoral project. I greatly enjoyed our scientific conversations and how I left her office motivated to continue doing science. I am grateful to Prof. Dr. Klüter, who trusted in my talent and has unconditionally supported my scientific career. I am grateful for the financial support of DRK-Blutspendedienst Baden-Württemberg - Hessen gGmbH

I express my sincere gratitude to Christina Schmuttermaier for her excellent technical assistance and her sincere encouragement. Likewise, I would like to thank the other members of the laboratory for their support and good humor: Xiaomin Li, Guanhao Li, Quan Liu, Youjing Sheng, Fangrong Xu and Jingxuan Xu. And to all the colleagues who greeted me with generous smiles and sympathetic glances, especially to my colleagues from the Institute for Transfusion Medicine and Immunology, who supported me during the writing of this dissertation.

I thank PD Dr. Thomas Worst, from the Urology Department, for his intellectual contribution to the development of this project.

Prof. Dr. Christel Weiß for valuable advices in statistical analysis.

I am deeply thankful for all the support and love I received from my friends during this journey. I thank Natthaly for her great experimental support and cheerleader attitude. To Camilo, who has always been a precious friend. For the motivating conversations and emotional support, I thank Jimmy, Angela, Misaela, Nora, Patrick, Jose and Jonas. I hope that one day I will be able to give back all the amazing blessings I have received so far.

To Tatyana, who taught me the techniques of the lab and offered me her friendship. To Ernesto, who will remain in my thoughts as a good friend.

To my first mentor in science, Prof. Dr. Mendivil, who has inspired me since the beginning of my research path by being an example of a great teacher and a wonderful person.

Finally, I dedicate this achievement, as well as all the others that will follow, to my parents, Ramiro and Susana, and to my brother, Ramiro D, without whom none of this would make sense.